PETROS CHATZOPOULOS

SCHOOL OF MECHANICAL ENGINEERING

Gas Turbine Operation with CO_2 as Working Medium

Section: Fluids

Supervisor: Mathioudakis Konstantinos, Professor NTUA

Athens 2024

This Page Intentionally Left Blank

<u>Υπεύθυνη δήλωση</u> για λογοκλοπή και για κλοπή πνευματικής ιδιοκτησίας:

Έχω διαβάσει και κατανοήσει τους κανόνες για τη λογοκλοπή και τον τρόπο σωστής αναφοράς των πηγών που περιέχονται στον οδηγό συγγραφής Διπλωματικών Εργασιών. Δηλώνω ότι, από όσα γνωρίζω, το περιεχόμενο της παρούσας Διπλωματικής Εργασίας είναι προϊόν δικής μου εργασίας και υπάρχουν αναφορές σε όλες τις πηγές που χρησιμοποίησα.

Οι απόψεις και τα συμπεράσματα που περιέχονται σε αυτή τη Διπλωματική εργασία είναι του συγγραφέα και δεν πρέπει να ερμηνευθεί ότι αντιπροσωπεύουν τις επίσημες θέσεις της Σχολής Μηχανολόγων Μηχανικών ή του Εθνικού Μετσόβιου Πολυτεχνείου.

Χατζόπουλος Πέτρος

This Page Intentionally Left Blank

Abstract

In an effort to address and reverse the greenhouse effect, there is a particular interest in potential solutions. If we focus on the causes of the problem, we find out that carbon dioxide emissions are a significant aggravating factor. Therefore, it is deemed crucial to engage with and understand such substance, as well as delve into various fields where it can be utilized.

In this context, this thesis marks the first interaction of the Laboratory of Thermal Turbomachines at the National Technical University of Athens with carbon dioxide as a working fluid in gas turbines.

Specifically, by gathering relevant sources from international literature and using them as references throughout the work, an initial study of the properties of carbon dioxide is conducted, with emphasis on its supercritical region, where it exhibits outstanding properties. However, its unique properties compared to other substances require special computational treatment, given its behavior as a real gas. Concurrently, it emerges as a rising working medium for power cycles.

Power cycles are one of the primary applications using carbon dioxide. Its nature allows for efficiency across a broad range of temperatures and pressures, facilitating collaboration with various heat sources, such as solar energy. The second stage of this work focuses on modeling and developing computational tools for calculating power cycles using carbon dioxide as a working fluid. These tools go beyond determining the operating point of each cycle; they extend to off-design analysis, covering the entire operating range of a gas turbine.

With a better understanding of carbon dioxide behavior and the computational tools developed, this thesis serves as the foundation for further studies in the Laboratory of Thermal Turbomachines.

Key words:

Carbon Dioxide, Supercritical Region, Equations of State, Power Cycles, Gas Turbines.

Περίληψη

Σε μια προσπάθεια αντιμετώπισης και αντιστροφής του φαινομένου του θερμοκηπίου, υπάρχει ιδιαίτερο ενδιαφέρον για πιθανούς τρόπους επίλυσης του. Αν επικεντρωθούμε στα αίτια του προβλήματος, διαπιστώνουμε ότι οι εκπομπές διοξειδίου του άνθρακα αποτελούν σημαντικό παράγοντα επιδείνωσης του φαινομένου. Έτσι λοιπόν, κρίνεται ως επιτακτική ανάγκη η επαφή και η γνωριμία με την εν λόγω ουσία, όπως επίσης και εμβάθυνση στους διάφορους τομείς στους οποίους μπορεί να χρησιμοποιηθεί.

Στο πλαίσιο αυτό, η παρούσα διπλωματική εργασία, αποτελεί την πρώτη επαφή του Εργαστηρίου Θερμικών Στροβιλομηχανών του Εθνικού Μετσόβιου Πολυτεχνείου, με το διοξείδιο του άνθρακα ως εργαζόμενο μέσο σε αεριοστρόβιλους.

Πιο συγκεκριμένα, έχοντας συλλέξει τις κατάλληλες πηγές από την διεθνή βιβλιογραφία και χρησιμοποιώντας τες σαν αναφορά καθ' όλη την διάρκεια της εργασίας, πραγματοποιείται σε πρώτο στάδιο μια ενδεικτική μελέτη των ιδιοτήτων του διοξειδίου του άνθρακα, με έμφαση στην υπερκρίσιμη περιοχή του, όπου και παρουσιάζει εξέχουσες ιδιότητες. Ωστόσο, η διαφοροποίηση στις ιδιότητές του σε σχέση με άλλες ουσίες, το χρίζουν ιδιαίτερης υπολογιστικής μεταχείρισης, αφού συμπεριφέρεται σαν πραγματικό αέριο. Παράλληλα όμως, καθίσταται και ανερχόμενο εργαζόμενο μέσο για κύκλους ισχύος.

Οι κύκλοι ισχύος αποτελούν μία από της βασικότερες εφαρμογές που χρησιμοποιείται το διοξείδιο του άνθρακα. Η φύση του, του επιτρέπει να είναι αποδοτικό σε ένα ευρύ φάσμα θερμοκρασιών και πιέσεων, επιτρέποντας έτσι την συνεργασία του με διάφορες πηγές θερμότητας, όπως η ηλιακή. Το δεύτερο στάδιο της παρούσας εργασίας, επικεντρώνεται στην μοντελοποίηση και την ανάπτυξη υπολογιστικών εργαλείων, που στόχο έχουν τον υπολογισμό κύκλων ισχύος, με το διοξείδιο του άνθρακα ως εργαζόμενο μέσο. Τα εργαλεία δεν περιορίζονται μόνο στον υπολογισμό του σημείου λειτουργίας του εκάστοτε κύκλου, αλλά επεκτείνονται και σε σχεδιασμό εκτός λειτουργίας, ώστε να καλυφθεί πλήρως το εύρος λειτουργίας ενός αεριοστρόβιλου.

Αποκτώντας πλέον μια καλύτερη εικόνα για την συμπεριφορά του διοξειδίου του άνθρακα, σε συνδυασμό με τα υπολογιστικά εργαλεία που αναπτύχθηκαν, η παρούσα διπλωματική εργασία αποτελεί την βάση για περαιτέρω μελέτες του εργαστηρίου.

Λέξεις κλειδιά:

Διοξείδιο του Άνθρακα, Υπερκρίσιμη Περιοχή, Εξισώσεις Κατάστασης, Κύκλοι Ισχύος, Αεριοστρόβιλοι.

Ευχαριστίες

Από την θέση αυτή, θα ήθελα να ευχαριστήσω θερμά τον καθηγητή μου κ. Κωνσταντίνο Μαθιουδάκη, για την ευκαιρία που μου έδωσε, να εκπονήσω υπό την επίβλεψή του την διπλωματική μου εργασία. Η -σχεδόν- καθημερινή μας αλληλεπίδραση, αποτέλεσε πηγή έμπνευσης και σιγουριάς, και η καθοδήγησή του ήταν καίρια για την επιτυχή περάτωση της εργασίας.

Φυσικά, δεν μπορώ να παραλείψω τα υπόλοιπα μέλη του Εργαστηρίου Θερμικών Στροβιλομηχανών, με ιδιαίτερη μνεία στον Δρ. Ιωάννη Κόλια, του οποίου η πόρτα ήταν διαρκώς ανοιχτή για την επίλυση οποιασδήποτε απορίας στο υπολογιστικό κομμάτι της εργασίας.

Εν συνεχεία, ένα ιδιαίτερο και ειλικρινές ευχαριστώ στην οικογένειά μου, για την στήριξη που μου προσφέρει απλόχερα τόσα χρόνια, και για την δυνατότητα που μου παρείχε να αφοσιωθώ στις σπουδές μου και να κυνηγήσω τους στόχους μου.

Τέλος, οφείλω πολλά στους φίλους μου και στην Η., για τις στιγμές που περάσαμε και την συμπαράστασή τους σε εύκολες και δύσκολες καταστάσεις, όλα αυτά τα χρόνια.

This Page Intentionally Left Blank

TABLE OF CONTENTS

1. INTRODUCTION

The emissions of greenhouse gases are the major cause of global climate change. Those gases have the ability to absorb heat that is radiated by the Earth's surface and trap it inside the atmosphere. Even though their presence is essential to maintain a normal average temperature on Earth, around 15°C, human activities have led to increased emissions of greenhouse gases, which has as a consequence the increment of global surface temperature. Carbon dioxide (CO_2) is considered to be the largest contributor among greenhouse gas, as depicted in **Figure 1**, and its annual emissions gradually increase over the years, according to **Figure 2**.

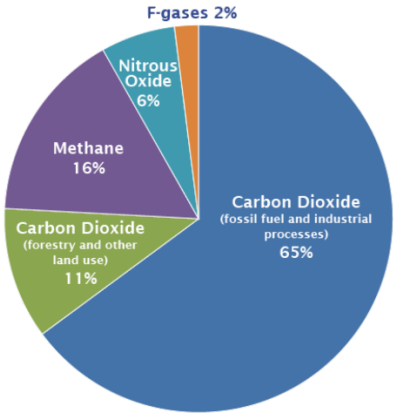

Figure 1. Total U.S. emissions of greenhouse gasses in 2021 [1].

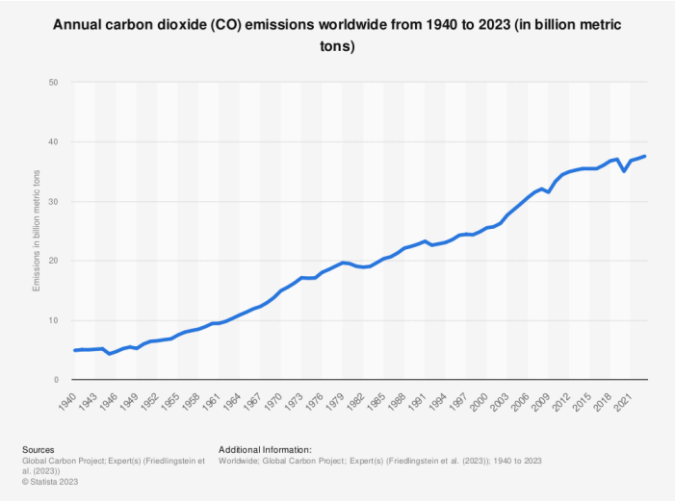

Figure 2. Annual carbon dioxide emissions worldwide [2].

To reduce those emissions, the utilization of renewable energy sources is highly promoted. However, conventional energy sources, such as oil, coal and natural gas, still constitute the lion's share of the energy production, since they fulfill the 85% of global energy demand [3]. So far, especially for the case of coal, it is highly competitive with respect to cleaner energy sources. As a result, coal-burning power plants, for example, are responsible for nearly 40% of carbon dioxide emissions [4]. If those emissions cannot be avoided, ways to overcome their impact on the environment must be established.

1.1 Applications of sCO_2

A promising method for avoiding emissions is Carbon Capture Use and Sequestration (CCUS or CCS) which consists of three steps,

1. The capture of carbon dioxide after it is produced by power plants,
2. its transportation and
3. its use or storage in deep underground locations [5].

For this process, CO_2 must be compressed to high pressures and possibly reach its supercritical state, in which it behaves as a real gas, but it has the density of a liquid. The importance of CCS towards the reduction of CO_2 emissions is illustrated in **Figure 3**.

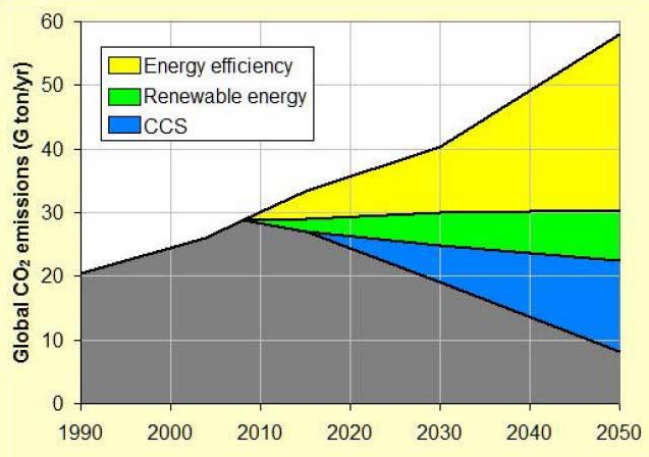

Figure 3. Strategy to reduce global CO_2 emissions, as presented in [5].

Apart from CCS, sCO_2 can be used in Enhanced Oil Recovery [4]. Its use is also possible in many power generation applications, which is the main interest of the present thesis. **Table 1** summarizes the power generation applications that sCO_2 can be used, within a working range for each case. Further explanation will be given for the first three applications, starting with nuclear power generation.

1.1.1 Power Generation Applications

In pursuit of more efficient, cost-effective, and safer nuclear power generation, fourth-generation reactors (IV Generation) are emerging. The Sodium-cooled Fast neutron Reactor is a leading contender, utilizing molten sodium for improved heat transfer. However, challenges arise when coupling sodium with traditional steam Rankine Cycles due to safety concerns. An alternative solution lies in sCO_2 Brayton power cycles, leveraging CO_2's lower reactivity with sodium and enhancing safety features. This approach offers versatility across various energy industries, potentially reducing manufacturing costs and enhancing competitiveness in both capital and operational expenditures ([6], [7], [8]).

In addition, sCO_2 power cycles show potential as replacements for conventional fossil fuel-based power systems. They offer cost-effective integration for carbon capture and storage, especially in direct-fired setups. Despite challenges in combustor chamber design and energy-intensive oxygen production, the Allam cycle provides a promising solution, currently under assessment in a 50 MW thermal pilot plant. The use of sCO_2 power cycles in fossil fuel applications brings added advantages, including higher efficiency at partial loads and faster dynamics compared to traditional steam Rankine systems. Additionally, the compact footprint and reduced cooling water requirements make sCO_2 power systems a flexible choice ([7], [8]).

Finally, sCO_2 power cycles are seen as a key solution to enhance the efficiency of Concentrated Solar Power (CSP) plants, making them economically competitive with photovoltaic systems. By using sCO_2 as a working fluid, these cycles improve efficiency and reduce capital costs in the power block. The approach eliminates the need for intermediate heat transfer loops, common in conventional CSP systems with steam Rankine Cycle units and molten salts. However, challenges arise in designing solar collectors due to the high pressures of CO_2. Moreover, addressing the lack of water sources in economically viable CSP areas involves ongoing research on CO_2 mixtures to enable dry cooling even in warmer climates ([7], [8]).

Table 1. Potential applications for sCO_2 for power conversion, as presented in [8].

Application	Cycle type	Motivation	Size (MWe)	Temperature (°C)	Pressure (MPa)
Nuclear	Indirect sCO_2	Efficiency, size, water reduction	10–300	350–700	20–35
Fossil fuel (PC, CFB, …)	Indirect sCO_2	Efficiency, water reduction	300–600	550–900	15–35
Concentrating solar power	Indirect sCO_2	Efficiency, size, water reduction	10–100	500–1000	35
Shipboard propulsion	Indirect sCO_2	Efficiency, size	<10–10	200–300	15–25
Shipboard house power	Indirect sCO_2	Efficiency, size	<1–10	230–650	15–35
Waste heat recovery	Indirect sCO_2	Efficiency, size, simple cycles	1–10	<230–650	15–35
Geothermal	Indirect sCO_2	Efficiency	1–50	100–300	15
Fossil fuel (syngas, natural gas)	Direct sCO_2	Efficiency, water reduction, CO_2 cap	300–600	1100–1500	35

Apart from the higher efficiencies which can be achieved by the alternation of conventional working fluids to sCO_2, supercritical power systems offer some other solutions in each industry sector, which promote their usage. Those solutions include the following abilities, which are listed in [8]:

1. Efficiency improvement, as mentioned above,
2. Make that market profitable, given that the heat source and sCO_2 technology are sufficiently integrated (CSP, geothermal, fossil fuel with zero emissions),
3. Being innovative as a technology, sets new standards which create a new market,
4. Fill an underutilized market niche (Waste Heat Recovery on intermediate to small-sized gas turbines, biofuels, and bulk energy storage).

1.2 Properties and Challenges

Carbon dioxide has a relatively low critical point (**Figure 4**) and is nonflammable and nontoxic [9]. Those properties, combined with its availability, since it can be obtained directly from industrial processes, make it a promising working fluid for the aforementioned applications. Moreover, as a supercritical fluid, it has high solubility and diffusivity, attributes which make it an excellent solvent and allow its usage in applications like manufacturing and sterilization.

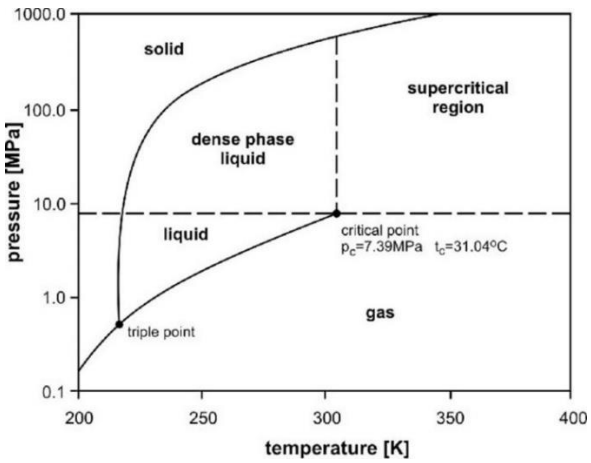

Figure 4. A state diagram for CO_2 and its critical point [10].

It needs to be mentioned that working above critical point, comes with some challenges, which arise from the fluctuations of thermodynamic properties. Nikolai et al. [9] have excessively studied the properties of CO_2, and **Figure 5** is a representative example

of the deviation from ideal gas behavior. This makes clear that real gas equation of state modeling, is essential to calculate the properties of such working fluid.

Böttcher et al. [11] compare four equations of state for CO_2 with many measurement data taken from literature. This comparison showed that complex equations of state are more accurate than simple ones. Moreover, they examine if the differences in accuracy have an influence on numerical simulations, which proves that the difference between ideal gas and real gas behavior is quite large, but the differences among the real gas equations have no noteworthy influence on the simulation results. However, they distinguish Span and Wanger equation of state for its accuracy.

Span and Wanger [12] have reviewed an excessive body of experimental data specifically for CO_2 and they have fitted to these data their equation of state. It provides with fully accurate results, even around critical point, and it is considered as the most accurate reference equation for CO_2.

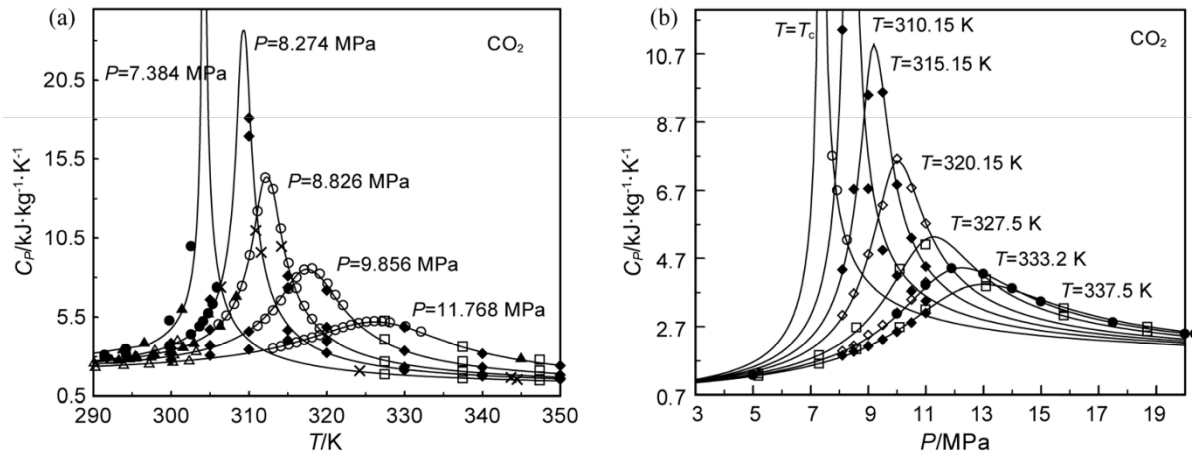

Figure 5. (a) C_p - T diagram for constant pressures; (b) C_p - p diagram for constant temperatures as presented in [9].

The properties that were discussed, set new opportunities and challenges in turbomachinery design. For instance, the high density of sCO_2 lowers the volumetric flows in the turbomachinery, which allows the making of compact components and may lead to a significant decrease in the size and consequently the cost of the entire plant.

For example, a 1 MW_e power cycle could have a single-stage compressor with an impeller diameter of 10 cm [8]. This also leads to high power density turbomachinery, and, for low power output below a few MW_e, high rotational speed is essential to maintain high isentropic efficiency [13]. Some results of a study carried out by Musgrove et al., are presented in **Figure 6**, which illustrates the range of sizes and speed for sCO_2 radial turbomachinery, in a range up to 20 MW_e.

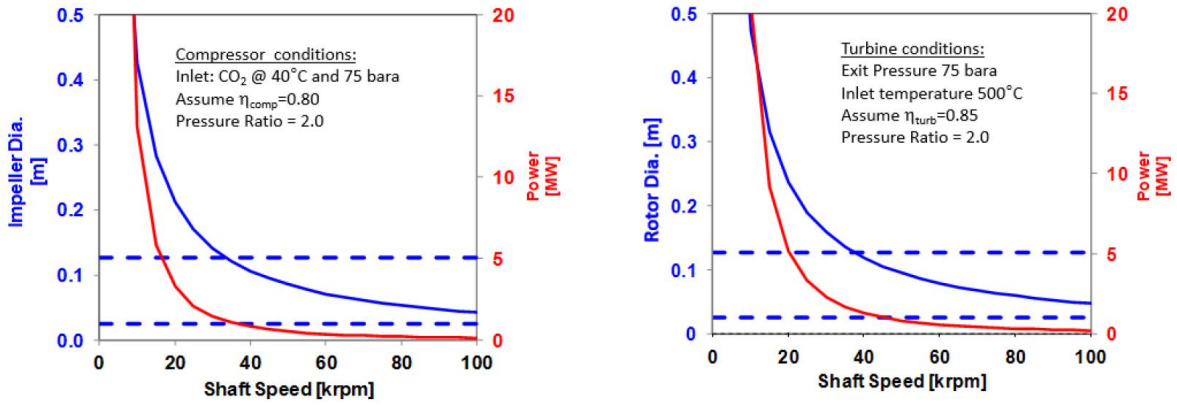

Figure 6. Example sizes and speeds for radial sCO_2 turbomachinery as presented in [14].

From the relative information that was mentioned, designing, analyzing and calculating systems that involve sCO_2, require a comprehensive understanding of its unique properties. The need for precision arises from the distinct thermodynamic behavior of CO_2, particularly when operating in supercritical conditions. For this reason, accurate computational tools must be used and developed to ensure the reliability of the numerical simulations. The present Thesis is the first systematic approach undertaken in the Laboratory of Thermal Turbomachines with such working fluid, setting as main goals to examine the accuracy of existing tools and develop new tools, specifically for sCO_2.

1.3 Thesis Structure

The thesis is structured as follows:

Chapter 2 provides a literature review, which delves into the subject that will be explored in subsequent sections. Initially, the review provides historical insights, tracing the development of sCO_2 power cycles over time. Then, a detailed examination of sCO_2 and its properties is presented, with a specific focus on calculating its key characteristics. The concluding segment of the literature review explores various studies pertaining to power generation cycles integrated with Concentrated Solar Power (CSP).

Chapter 3 provides insights into the characteristics of sCO_2, and the methods used for their calculation. Initially, the focus is on modeling the properties of sCO_2 using an appropriate Equation of State (EoS). The examination involves assessing the capabilities of various models within the RGTM library from LTT|NTUA to accurately represent the real gas behavior of sCO_2. Once the optimal EoS of RGTM is identified, a comparative analysis with REFPROP's database is conducted to determine the relative error. The chapter also includes a concise overview of the EoS employed by REFPROP and introduces the CoolProp library, which will be employed for subsequent calculations. In the second section of this chapter, specific properties of sCO_2 around its critical point are presented to highlight its

unique characteristics. The chapter concludes by explaining the preference for a compression process in proximity to the critical point.

Chapter 4 explores the foundational principles of heat transfer, fluid dynamics relationships, and the equilibrium of energy and entropy. Additionally, it elucidates specific considerations relevant to sCO_2. Commencing with the definition of key terms such as heat engine, open and closed thermodynamic systems, the chapter proceeds to outline the essential equations required for describing a thermodynamic cycle. Emphasis is placed on delineating the components integral to the thermodynamic cycle.

Chapter 5 critically examines various cycle configurations. Following a brief categorization of power cycles, the initial phase of this investigation involves illustrating the impact of assuming ideal gases instead of real gases on the efficiency of an open cycle. Subsequently, the equations introduced in the preceding chapter are applied to characterize diverse thermodynamic cycles, allowing for a thorough analysis of their performance and the conduct of various parametric studies. These studies are conducted using source codes and schematics developed in the PROOSIS environment, and their reliability is substantiated by referencing data available in the literature. The ultimate objective of this chapter is to compare distinct layouts and scrutinize the distinctive characteristics of each configuration.

The preceding chapter exclusively focuses on design point analysis, a valuable approach for assessing the comprehensive performance of the cycle and determining the optimal combination of design variables for a specific configuration. It consist of the starting point for any new design development. Another aspect useful for applications of existing layouts is the study of operation across a range of conditions. Factors such as fluctuations in power production requirements, ambient conditions, and various other considerations make it imperative for the cycle to adapt to varying circumstances. Consequently, off-design analysis becomes essential, serving the purpose of predicting the cycle's performance across its entire operating envelope, and this is the goal of **Chapter 6**.

2. LITERATURE REVIEW

To begin with, some historical information is included, which refer to the evolution of sCO_2 power cycles. Then, sCO_2 and its properties are discussed with emphasis on the calculation of its characteristics. The final part of consists of different research into power generation cycles integrated with CSP.

2.1 Historical Background

Early in 1800's, the experiments of the French physicist Baron Charles Cagniard de la Tour lead to the discovery of the critical point of a substance, which was first step towards the exploration of the supercritical state. Half a century later, Andrews examined the applicability of Boule's law across a board spectrum of pressures and approached the real gas behavior of CO_2. Nevertheless, it was not until the middle of the 20^{th} century that CO_2 gained recognition as a potential working fluid for power generation system, in a timeframe when researchers directed their efforts towards addressing the constraints associated with open Joule-Brayton and steam Ranking cycles. The genesis of closed-loop CO_2 power cycles is commonly attributed to Sulzer in 1950 [13].

Almost 20 years later, Feher in 1968 [15] and Angelino in 1969 [16] conduct more in-depth researchers in sCO_2 power systems. Feher explored a basic recuperated supercritical cycle and analyzed how the cycle's performance is influenced by operational factors and component efficiency. The research delved into the issue of heat capacity mismatch between the hot and cold fluids in the recuperator, introducing an element of irreversibility to the cycle. Building on this work, Angelino examined both supercritical and transcritical cycles, exploring various cycle configurations to mitigate the introduced irreversibility associated with the heat capacity disparity between the hot and cold fluids in the recuperator.

The PhD Thesis of Dostal in 2004 [6], revitalized the enthusiasm for sCO_2 cycles, which had been declined after the publications of Feher and Angelino. His work was focused on nuclear power applications, while he scrutinized various cycle configurations, introducing ways to improve the efficiency such intercooling and recompression. The impact of his work is depicted in **Figure 7**, which highlights the growing interest in sCO_2 as a working fluid in recent years.

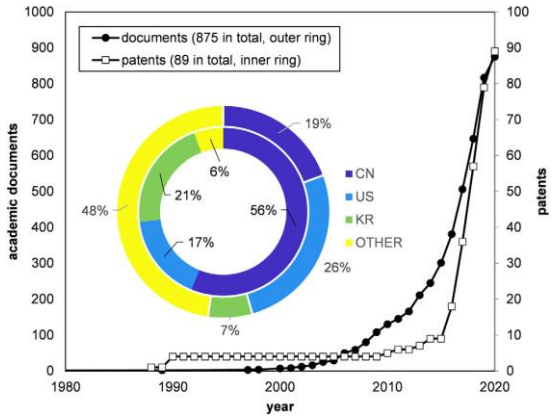

Figure 7. Historical evolution and geographical distribution of intellectual property outputs in the field of sCO_2 power systems, as presented in [13].

2.2 Properties of CO_2

Carbon dioxide holds significance as a crucial natural substance and finds extensive applications across various commercial and industrial sectors. In recent years, there has been a growing enthusiasm for employing CO_2 due to its favorable thermodynamic and transport characteristics under supercritical conditions, coupled with its positive environmental attributes.

Many researchers ([5], [9], [17]) have mentioned the unique advantages of sCO_2, which distinguish it from other supercritical fluids, starting with its relatively low critical pressure and temperature. Its distinctive attributes, such as high density and convective heat transfer coefficient, allow for the downsizing of turbomachines and heat exchangers. Remarkably, sCO_2 turbines are about 1/100 of the size of steam turbines, as illustrated in **Figure 8**, presenting a considerable cost advantage in constructing sCO_2 Brayton cycles. The low viscosity and high mobility of sCO_2 contribute to reduced flow resistance, enhancing its efficiency across various applications. Additionally, the low compressibility factor of sCO_2 significantly diminishes compression work—approximately 20–30% of the turbine output power—leading to a notable improvement in the overall efficiency of thermal cycles. In essence, sCO_2's unique properties position it as a highly advantageous fluid, particularly in power generation, offering benefits such as size reduction, improved flow characteristics, and enhanced efficiency in thermal cycles [18].

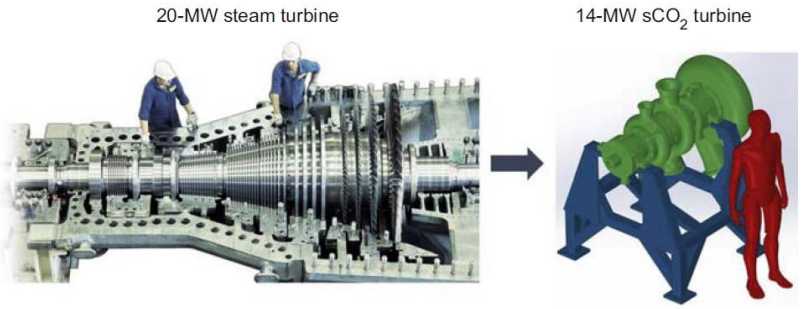

Figure 8. Size comparison of steam turbine and sCO_2 turbine [8].

The unique properties of sCO_2 come with the real gas behaviour of the fluid, which requires the suitable EoS and computational tools. Li [5], categorizes the EoSs into general and specialized EoSs. General EoSs have broader applicability, covering a diverse array of substances and conditions. These are typically categorized into two subgroups: simple structure equations and complex structure equations and they are mostly covered in the RGTM Library of LTT|NTUA [19]. Specialized EoSs are formulations designed to forecast properties specific to certain elements, compounds, or mixtures within specified conditions. These equations remain applicable solely within the defined constraints, exemplified by EoSs developed by Span and Wagner [12], which is characterized as the most suitable EoS for CO_2 [11]. Span and Wanger EoS is one EoS among others, which is incorporated into the available commercial software like NIST'S REFPROP [20] and CoolProp [21] which are able to calculate thermodynamic and physical properties of substances at steady-state conditions.

2.3 Power Generation Cycles Integrated With CSP

The previous years, several studies have been carried out examining different cycle configurations ([22] [23], [24], [25]). They focus on different applications and investigate various cycle parameters. Three relevant studies concerning concentrated solar power as the heat source, are described more in detail.

After reviewing previous modeling studies, concerning sCO_2 Brayton cycles configurations and their applications, Neises and Turchi [26], focus on the optimization of three configurations (simple, recompression, and partial cooling) using an effectiveness heat exchanger model. For compressor and turbine, a simple isentropic efficiency model is used and for the pre-cooler, an already developed model. Their main assumptions are relevant to concentrated solar power applications and have to do with the inlet temperature of compressor and turbine, upper pressure, and efficiency. Moreover, they neglect pressure drops in heat exchangers and they optimize pressure ratio for each design case. Those assumptions lead to the calculation of recuperator conductance and cycle thermal efficiency, and it is shown, that for the same conductance and up to 15 MW/K, partial cooling cycle has the best thermal efficiency and recompression cycle circulates the lowest pre-cooler mass. At first sight, partial cooling cycle seems to qualify for CSP

applications, since the temperature differential across the primary heat exchanger is larger, and this lead to lower cost of sensible thermal energy storage systems and more efficient CO_2 receivers.

In their work, van der Westhuizen and Dobson [17], set as main objectives to contribute to the design, optimization, and control of CSP-sCO_2 systems. Their simulation is based on a simple recuperated Brayton cycle, where the heater is a solar receiver. A centrifugal compressor is used, along with a radial inflow turbine, which are not mechanically connected. The heat sink is modelled as a natural cooled finned tube and the recuperator is a counter flow printed-circuit type. For every component of the cycle, the corresponding model is created with certain inputs and outputs. Turbine is modelled first, with a goal of a specified power output which will determine the mass flow rate and temperatures and pressures around turbine. Then, comes the compressor, which is responsible to achieve a pressure at least as high as the pressure at the turbine. Next is the recuperator and finally heat sink and solar receiver, which must be designed so that for certain mass flow and conditions in their entrances, achieve compressor and turbine conditions in their exit. Thermodynamic diagrams are presented as results, in addition to diagrams that concern optimization and control.

Binotti et al. [27] study three different sCO_2 power cycles (Recompression, Partial Cooling and Main Compression Intercooling), in which heat is collected from an elevated temperature solar tower system. After explaining the components of each cycle and mentioning certain details and assumptions, they describe the solar plant which is like the existing Gemasolar plant, and they refer to heat transfer fluid which is KCl-$MgCl_2$. The performance of each cycle is given as a function of turbine inlet temperature and the better results are provided with Main Compression Intercooling cycle, which is selected for a yearly simulation. Further investigation is made on this cycle, to optimize turbomachinery design and examine if the assumptions that were made affect the results.

2.4 Literature Gap and Future Work

Even though CO_2 has been investigated as a working medium for over five decades, it's been the last years that it has aroused the attention of the researchers. White et al. [14] in their review of the current state-of-the-art sCO_2 systems, identifie the future research trends in different parts of a power cycle, such as the turbomachinery, the heat exchanger and the control systems. Specifically, the control systems of the cycle, in combination with the off-design performance prediction and the investigation of similitude models is an upcoming topic studied recently by different researchers ([29], [30], [31]). The final chapter of the thesis is a first approach of the author towards relative studies.

The literature research that the author conducted, concludes that there is a solid background in the modeling of CO_2 and in the analysis of power cycles. Thus, the goal of the current thesis is not to produce an innovative output on those topics. It consists of a preparatory work for future, novel studies.

2.5 Summary

The previous literature review includes papers and studies that work as a guideline for the present Thesis. The two main topics that are being covered in this thesis; properties of sCO_2 and power cycles, have been extensively studied in the global literature, and in an effort to introduce sCO_2 as a working fluid in the Laboratory of Thermal Turbomachines of NTUA, similar work has been carried out, starting with modeling the properties of sCO_2.

3. MODELING OF sCO_2 PROPERTIES

This chapter includes information about the properties of sCO_2 and their calculations. The first step is to model properties with the appropriate Equation of State (EoS). For this reason, it is examined whether the available models offered by the RGTM library from LTT|NTUA, are able to capture the real gas behavior of sCO_2. After it is figured out which is the best EoS that RGTM offers for sCO_2, it is compared with REFPROP's database to calculate the relative error. Then, there is a brief description of the EoS that REFPROP utilizes, and an introduction to CoolProp's library, which will be used for further calculations. In the second part of this chapter, the properties of sCO_2 around critical point are presented, to depict its particularities. Finally, it is shown why a compression process near the critical point is preferred.

3.1 Equations of State

To describe the thermodynamic properties of a fluid, an Equation of State (EoS) is required. It consists of a relationship between state variables, such that specification of two state variables permits the calculation of the others. State variables may differ from one scientific field to the other; usually, in fluid dynamics, pressure, temperature, and density are the main variables since they appear in the equation of motion [26]. For a certain range of temperatures and pressures, e.g., high temperatures and low pressures, the properties of a fluid, can be calculated from the EoS for the ideal gases, which can be written as:

$$p v_m = R_g T \tag{3.1}$$

where p is pressure, v_m is molar volume, R_g is the universal gas constant with R_g = 8.31451 J mol^{-1}, and T is temperature.

However, modern applications, take place in a wide range of temperatures and pressures, in which the fluid deviates from the ideal behavior. For this reason, many real gas models and their EoS have been developed through the years. The first attempt to approach the real gas behavior, was made by van der Waals in his 1873 Ph.D. thesis [27], who provided the well-known formula:

$$p = \frac{R_g T}{v - b} - \frac{a}{v^2} \tag{3.2}$$

Parameters a and b can be either estimated from the critical point and considered constants for every substance or be a function of temperature. The simplicity of the equation provided scientist with enough space, to develop more complex EoS and get better results, depending on the application.

When it comes to CO_2 as the working fluid, a recent comparison of EoS was made by Böttcher et al [11]. They included van der Waals-type EoS, like the Peng & Robinson EoS (PR-EoS, 1976) and Duan-Møller-Weare (DMW-EoS, 1992) in addition to Span and Wanger EoS (SW-EoS, 1996) and ideal gas EoS. It was shown that the complexity of the model goes along with its accuracy, and they declare Span and Wanger as the most accurate EoS. In his Master's Thesis [5], Hailong Li utilizes a modified Redlich and Kwong EoS (RK EoS, 1949) to approach better gaseous CO_2 and mixtures of CO_2 and H_2O. The original equation for RK model is given by the formula:

$$p = \frac{R_g T}{v - b} - \frac{a}{v(v + b)\sqrt{T_r}} \tag{3.3}$$

Where $T_r = T/T_{cr}$ is the reduced temperature and a and b are the model's constants determined by the behavior of a substance at its critical point. These are given by [19]:

$$a = 0.42747 \frac{R_g^2 T_c^2}{P_{cr}}, \qquad b = 0.08664 \frac{R_g T_{cr}}{P_{cr}} \tag{3.4}$$

The goal of this research is to depict the temperature entropy diagram for CO_2 near the critical point (**Figure 9**), which is presented in Sandia's Report [28] at page 22. This will certify that the computational tools that will be used for the calculations of properties are sufficient. To do so, different EoS will be tested to examine the accuracy of the results that they provide for sCO_2. The first part of the study is to find out if the EoS that the RGTM library -created by LTT|NTUA- provides with, capture satisfactorily the real gas behavior of sCO_2. If not, the second part of the study will be applied, which is the implementation of specialized EoS, such as Span and Wanger for the rest of this thesis.

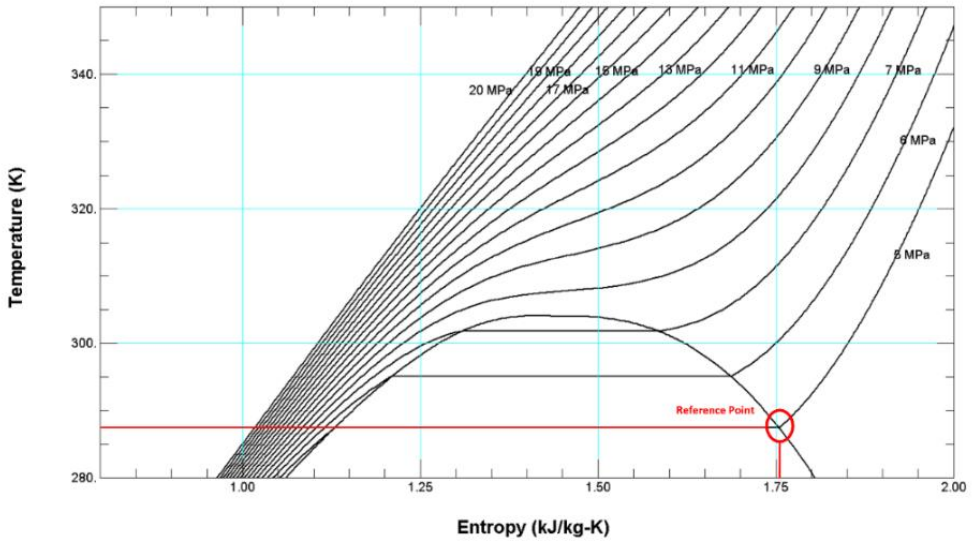

Figure 9. Temperature entropy diagram for CO_2 near the critical point [28].

3.2 Development of Calculation Tools

To calculate the real gas behavior, a PROOSIS library named RGTM is used, created, and provided by LTT|NTUA, which includes eight state models for estimating system fluid and thermodynamic properties [19]. Moreover, for the saturation curve of CO_2, data was taken from NIST [29], inserted in PROOSIS and interpolated linearly to form the curve. RGTM library could not calculate the saturation curve for the CO_2 accurately, so the data taken from NIST was implemented especially for this study by the author. Among the EoS, which are previously assessed for CO_2, RGTM incorporates van der Waals EoS and Redlich and Kwong EoS. For those models, a temperature entropy diagram is printed, to examine how close they are to Sandia's diagram. The comparison is shown in **Figure 10** for van der Waals EoS and in **Figure 11** for RK EoS. A graphical process was used, through which it was possible to define the specific entropy reference and calibrate the diagrams, since they were produced from different sources. The reference for this process, was the known intersection point of saturation curve and isobaric line of 5 MPa, as indicated with red in **Figure 9**.

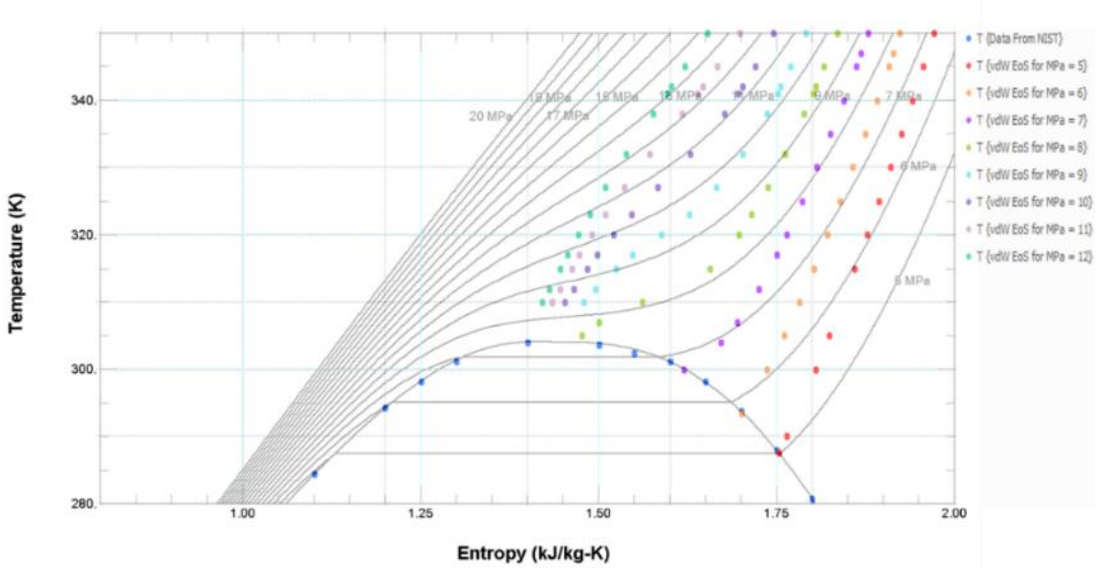

Figure 10. Temperature entropy diagram for CO_2 near the critical point (Solid line) and the diagram produced using van der Waals EoS (Dots).

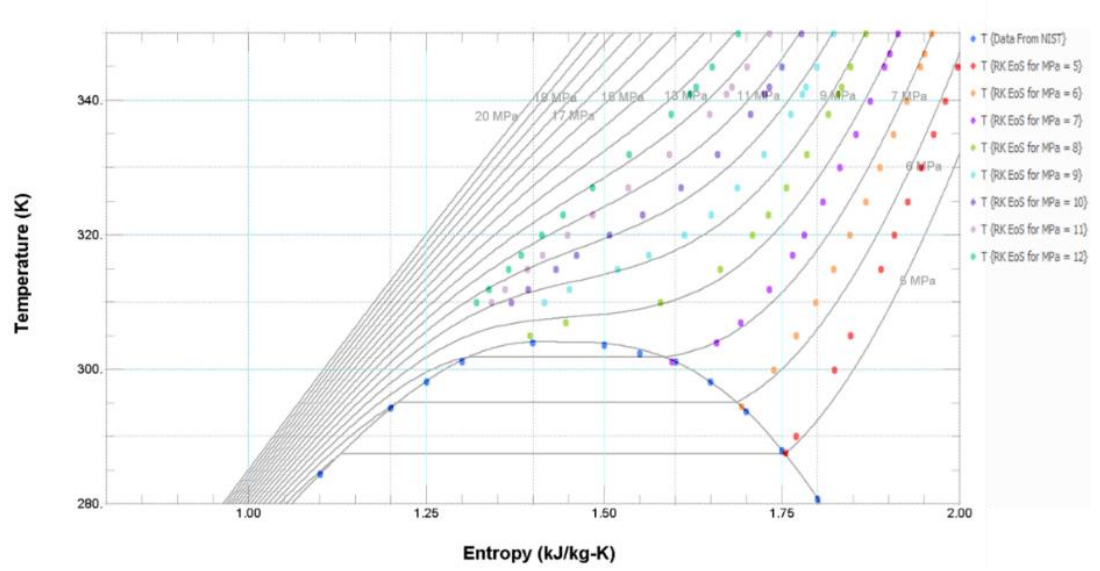

Figure 11. Temperature entropy diagram for CO_2 near the critical point (Solid line) and the diagram produced using Redlich-Kwong EoS (Dots).

The comparison reveals better results with the more complex RK EoS, but they are not satisfactorily. In addition, the accuracy of every other EoS that the RGTM library includes was examined through the same process, and only Berthelot EoS appeared to be competitive. For this reason, Berthelot EoS will undergo further investigation.

3.2.1 Berthelot Equation of State

Twenty-seven years after van der Waals equation was released, an improved version of the equation was published, by the French scientist Daniel Berthelot, who made the term a/v^2 a function of the temperature. His study concludes to the following formula:

$$p = \frac{R_g T}{v - b} - \frac{a}{v^2 T} \tag{3.5}$$

Variables a and b have the same formula as van der Waals equation, and they can be written as [19]:

$$a = \frac{27 R_g^3 T_c^3}{64 P_{cr}}, \qquad b = \frac{R_g T_{cr}}{8 P_{cr}} \tag{3.6}$$

The previous equations are utilized by RGTM library, and **Figure 12** can be created. The results are now much closer to Sandia's diagram, and for this reason, Berthelot EoS is qualified to be evaluated in a wider range of temperatures and pressures.

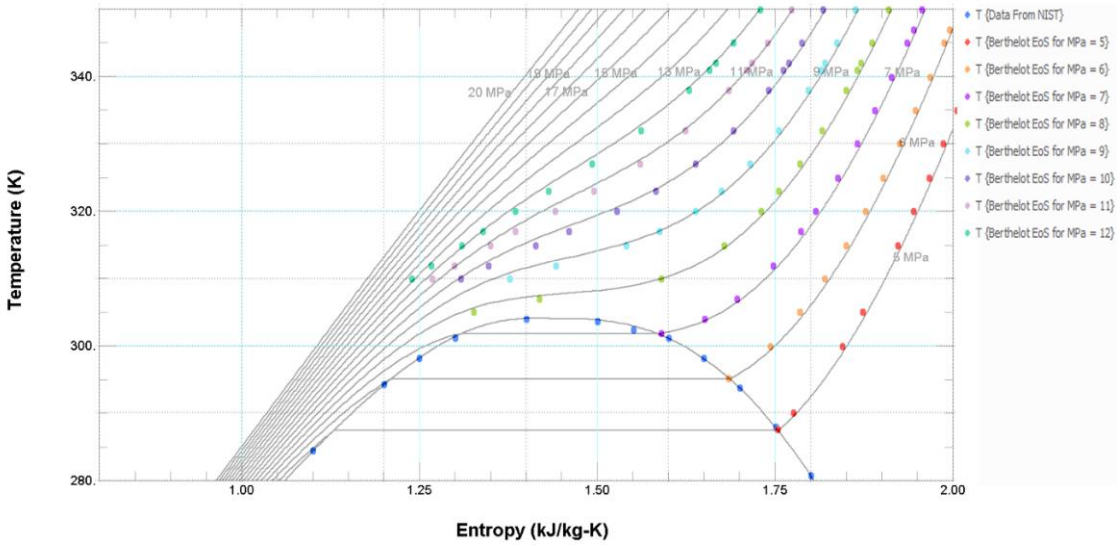

Figure 12. Temperature entropy diagram for CO_2 near the critical point (Solid line) and the diagram that occurs using Berthelot EoS (Dots).

In their work, Kurz et al. [30] set the limits of pressure range for carbon capture and sequestration. Specifically, CO_2 becomes available at low pressures, which can vary near atmospheric. The ultimate pressure requirements for sequestration, is a function of the depth of the sequestration site, and for very deep formations it can lead to pressures above 50 MPa. Moreover, in a recuperated cycle integrated with CSP [17], which will be the topic for a next section, the highest temperature is around 825K. Even though some

applications operate in more extreme conditions, the boundaries that were considered are sufficient for the initial comparison.

Considering those applications, it is reasonable to examine whether Berthelot EoS provides with satisfactory results in a temperature range from 225 to 850 K and pressure range from 0.1 to 40 MPa. For this reason, the values of specific entropy and enthalpy obtained by Berthelot's EoS were directly compared to those from mini-REFPROP [20], which is a free sample version of the full REFPROP program provided by NIST. The relative error, which is the contour in the following figures, is given by the equation:

$$RelError\% = 100\frac{|X_{REFPROP} - X_{Berthelot}|}{X_{REFPROP}} \tag{3.7}$$

The representation of specific entropy error is presented in **Figure 13**.

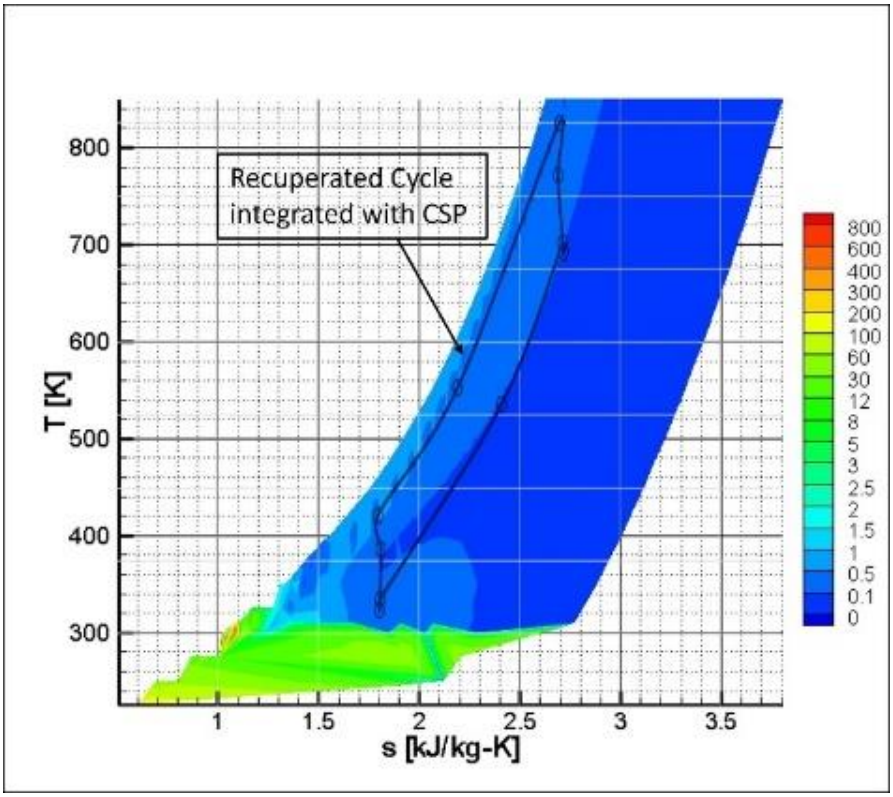

Figure 13. Relative error of specific entropy in a T-s diagram and the recuperated cycle of a CSP application.

A zoomed-in representation is shown in **Figure 14**, focusing on the area where the error seems to rise.

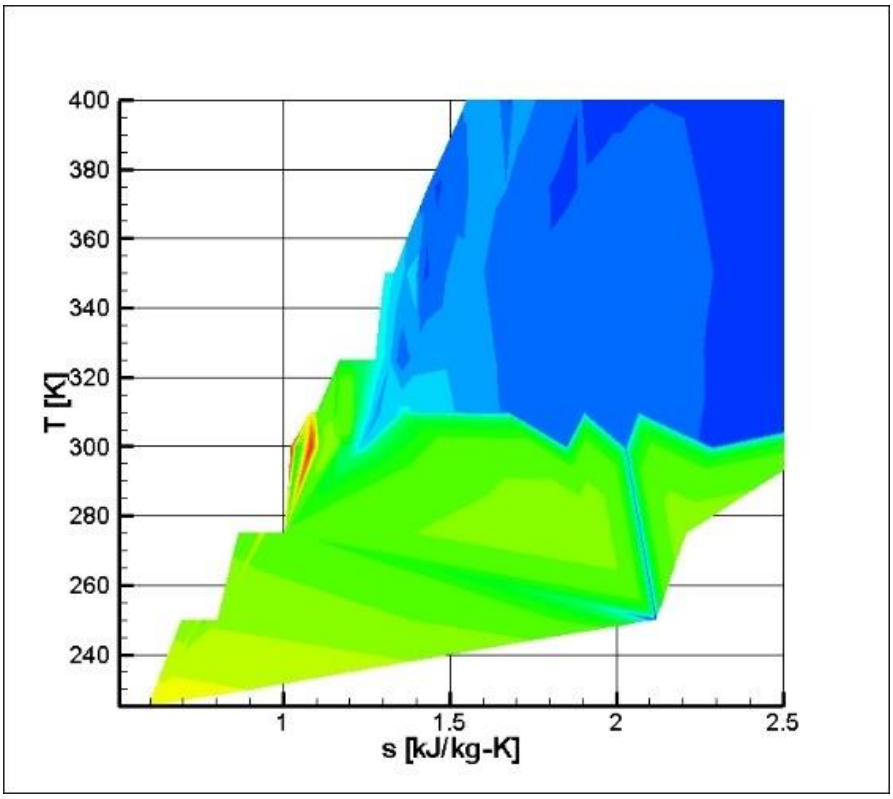

Figure 14. Zoomed-in relative error of specific entropy.

Figure 14 demonstrates the incapability of Berthelot EoS to capture the entropy of CO_2 at low temperatures, below critical point. However, in this thesis, we are interested in supercritical applications of CO_2. The accuracy of Berthelot's EoS in supercritical region, is considered as sufficient, if we exclude big values of pressure, i.e. above 13 MPa, close to critical temperature. This would be a problem if we were studying transcritical cycles, where, for instance, the outlet of the compressor was close to those points.

The same process is conducted for specific enthalpy. After calibrating the enthalpy reference between RGTM library and REFPROP's dataset, the relative error is calculated and represented in **Figure 15**.

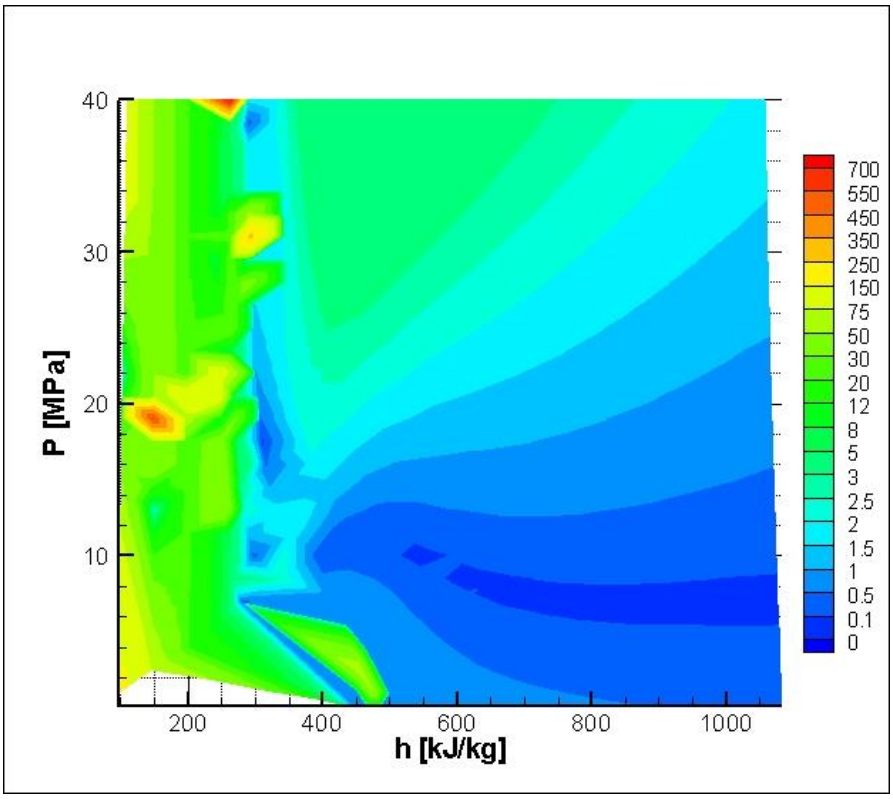

Figure 15. Relative error of specific enthalpy in a P-h diagram.

In general, it appears that enthalpy has a larger relative inaccuracy than entropy. This could be a reason why many researchers ([4], [30]) suggest Span and Wanger EoS for pure CO_2. This model, focuses specifically on CO_2, is highly accurate and correlates well with experimental data. This is also the model used by NIST to reproduce the properties of CO_2. For this reason, Span and Wanger EoS is preferred in this thesis for the upcoming calculations.

3.2.2 Span and Wanger Equation of State

Considering the great interest in the properties of CO_2 and the need for more accurate correlations for their calculation, Span and Wanger propose a new equation of state, specifically for CO_2, which is expressed in form of a dimensionless Helmholtz energy a_H. This, consists of the ideal-gas a_H^0 behavior and a part which considers the residual fluid behavior a_H^r, namely:

$$\varphi_H(\delta,\tau) = a_H^r(\delta,\tau) + a_H^0(\delta,\tau) \tag{3.8}$$

Where $\delta = \rho/\rho_c$ is the reduced density and $\tau = T_c/T$ is the inverse reduced temperature.

By considering Helmholtz energy as a fundamental equation which is a function of temperature and density, all the other thermodynamic properties can be obtained as a

function of Helmholtz energy and its derivatives, as presented in [12]. To obtain the ideal-gas term, authors follow an analytical approach, apart from c_p^o, which has been established by a nonlinear fitting in existing data. They get:

$$a_H^0(\delta,\tau) = \ln(\delta) + \beta_1^o + \beta_2^o\tau + \beta_3^o \ln(\tau) + \sum_{i=4}^{8} \beta_i^o \ln\left(1 - exp(-\tau\theta_i^o)\right) \tag{3.9}$$

where the coefficients β_i^o and θ_i^o are coming from the expression of c_p^o.

An analytical approach cannot be applied on the residual part of the equation. For this reason, they propose a complicated procedure which includes optimization and fitting to wide variety of experimental results, out of which the following empirical equation is determined:

$$a_H^r(\delta,\tau) = \sum_{i=1}^{7} n_i \delta^{d_i}\tau^{t_i} + \sum_{i=8}^{34} n_i \delta^{d_i}\tau^{t_i} e^{-\delta c_i} + \sum_{i=35}^{39} n_i \delta^{d_i}\tau^{t_i} e^{\left[-alpha_i(\delta-\varepsilon_i)^2-\beta_i(\tau-\gamma_i)^2\right]}$$

$$+ \sum_{i=40}^{42} n_i \Delta^{b_i}\delta e^{\left[-C_i(\delta-1)^2-D_i(\tau-1)^2\right]} \tag{3.10}$$

For further explanations, reader should advise [12].

3.2.3 CoolProp Package

CoolProp [21] is an open-source library of thermodynamic properties, which is based on high accuracy EoS for each one of its working fluids (Span and Wanger EoS for CO_2), to calculate their thermodynamic and transport properties. Many wrappers have been developed that allow the use of CoolProp with many software and programming languages, including MATLAB, Python and Excel. Moreover, CoolProp is a cross-platform and can be used in every operating system. The Laboratory of Thermal Turbomachines, took advantage of its compatibility and utilized its publicly available static libraries, aiming for the cooperation with PROOSIS environment. This allows to calculate a property by calling the following function:

$$PropsSI(STRING\ output, STRING\ Name1, REAL\ Value1, STRING\ Name2, REAL\ Value2, STRING\ Ref)$$

A pair of known thermodynamic properties is required to calculate all the others. The properties that were calculated in this thesis are mainly Temperature T, Pressure P, Enthalpy h and Entropy s. They can be calculated from the following equations:

$$T = \begin{cases} PropsSI("T", "P", \mathrm{P}, "H", \mathrm{h}, "CO2") \\ PropsSI("T", "P", \mathrm{P}, "S", \mathrm{s}, "CO2") \\ PropsSI("T", "H", \mathrm{h}, "S", \mathrm{s}, "CO2") \end{cases} \quad P = \begin{cases} PropsSI("P", "T", \mathrm{T}, "H", \mathrm{h}, "CO2") \\ PropsSI("T", "T", \mathrm{T}, "S", \mathrm{s}, "CO2") \\ PropsSI("P", "H", \mathrm{h}, "S", \mathrm{s}, "CO2") \end{cases}$$

$$h = \begin{cases} PropsSI("H", "T", \mathrm{T}, "P", \mathrm{P}, "CO2") \\ PropsSI("H", "T", \mathrm{T}, "S", \mathrm{s}, "CO2") \\ PropsSI("H", "P", \mathrm{P}, "S", \mathrm{s}, "CO2") \end{cases} \quad s = \begin{cases} PropsSI("S", "P", \mathrm{P}, "T", \mathrm{T}, "CO2") \\ PropsSI("S", "P", \mathrm{P}, "H", \mathrm{h}, "CO2") \\ PropsSI("S", "T", \mathrm{T}, "H", \mathrm{h}, "CO2") \end{cases}$$

For example, to calculate enthalpy H of CO_2 at temperature T of 298 K and a pressure P of 101325 Pa, we type:

$$h = PropsSI("H", \mathrm{T}, 298, \mathrm{P}, 101325, \mathrm{CO2}) \tag{3.11}$$

This allows us to calculate every property directly from PROOSIS, which is what RGTM library does but for more inaccurate EoS.

3.3 CO_2 Properties

3.3.1 Thermodynamic Behavior of Supercritical CO_2

In an analogous way as Nikolai et al. [9] did, in this section some of the properties discussed in the previous section are presented, through several diagrams. Those diagrams aim to visualize the particularities around the region of critical point and point out some of the reasons why CO_2 is preferred as working fluid. All data was taken from mini-REFPROP's external database, which is based on Span and Wanger EoS, and introduced in Microsoft Excel to reproduce the following figures.

In **Figure 16** and **Figure 17**, we observe an expected sharp spikes in the specific isochoric and isobaric heat capacities around critical point, which exemplify the strong real gas behavior of sCO_2. Moreover, the fluid's ability to absorb more energy without raising its temperature, near the critical point, can be further illustrated by using its specific heat capacity.

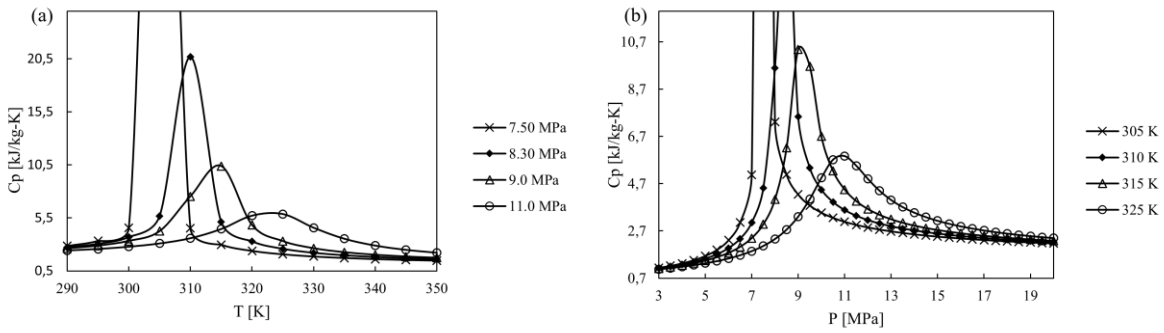

Figure 16. (a) C_p - T diagram for constant pressures; (b) C_p - P diagram for constant temperature.

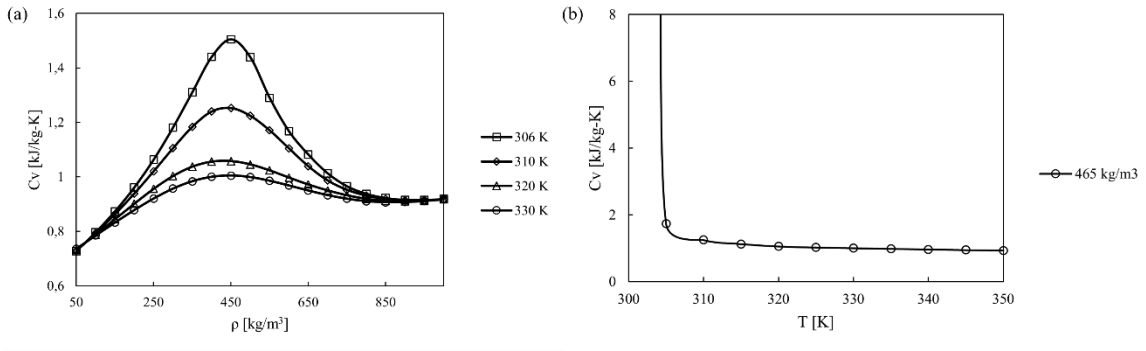

Figure 17. (a) C_v - ρ diagram for constant temperatures; (b) C_v - T diagram for a constant density near the critical value.

In addition, there are other physical properties which have an intense change near the critical point and require attention. More specifically, density presented in **Figure 18**, which is highly connected with the machinery, may affect the components or the operating conditions. Moreover, large variations in density lead to large variation in flow velocity and Reynolds number.

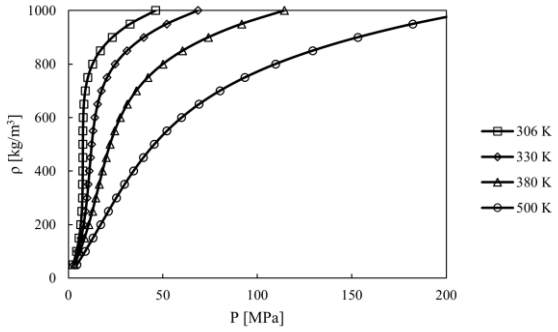

Figure 18. ρ - P diagram for constant temperatures.

Finally, the speed of sound, would be expected to be proportional to the square root of temperature, as is in the case of the air. However, for carbon dioxide in the critical region, speed of sound is significantly affected by the operating density as presented in **Figure 19**. It should be noted that Mach number is determined by the speed of sound, a fact that must be taken into consideration for the turbomachinery design.

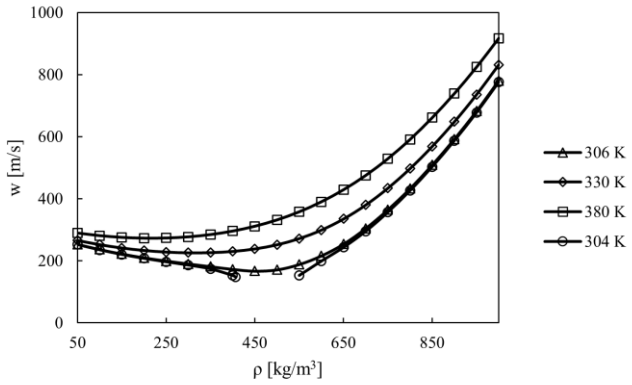

Figure 19. w - ρ diagram for constant temperatures.

3.3.2 Compression Process Around Critical Point

Because of its near-critical thermodynamic properties, using sCO_2 as the working fluid in a supercritical power cycle is generally associated with improved cycle performance. The process which takes place near the critical point is the compression, and for this reason, it requires bigger attention and deeper analysis.

To study a compression process near critical point, a parametric study was carried out in PROOSIS environment. The equations that were used for the creation of **Figure 20** will be described later. The inlet temperature varies in a range from 290 to 320 K, for 5 different pressures, around the critical for case a and for case b, the inlet pressure varies in a range from 6.5 to 10 MPa, for 4 different temperatures. For every case, the isentropic efficiency was set to 0.85 and the pressure ratio to 2.5.

In **Figure 20**, we observe rapid changes in outlet temperature, when the inlet conditions of the compressor are close to the critical point. Those changes exist due to the rapid changes in specific heat for slight changes in temperature and pressure, and for this reason compression work with minimal work input is achieved. The process gets smoother when working on supercritical region.

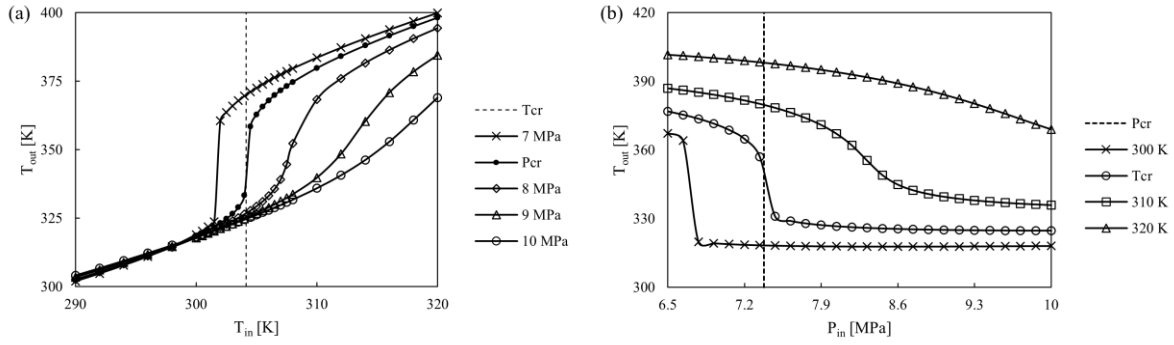

Figure 20. Compression process around critical point.

The specific work for an isentropic compression is demonstrated in a T-s diagram in **Figure 21**. The relative area is prefered. The low work of the compression, can be also justified from a T-h diagram, where the isobars have a low slope near the critical point. This practicly means that the energy can be added to the fluid with a little increase in its temperature.

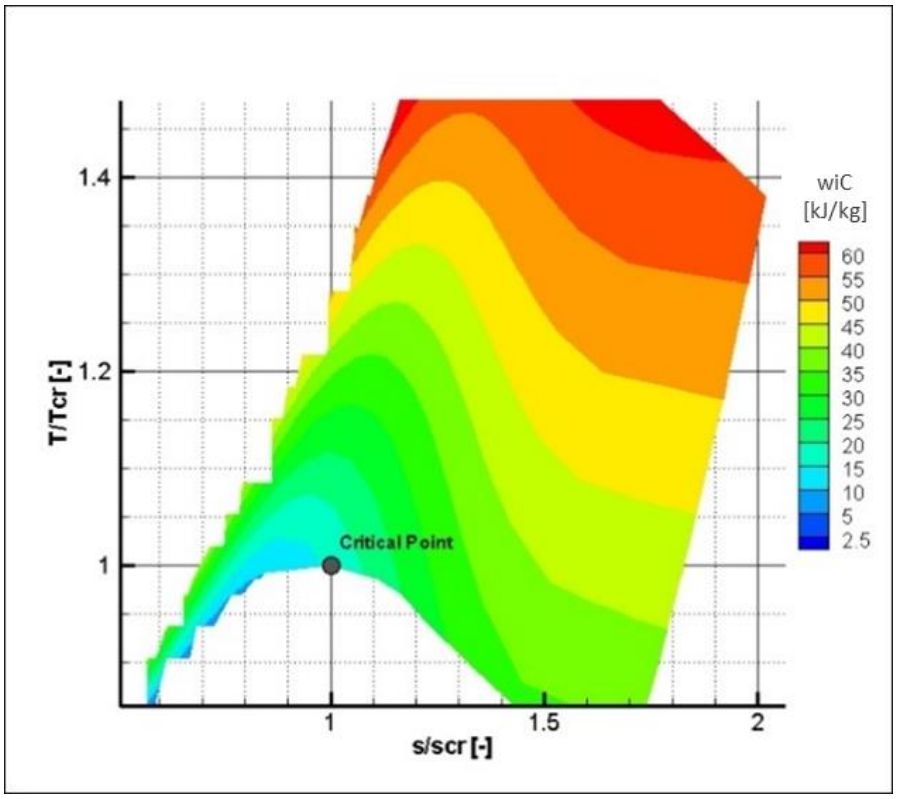

Figure 21. Specific work for an isentropic compression (PR = 2).

3.4 Summary

In summary, the thermodynamic properties of CO_2 in the supercritical region introduce certain particularities, which even though they add complexity and make the calculations harder, they offer a distinct advantage when it comes to compress the fluid near the critical point, since the compression process requires less work. By utilizing the proper EoS, the real gas behavior of sCO_2 can be captured in a sufficient way, without introducing big errors and deviations to the calculations. It was proven that obsolete and simpler EoS are not sufficient for the desired calculations (vdW EoS and RK EoS) while other (Berthelot EoS) could potentially consist of a mediocre solution. As the global literature suggest, the specialized Span and Wanger EoS is the optimum EoS for relevant calculations, and for this reason, it was introduced in PROOSIS in a way that it can be used for future calculations of the thermodynamic properties.

4. THEORETICAL BACKGROUND FOR CYCLE CALCULATIONS[1]

This chapter covers fundamental heat transmission, fluid dynamic relationships, and the balances of energy and entropy. Moreover, it clarifies where should be paid attention in the case of sCO_2. It begins with the explanation of terms such as heat engine, open and closed thermodynamic system and goes on with the equations that are needed to describe a thermodynamic cycle, focusing on the components that make it up.

4.1 Introduction

The relationships that will be discussed, are based on the laws of thermodynamics. The first law states that the energy is conserved, while the second law indicates that heat engines must reject a portion of the heat received to a lower temperature heat sink. Heat engines are thermodynamic systems that converts heat to usable energy, and a typical example is shown in **Figure 22**. A heat sink is typically an environmental component, such as the atmosphere. Instead of releasing the heat to the environment, it can also be utilized in a lower temperature heat engine. Later on Chapter 5, heat sink will be referred to as the precooler.

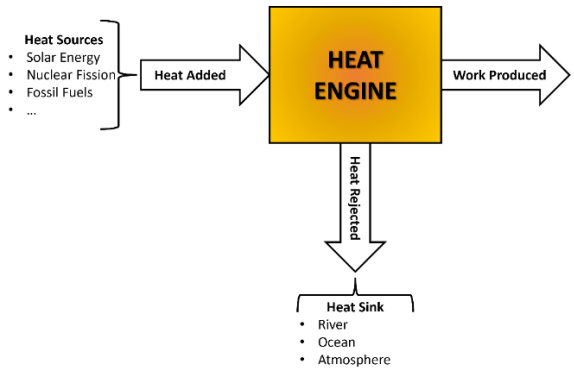

Figure 22. Example of a thermodynamic heat engine.

[1] The structure and the form of equation of this chapter, is based on Chapter 3 of [8].

The heat engine presented in **Figure 22** is considered a closed system, since it does not allow transfer of matter in or out of the system. On the other hand, turbines and compressors that will be discussed later on Chapter 5, are examples of open systems since they allow the passage of fluid through their boundaries. An example of an open thermodynamic system is shown in **Figure 23**.

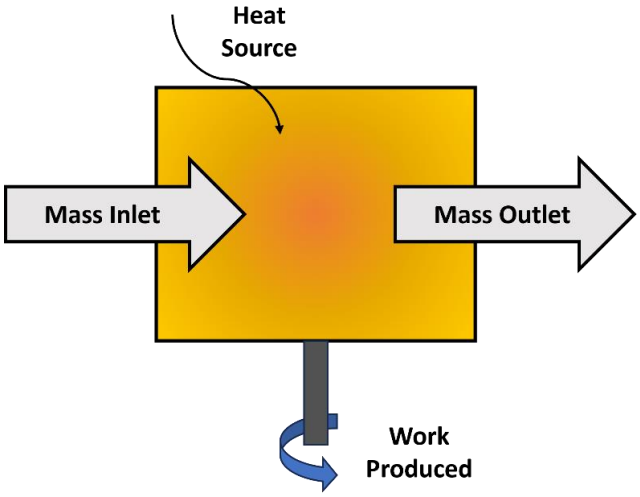

Figure 23. Example of a thermodynamic open system.

The processes that make up a heat engine cycle include compression, heat addition, expansion and waste heat rejection. Those processes are represented in Chapter 5 by a compressor, a heater, a turbine and a precooler, respectively. The simplest configuration that they can produce, is a closed Brayton cycle, as presented in **Figure 24**.

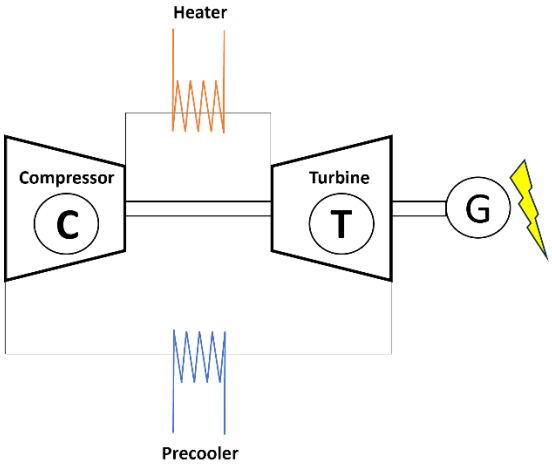

Figure 24. Closed Brayton cycle, in its simplest version.

In an effort to increase the effectiveness (the quantity of work generated for a specific heat input), the cycle might significantly increase in complexity and incorporate several intermediary steps, as it will be discussed later. However, a heat engine must always comprise the essential features of a heat supply and heat rejection and the efficiency must be below that of the ideal Carnot cycle.

4.2 Mass Energy and Entropy Equations

4.2.1 Conservation of Mass

For the open system presented in **Figure 23**, mass conservation can be described as:

$$[Inlet\ Mass\ Flow\ rate] - [Outlet\ Mass\ Flow\ rate] = [Mass\ Variation\ During\ Time]$$

or in a mathematical way:

$$\sum_{in} \dot{m} - \sum_{out} \dot{m} = \frac{dm}{dt} \tag{4.1}$$

where $\dot{m}$ is the mass flow rate and m is the mass of the system. For a given density, fluid velocity and flow area, mass flow rate can be calculated by:

$$\dot{m} = \rho V A \tag{4.2}$$

4.2.2 Conservation of Energy

As it was previously stated, by the first law of thermodynamics, the total quantity of energy is conserved. For an open and transient system, this statement can be described as:

$$\begin{bmatrix} The\ net\ heat \\ transfer \\ rate \end{bmatrix} - \begin{bmatrix} System's \\ generated \\ power \end{bmatrix} + \begin{bmatrix} The\ net\ rate\ energy \\ is\ introduced\ the\ system \\ through\ mass\ flow \end{bmatrix} = \begin{bmatrix} The\ overall\ rate \\ of\ energy \\ alteration\ within \\ the\ system \end{bmatrix}$$

or in a mathematical way:

$$\dot{Q} - \dot{W}_{shaft} - P\frac{dV}{dt} + \sum_{in} \dot{m}\,(h + pe + ke) - \sum_{out} m(h + \dot{pe} + ke) =$$

$$= \frac{d}{dt} m(u + pe + ke) \tag{4.3}$$

The term $P\frac{dV}{dt}$ is the rate of boundary work, and in combination with the shaft power $\dot{W}_{shaft}$, consist of the power produced by the system. For steady state conditions and for system that have rigid boundaries, boundary work is zero. The associated energy that the flow streams carries is:

$$e = u + pe + ke \tag{4.4}$$

Streams entering the system perform flow work on the stream at a rate of $\dot{m}pv$ ant the system performs flow work on exiting streams. Substituting the definition of enthalpy results in the mathematical expression of the first law of thermodynamics.

If we consider a steady state flow, derivatives of time are considered as zero, so there is no boundary work and energy storage. Eq. (4.3) can be simplified to:

$$\dot{Q} - \dot{W}_{shaft} = \sum_{out} \dot{m}\,(h + pe + ke) - \sum_{in} \dot{m}\,(h + pe + ke) \tag{4.5}$$

And since potential and kinetic energies are considered as negligible at the component level in a power plant analysis, the previous can be simplified in:

$$Q - W = \Delta h \tag{4.6}$$

For this final equation, a single inlet and outlet port is considered, so that the dots can be eliminated.

To quantify the performance of a component, we can use the first law of efficiency, which is an energy ratio:

$$\eta = \frac{Energy\ Output}{Energy\ Supplied} \tag{4.7}$$

And specifically for heat engines, thermal efficiency can be defined as:

$$\eta_{th} = \frac{w_{net}}{q_{added}} = 1 - \frac{q_{rejected}}{q_{added}} \tag{4.8}$$

4.2.3 Entropy and the Second Law of Thermodynamics

The second law of thermodynamics implies the irreversibility of certain processes, like heat moving from high to low temperatures. This principle is reflected in two equivalent statements: the Kelvin-Plank statement, stating the impossibility of constructing a cyclic device converting heat from a single thermal reservoir entirely into work, and the Clausius statement, asserting the impossibility of creating a cycle that only transfers heat from a low-temperature reservoir to a higher one without affecting the environment. Both

statements are derived from the principle of increasing entropy, which ensures that the total entropy change in any process is always greater than or equal to zero.

$$\Delta S|_{Total} \geq 0 \tag{4.9}$$

The term "total" suggests that entropy in a system can decrease as heat is transferred out, but the rise in entropy outside the system surpasses the reduction within it. In a physical sense, entropy quantifies the energy unavailable for work production. Usable work and mechanical energy lack associated entropy, making any entropy-generating process irreversible.

Entropy is formally defined as the integral of the added heat divided by the absolute temperature along any internally reversible path connecting two states as:

$$\Delta S = \int \frac{\delta Q}{T} \tag{4.10}$$

And for an isothermal system:

$$\Delta S = \frac{Q}{T} \tag{4.11}$$

The entropy balance of a system, can be described as:

$$\begin{bmatrix} The\ net\ rate\ at \\ which\ entropy\ is \\ transported \\ through \\ heat\ tranfer \end{bmatrix} + \begin{bmatrix} Entropy's \\ Generation \\ Rate \end{bmatrix} + \begin{bmatrix} The\ net\ influx\ rate \\ of\ entropy\ through \\ mass\ flows \end{bmatrix} = \begin{bmatrix} The\ overall\ rate \\ of\ entropy \\ alteration \\ within \\ the\ system \end{bmatrix}$$

Or in a mathematical way:

$$\sum_i \frac{\dot{Q}_i}{T_i} + \dot{S}_{gen} + \sum_{in} \dot{m}\, s - \sum_{out} \dot{m} s = \frac{dS}{dt} m \tag{4.12}$$

Where T_i is the temperature at the system boundary. For a single port system, at steady state conditions, the entropy balance can be written as:

$$s_{gen} = s_2 - s_1 - \frac{q}{T}\Big|_{Boundary} \tag{4.13}$$

Since the second thermodynamic law states that the entropy increases, the maximum thermal efficiency is limited by Carnot efficiency:

$$\eta_{Carnot} = 1 - \frac{T_{cold}}{T_{hot}} \tag{4.14}$$

4.3 Components of a Power Cycle

4.3.1 Compressor and Turbine

The equations that were discussed previously, will be applied on the components which a power cycle consists of. To begin with, the energy balance for a compressor presented in **Figure 25**, is:

$$w_{iC} = h_2 - h_1 = f(T_2, p_2) - f(T_1, p_1) < 0 \tag{4.15}$$

It needs to be mentioned that the calculation of enthalpy and every other property, is a function of two state variables, for example temperature and pressure. This is obligatory, since sCO_2 behaves as a real gas in its supercritical region, and a consideration that enthalpy is solely a function of temperature, as is in ideal gases, will lead to huge deviations.

Moreover, if we assume that there are no bleeds in between, mass flow rate remains the same:

$$\dot{m}_{inlet} = \dot{m}_{outlet} \tag{4.16}$$

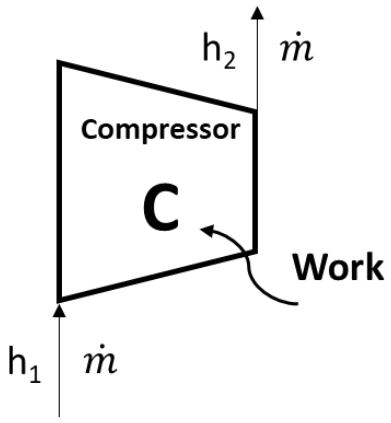

Figure 25. Inlet and outlet of a compressor.

By considering an efficiency rate for the compression process, we can correlate the inlet and the outlet value of enthalpy. Isentropic efficiency, which compares the actual work of a real process with the corresponding work of an isentropic process, allows us to do so. The difference between those processes, is depicted in **Figure 28**. The isentropic efficiency is defined as:

$$\eta_{c,is} = \frac{h_{2is} - h_1}{h_2 - h_1} = f(T, p) \tag{4.17}$$

The assumption that isentropic efficiency is a function of temperatures and pressure ratio is not sufficient when the working fluid behaves as a real gas. For this reason, the previous definition is used, where the enthalpies are a function of temperature and pressure, covering the real gas case.

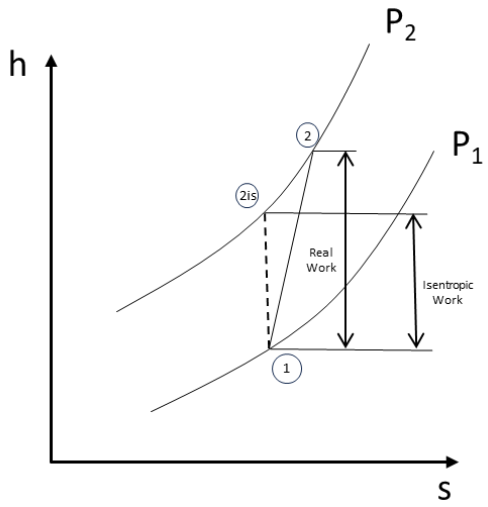

Figure 26. h-s diagram of a compression process. 1-2 is the real process while 1-2is is the ideal-isentropic process.

In a similar way, for a turbine presented in **Figure 27**, the energy balance is:

$$w_{iT} = h_1 - h_2 = f(T_1, p_1) - f(T_2, p_2) > 0 \tag{4.18}$$

As in case of the compressor, the calculation of enthalpy is a function of two state variables: temperature and pressure. This is obligatory, since sCO_2 behaves as a real gas in its supercritical region, and a consideration that enthalpy is solely a function of temperature, as is in ideal gases, will lead to huge deviations.

Moreover, if we assume that there are no bleeds in between, mass flow rate remains the same:

$$\dot{m}_{inlet} = \dot{m}_{outlet} \tag{4.19}$$

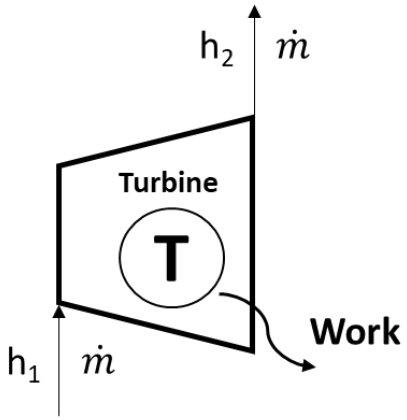

Figure 27. Inlet and outlet of a turbine.

The isentropic efficiency for the turbine is:

$$\eta_{T,is} = \frac{h_1 - h_2}{h_1 - h_{2is}} = f(T, p) \tag{4.20}$$

The assumption that isentropic efficiency is a function of temperatures and pressure ratio is not sufficient when the working fluid behaves as a real gas. For this reason, the previous definition is used, where the enthalpies are a function of temperature and pressure, covering the real gas case.

And the expansion process is depicted in **Figure 28**.

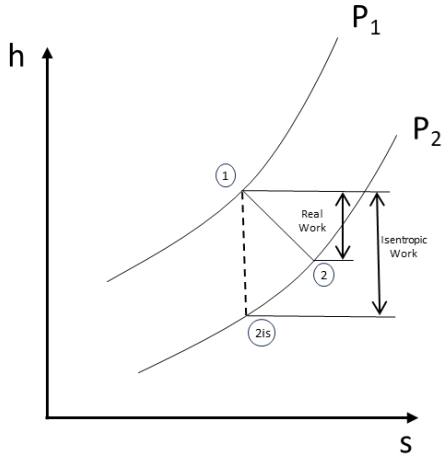

Figure 28. h-s diagram of an expansion process. 1-2 is the real process while 1-2is is the ideal-isentropic process.

4.3.2 Heat Exchangers

The cycles that will be studied in Chapter 5, require heat exchangers in which the two streams are either both part of the cycle, i.e., Recuperators of **Figure 29** , or the stream of the cycle is being cooled or heated by an outside source i.e., Precoolers and Heaters of **Figure 30**.

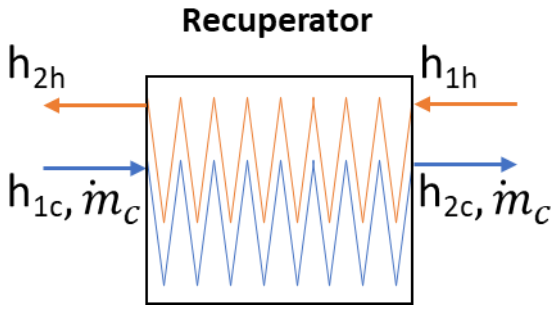

Figure 29. Typical recuperator with hot and cold stream.

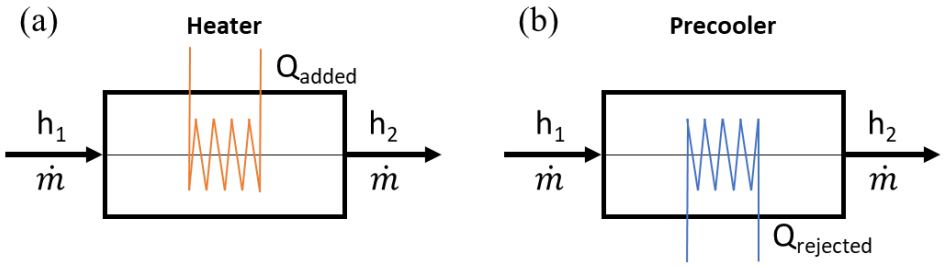

Figure 30. Typical heater (a) and precooler (b).

To begin with the simplest case, when the temperature of the main flow changes due to an outside source (**Figure 30**), the mass flow rate remains the same:

$$\dot{m}_{inlet} = \dot{m}_{outlet} \tag{4.21}$$

From energy balance of the heater:

$$\dot{Q}_{added} = \dot{m}(h_1 - h_2) < 0 \tag{4.22}$$

While for the precooler:

$$\dot{Q}_{rejected} = \dot{m}(h_1 - h_2) > 0 \tag{4.23}$$

In such components, there could also be a user-defined a pressure drop.

In case of recuperators, the mass flow rate of the two streams, remains the same:

$$\dot{m}_{inlet,h} = \dot{m}_{outlet,h} \tag{4.24}$$

$$\dot{m}_{inlet,c} = \dot{m}_{outlet,c} \tag{4.25}$$

And from energy balance assuming that there is no heat loss to the environment:

$$\dot{m}_c(h_{2c} - h_{1c}) = \dot{m}_h(h_{1h} - h_{2h}) \tag{4.26}$$

In this thesis, except from Section **5.5**, and for simplicity reasons, the effectiveness of the recuperators is defined as:

$$\varepsilon = \frac{T_{2c} - T_{1c}}{T_{1h} - T_{1c}} \tag{4.27}$$

4.4 Summary

The thermodynamic analysis of sCO_2 systems components and the relationships that are used to describe the components of a cycle, are based on the fundamental equations of thermodynamics, as they are for other working fluids. However, ideal gas assumptions cannot be made since sCO_2 deviates significantly from the ideal gas behavior. For this reason, every thermodynamic property is a function of other two state variables. The components that were analyzed and their relevant equations, will be used in the following chapter to make up thermodynamic cycles for further investigation.

5. POWER CYCLES INVESTIGATION

The advantages of sCO_2 that were previously discussed, classifying it as a promising working fluid for thermodynamic cycles. In this chapter, different layouts of cycles are investigated. After a short classification of power cycles, the first step of this research is to illustrate the difference on the efficiency of an open cycle if ideal gasses assumptions are made instead of real gasses. Afterwards, the equations that were introduced in the previous chapter, are used to analyze several thermodynamic cycles, in order to examine their performance and carry out several parametric studies. Those studies are based on source codes and schematics that are developed in PROOSIS environment, and their credibility is certified by using data available from literature. The eventual goal of this chapter is to compare the different layouts and examine the characteristics of each configuration.

5.1 Classification of Thermodynamic Power Cycles

Thermodynamic power cycles are categorized here, in a way similar to White et al. [13]. Four basic processes make up a generic thermodynamic power cycle: compression, heat addition at high pressure (p_2), expansion, and heat rejection at low pressure (p_1). The cycle may be classified based on whether phase shift takes place during the cycle. The Joule–Brayton cycle stays in the vapor zone, while the Rankine cycle experiences phase changes in the working fluid as a result of the heat addition and heat rejection processes.

Another way to categorize thermodynamic cycles is based on whether the operating pressures are above or below the working fluid's critical pressure (p_{cr}). This permits the following three classifications: subcritical ($p_1 < p_{cr}$ and $p_2 < p_{cr}$), transcritical ($p_1 < p_{cr}$ and $p_2 > p_{cr}$) and supercritical ($p_1 > p_{cr}$ and $p_2 > p_{cr}$). The previous are summarized in **Figure 31**, where four different cycles are depicted in a T-s diagram.

For every case, the highest temperature of the cycle remains the same, as well as some other cycle parameters shown in **Table 2**. Those cycles, include recuperation and the set of equations which describes them is presented in Section **5.3**. Moreover, it should be noted that the intermediate points of the cycles, are illustrated in a graphical way.

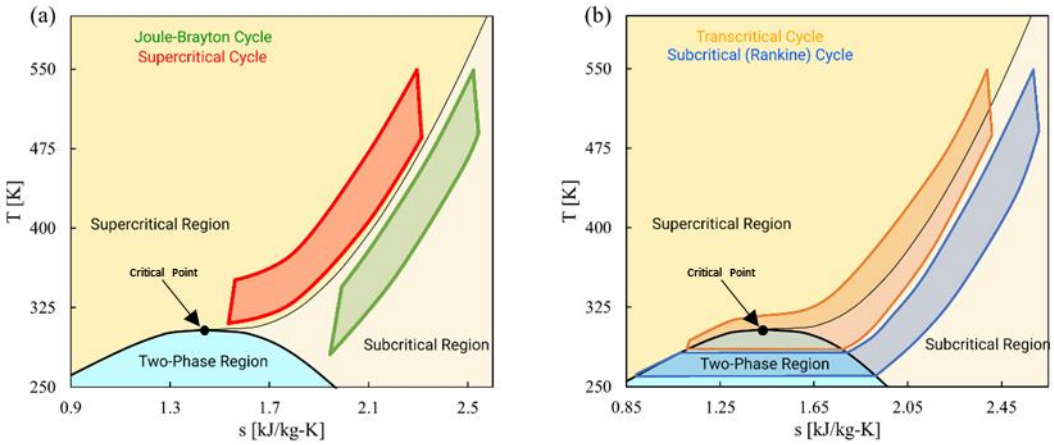

Figure 31. Classification of Thermodynamic Power Cycles; (a) non-Condensed cycles, (b) Condensed Cycles.

Table 2. Parameters of the examined cycles.

T_{high} [K]	η_{cmp} [-]	ε_{recup} [-]	η_{trb} [-]	PR [-]	$\dot{m}$ [kg/sec]
550	0.65	0.85	0.85	2	5

For each one of the four cycles, its efficiency was also calculated. Of course, they cannot be compared directly based on their efficiency, since the efficiency is a function of various parameters, which are not the same for every case. The results can be found in **Table 3**.

Table 3. Efficiency of different power cycles.

Power Cycle Type	Efficiency [%]
Joule-Brayton	10
Supercritical	25
Transcritical	40
Subcritical (Rankine)	53

5.2 Open Cycle Analysis

For a single shaft simple turbojet layout, as it is shown in **Figure 32**, to calculate the open cycle characteristics, the following data are needed.

$$T_0, p_0, K_{in}, \pi_c, \eta_c, K_b, T_{t4}, \eta_m, \eta_t, K_{ex}$$

T_0, p_0 refer to ambient conditions. K_{in}, K_b and K_{ex} are the pressure loss coefficients for inlet duct, burner and exit duct respectively. η_c and η_t represent the efficiency ratios for the compressor and turbine, while η_m is the mechanical efficiency ratio. π_c is the pressure ratio of compressor, and finally, T_{t4} is the total inlet temperature of the turbine.

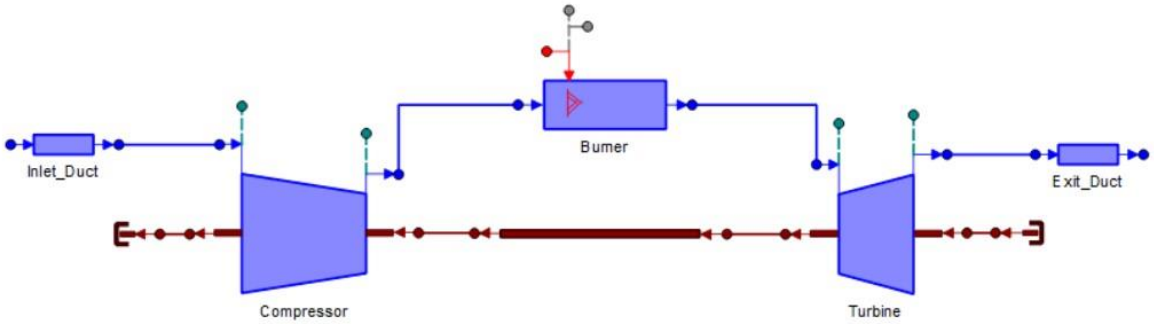

Figure 32. Single shaft turbojet layout.

To begin with the calculations, inlet duct creates a pressure drop, which is described by its coefficient. Thus:

$$T_{t2} = T_{t0} = T_0 \tag{5.1}$$

$$p_{t2} = p_{t1}(1 - K_{in}) = p_0(1 - K_{in}) \tag{5.2}$$

Compressor

For the compressor, we have assumed its pressure ratio, so:

$$p_{t3} = \pi_c p_{t2} \tag{5.3}$$

To calculate its outlet total temperature, it needs to be defined whether the working gas characteristics $(C_p,\ \gamma)$ are considered as constants or they are calculated through real gas model equations. In the simple occasion of constant characteristics, the total temperature is given by:

$$T_{t3} = T_{t2}\left[1 + \frac{1}{\eta_c}\left(\pi_c^{\frac{\gamma-1}{\gamma}} - 1\right)\right] \tag{5.4}$$

and the specific work of compressor is calculated through:

$$w_{iC} = C_{p_3}(T_{t3} - T_{t2}) \tag{5.5}$$

When it comes to real gas models, the conditions before and after the compression process can be defined through the definition of isentropic efficiency. Condition *2* refers to the entry, of the compressor, where T_{t2} and p_{t2} are already known, and so are the specific entropy and enthalpy since:

$$s_{t2} = f(T_{t2}, p_{t2}) = s_{t3,is} \tag{5.6}$$

$$h_{t2} = f(T_{t2}, p_{t2}) \tag{5.7}$$

The known pressure p_{t3} and specific entropy $s_{t3,is}$, allow us to calculate the temperature and the specific enthalpy, if the compression was isentropic, since:

$$T_{t3,is} = f\left(s_{t3,is}, p_{t3}\right) \qquad h_{t3,is} = f\left(T_{t3,is}, p_{t3}\right) \tag{5.8}$$

Now, h_{t3} can be calculated from isentropic efficiency definition for compressors:

$$h_{t3} = h_{t2} + \frac{h_{t3,is} - h_{t2}}{\eta_c} h_{t3,is} \tag{5.9}$$

Total temperature from:

$$T_{t3} = f(h_{t3}, p_{t3}) \tag{5.10}$$

And the specific work of compressor from:

$$w_{iC} = h_{t3} - h_{t2} \tag{5.11}$$

Burner - Heater

The pressure drop in the burner is calculated by:

$$p_{t4} = p_{t3}(1 - K_b) \tag{5.12}$$

It needs to be mentioned that in this thesis, the working fluid will be sCO_2. So, the term "Burner" of this section refers to a heater in general case.

Turbine

For the turbine, the similar process is considered, as the compressor. From the pressure drop of the exit duct, the outlet pressure of the turbine can be calculated and thus, the pressure ratio of the turbine:

$$p_{t5} = \frac{p_{t6}}{1 - K_{ex}} \tag{5.13}$$

$$\pi_T = \frac{p_{t4}}{p_{t5}} \tag{5.14}$$

For constant gas properties, outlet total temperature of the turbine can be calculated directly from:

$$T_{t5} = T_{t4}\left[1 - \eta_t\left(1 - \pi_T^{-\frac{\gamma-1}{\gamma}}\right)\right] \tag{5.15}$$

and the specific work of turbine from:

$$w_{iT} = C_{p_4}(T_{t4} - T_{t5}) \tag{5.16}$$

When it comes to real gas models, the conditions before and after the expansion process can be defined through the definition of efficiency ratio. The condition *4* refers to the entry, of the turbine, where T_{t4} and p_{t4} are already known, and so are the specific entropy and enthalpy since:

$$s_{t4} = f(T_{t4}, p_{t4}) = s_{t5,is} \tag{5.17}$$

$$h_{t4} = f(T_{t4}, p_{t4}) \tag{5.18}$$

The known pressure p_{t5} and specific entropy $s_{t5,is}$, allow us to calculate the temperature and the specific enthalpy, if the expansion was isentropic, since:

$$T_{t5,is} = f\left(s_{t5,is}, p_{t5}\right) \quad h_{t5,is} = f\left(T_{t5,is}, p_{t5}\right) \tag{5.19}$$

Now, h_{t5} can be calculated from isentropic efficiency definition for turbines:

$$h_{t5} = h_{t4} - \eta_t\left(h_{t4} - h_{t5,is}\right) \tag{5.20}$$

Total temperature from:

$$T_{t5} = f(h_{t5}, p_{t5}) \tag{5.21}$$

And the specific work of turbine from:

$$w_{iT} = h_{t4} - h_{t5} \tag{5.22}$$

If the gas properties are considered as constants and the enthalpy reference is the same, the specific heat added is given through the following simplified relationship:

$$q_i = C_{p_4} T_{t4} - C_{p_3} T_{t3} \tag{5.23}$$

Otherwise, it is given directly from the enthalpy difference:

$$q_i = h_{t4} - h_{t3} \tag{5.24}$$

Finally, the thermal efficiency is calculated from Eq. 5.25, and printed in **Figure 33**.

$$\eta_{th} = \frac{w_i}{q_i} = \frac{\eta_m (w_{iT} - w_{iC})}{q_i} \tag{5.25}$$

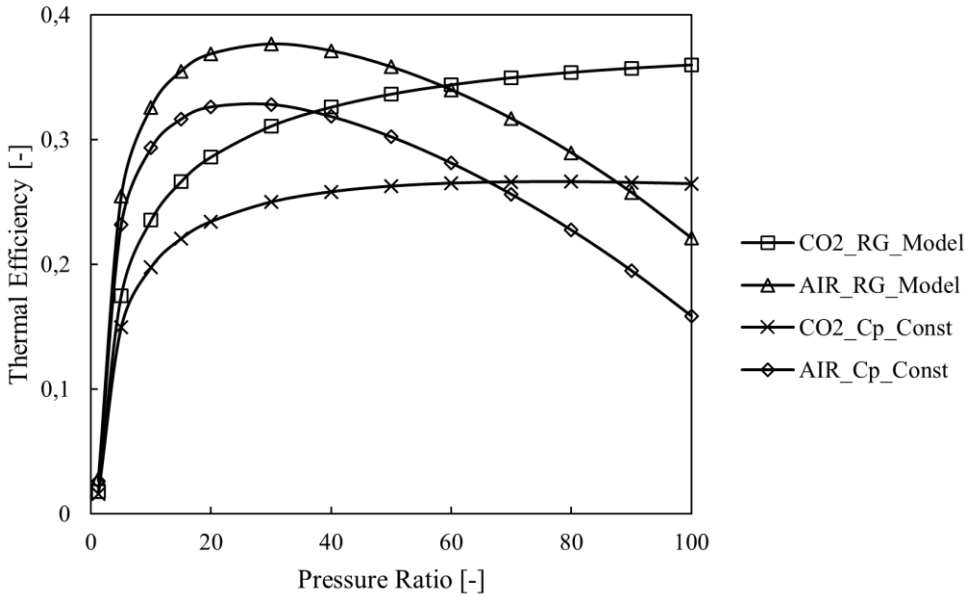

Figure 33. Thermal Efficiency vs Pressure ratio for CO_2 and Air

Figure 33 is the first tangible example on how the working fluid affects the efficiency and the pressure ratios in which a cycle can operate efficiently. While air provides with the biggest thermal efficiency, its operation is limited to a small range of pressure ratios, comparing to CO_2, which is more "robust", and the thermal efficiency with such working fluid is acceptable for a wider range of pressure ratios. Moreover, there is a clear

difference between real and ideal gas models, with the ideal gas model underestimating the efficiency of the cycle .

For **Figure 33**, data on **Table 4** and **Table 5** are used.

Table 4. Open cycle characteristics.

OPEN CYCLE CHARACTERISTICS			
T_0 [K]	288.15	K_b [-]	0.01
p_0 [Pa]	101325	T_{t4} [K]	1473.15
K_{in} [-]	0.01	η_m [-]	1
π_c [-]	1.2:100	η_t [-]	0.87
η_c [-]	0.85	K_{ex} [-]	0.01

Table 5. Constant gas properties for CO2 and Air.

CO_2		AIR	
C_{p_3} [J/kgK]	862	C_{p_3} [J/kgK]	1005
C_{p_4} [J/kgK]	1322	C_{p_4} [J/kgK]	1157
γ_3 [-]	1.30	γ_3 [-]	1.40
γ_4 [-]	1.182	γ_4 [-]	1.33

5.2.1 PROOSIS Components

The equations of Section **5.2** were not only written down as a script in an empty experiment, but also were used to create components and symbols in PROOSIS environment. Even though the equation for the open and closed cycles are almost the same, the development of the components is focused on the closed cycles which follow, since it contains extra equations and components, for example the recuperator.

To begin with, PROOSIS uses ports to achieve connection and communication between the components. In our case, we are using Fluid (F) and Mech (Me) Ports. Then, abstract components were created, which are the basis of the actual components, and they perform certain calculations, mostly for state variables. For compressor and turbine, a simple model based on their isentropic efficiency is used, and the symbols created are shown in **Figure 34**.

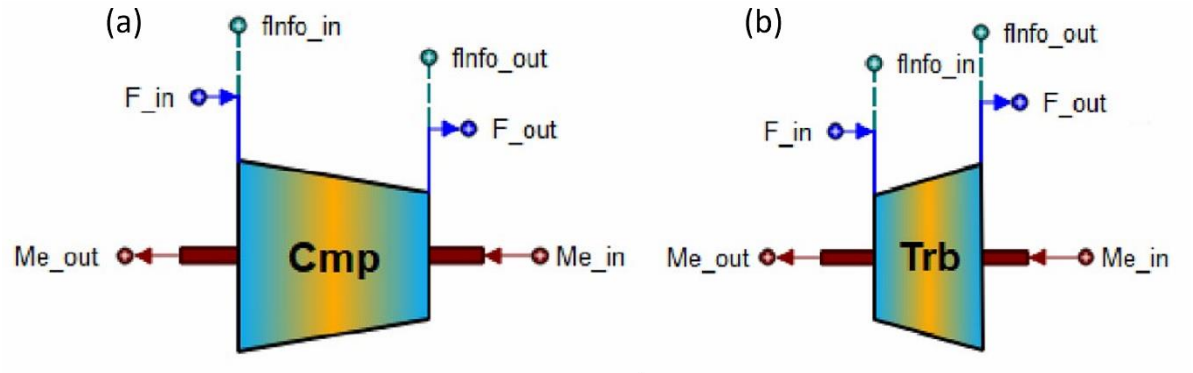

Figure 34. Symbols created in PROOSIS; (a) for Compressor, (b) for Turbine.

Recuperator is modelled as a simple heat exchanger, which utilizes thermal effectiveness definition and power equilibrium between cold and hot stream. Ducts can either add or abduct heat to the cycle, in combination with pressure drop. Their symbols are presented in **Figure 35**.

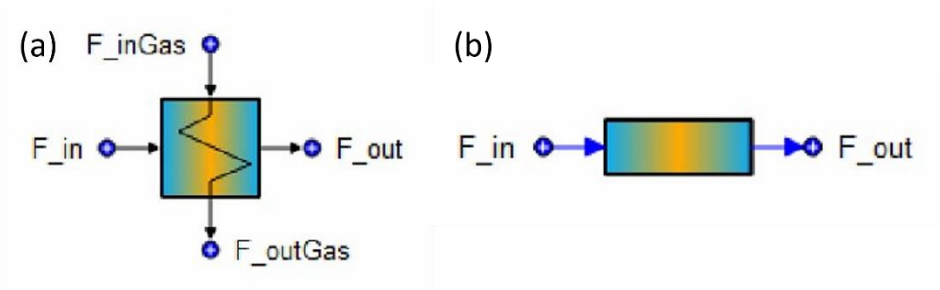

Figure 35. Symbols created in PROOSIS; (a) for Recuperator, (b) for Duct.

Finally, components related to the shaft are responsible for mechanical properties, e.g. inertia, torque and rotational speed. When the component ShaftStart is not used, we need to set inertia and rotational speed as input data. Their symbols are presented in **Figure 36**.

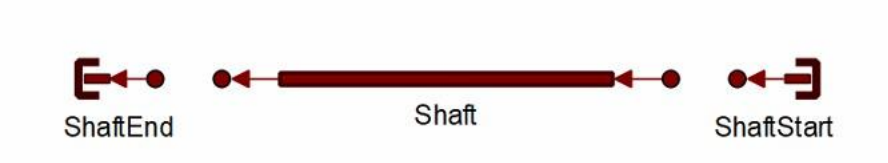

Figure 36. Symbols created in PROOSIS for Shaft Components.

5.3 Recuperated Power Cycle Analysis

In our case, we are interested in closed cycle configurations. For this reason, a recuperator and a precooler are added to the current open cycle. Moreover a heater duct has replaced the burner and the inlet and exit ducts have been removed, since their influence can be embedded in the precooler. The previous, are summarized in **Figure 37**. This consists of a typical Brayton cycle layout, in which the fluid is compressed in the compressor from Point 1 to Point 2. Then, it is preheated in the recuperator by the exhaust gas from the turbine (Point 2 to Point 3). Then, the fluid passes through the heater and reaches its highest temperature (Point 3 to Point 4). After the heat addition, there is an expansion in the turbine (Point 4 to Point 5), and the fluid is used later in the recuperator for preheating (Point 5 to Point 6). Finally, the heat is rejected in the precooler (Point 6 to Point 1).

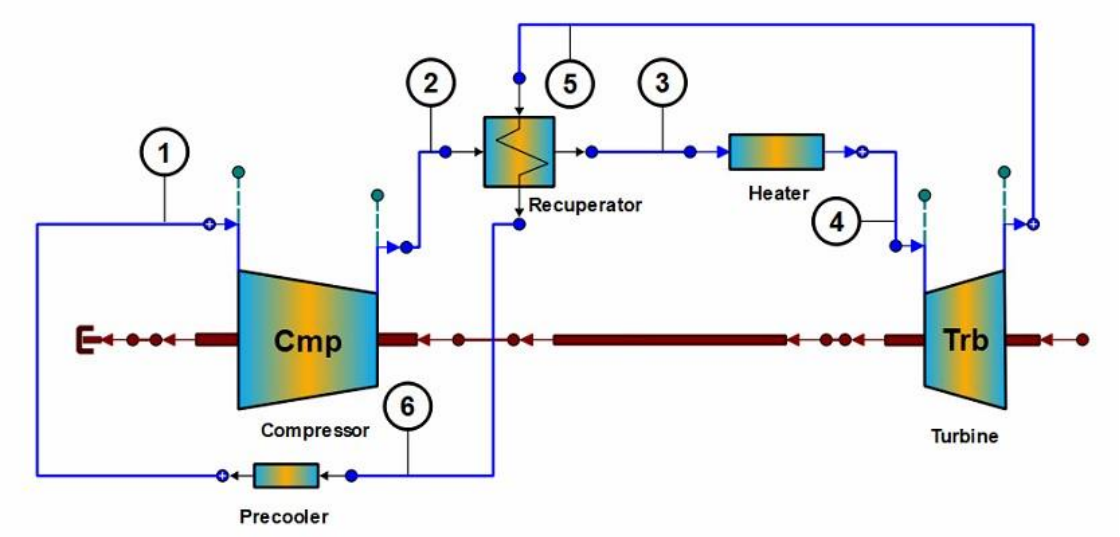

Figure 37. Closed cycle layout with Precooler, Recuperator and Heating Duct.

To solve such configurations, we need to know the following data:

$$T_{t1}, p_{t1}, T_{t4}, \eta_C, \eta_T, \varepsilon_R, \pi_C, K_{R,c}, K_{R,h}, K_h, K_{pc}, \dot{m}$$

Starting off from Point 1, by knowing temperature and pressure, we can calculate all the other properties, since:

$$s_{t1} = f(T_{t1}, p_{t1}) = s_{t2,is} \tag{5.26}$$

$$h_{t1} = f(T_{t1}, p_{t1}) \tag{5.27}$$

Compressor

We can proceed to Point 2, in which we can directly calculate the pressure from:

$$p_{t2} = p_{t1}\pi_C \tag{5.28}$$

The known pressure p_{t2} and specific entropy $s_{t2,is}$, allow us to calculate the temperature and the specific enthalpy, if the compression was isentropic, since:

$$T_{t2,is} = f(s_{t2,is}, p_{t2}) \qquad h_{t2,is} = f(T_{t2,is}, p_{t2}) \tag{5.29}$$

Now, h_{t2} can be calculated from isentropic efficiency definition for compressors:

$$h_{t2} = h_{t1} + \frac{h_{t2,is} - h_{t1}}{\eta_C} \tag{5.30}$$

and the total temperature from:

$$T_{t2} = f(h_{t2}, p_{t2}) \tag{5.31}$$

By knowing the pressure loss factors in every component, we can calculate the pressure in each Point:

$$p_{t3} = \frac{p_{t2}}{K_{R,c}} \quad p_{t4} = \frac{p_{t3}}{K_h} \quad p_{t6} = \frac{p_{t1}}{K_{pc}} \quad p_{t5} = \frac{p_{t6}}{K_{R,h}} \tag{5.32}$$

Turbine

For further calculations, we need to know turbine inlet temperature T_{t4}. Similarly with open cycle, T_{t4} and p_{t4} are already known, and so are the specific entropy and enthalpy since:

$$s_{t4} = f(T_{t4}, p_{t4}) = s_{t5,is} \tag{5.33}$$

$$h_{t4} = f(T_{t4}, p_{t4}) \tag{5.34}$$

The known pressure p_{t5} and specific entropy $s_{t5,is}$, allow us to calculate the temperature and the specific enthalpy, if the expansion was isentropic, since:

$$T_{t5,is} = f(s_{t5,is}, p_{t5}) \quad h_{t5,is} = f(T_{t5,is}, p_{t5}) \tag{5.35}$$

Now, h_{t5} can be calculated from isentropic efficiency definition for the turbines:

$$h_{t5} = h_{t4} - \eta_T\left(h_{t4} - h_{t5,is}\right) \tag{5.36}$$

And the total temperature from:

$$T_{t5} = f(h_{t5}, p_{t5}) \tag{5.37}$$

Recuperator

The definition of the effectiveness of recuperator allows us to calculate the inlet temperature of the heater:

$$T_{t3} = \varepsilon_R(T_{t5} - T_{t2}) + T_{t2} \tag{5.38}$$

and from this, the specific entropy and enthalpy at Point 3:

$$s_{t3} = f(T_{t3}, p_{t3}) \quad h_{t3} = f(T_{t3}, p_{t3}) \tag{5.39}$$

The energy balance in the recuperator, allows us to calculate h_{t6}:

$$h_{t6} = h_{t5} + h_{t2} - h_{t3} \tag{5.40}$$

and from this, the specific entropy and Temperature at Point 6:

$$s_{t6} = f(h_{t6}, p_{t6}) \quad T_{t6} = f(h_{t6}, p_{t6}) \tag{5.41}$$

In this case, p_{t6} no longer refers to ambient conditions. We consider a cooling stream with known inlet enthalpy $h_{c,c}$ which abducts heat Q_{pc} from the main stream and reduces the temperature from T_{t6} to T_{t1}. The amount of heat is given by:

$$Q_{pc} = \dot{m}(h_{t6} - h_{t1}) \tag{5.42}$$

And the amount of heat that has been added to the configuration from the heater:

$$Q_h = \dot{m}(h_{t4} - h_{t3}) \tag{5.43}$$

Cycle efficiency can be calculated if we divide the net work with the amount of heat that has been added. Specifically:

$$\eta_{Cycle} = \frac{w_{iT} - w_{iC}}{Q_h} \tag{5.44}$$

5.3.1 Validation

Yoonhan et al. [22] have already studied similar layouts. In their work, they propose the layout of **Figure 38**.

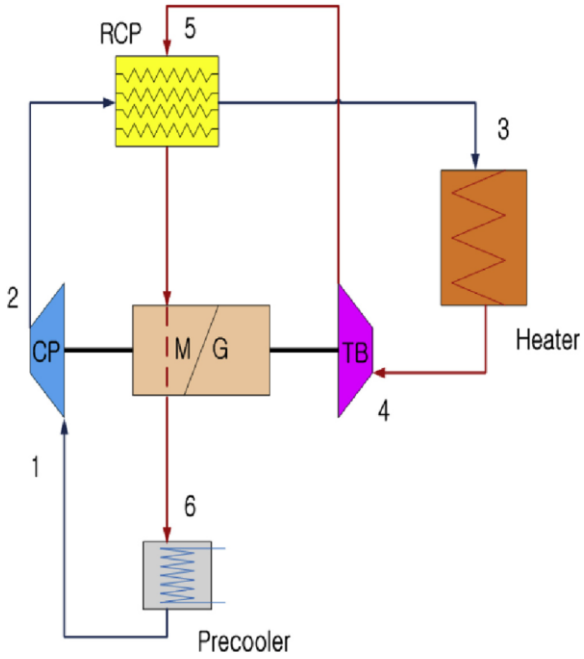

Figure 38. The first design layout (Single TAC feature-simple recuperated cycle of Yoonhan et al [22].

For this design, they set the variables as they are presented in **Table 6**.

Table 6. The first design variables [22].

Heat, kW	1320	**Mass flow rate, kg/s**	4.6
Net efficiency, %	25.6	**Turbine work, kW**	484
Rotating speed, krpm	111	**Compressor work, kW**	147
Recuperator ΔT, ℃	285.2	**Net work, kW**	337
Turbine N_s	0.48	**Compressor N_s**	0.65

With the previous assumptions, they get the following results (**Table 7**) which indicate the thermodynamic properties of every position.

Table 7. Section conditions of the first design [22].

No.	Section Conditions	P (MPa)	T (°C)	h (kJ/kg)	s (kJ/kg-K)
1	Compressor Inlet	7.78	33.2	329.6	1.42
2	Recuperator CS Inlet	20	74.3	361.2	1.45
3	Heater Inlet	19.9	269.1	688.8	2.23
4	Turbine Inlet	19.8	500	973.5	2.67
5	Recuperator HS Inlet	8.03	401.5	869.0	2.69
6	Precooler Inlet	7.93	116.2	541.4	2.06

The equations of **5.3** were inserted into PROOSIS environment, and the results are summarized in **Figure 39**, depicting the goal temperature of each point of the configuration with the relative error that occurs to the calculation of temperature, using Berthelot and Span and Wanger equation of state.

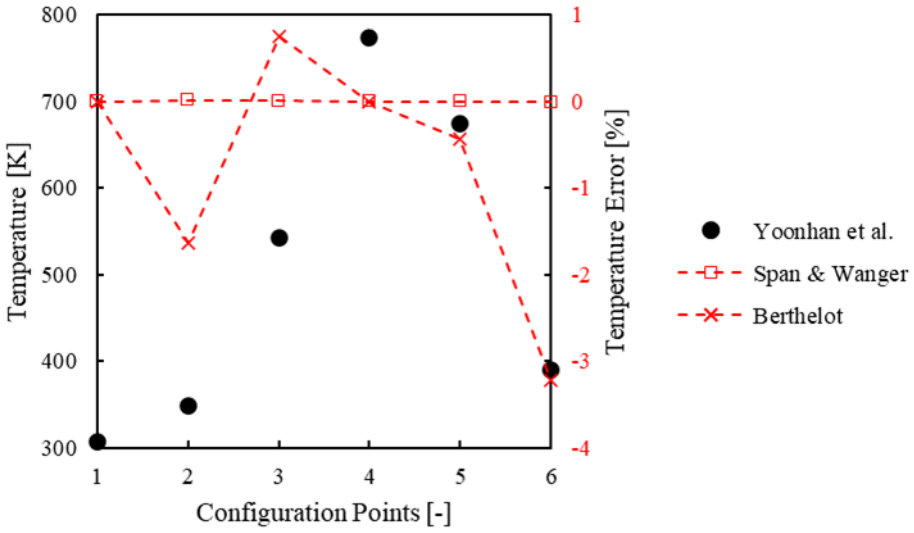

Figure 39. Goal temperature and relative error for the configuration of Figure 38.

The results of **Figure 39** come along with what it was mentioned in **3.2.1,** concerning the accuracy of Berthelot EoS for the CO_2 and how it could be an alternative solution is Span and Wanger EoS was not available. The error that the Berthelot EoS introduces is low, as indicates **Figure 39**. However the overall accuracy cannot be compared with Span and Wanger EoS.

5.3.2 Studies in Recuperated Cycle

Previously in **5.2** it was depicted how the efficiency and the operating pressure ratios are affected by the working medium in an open cycle. The same study is reconducted, this time for a closed recuperated cycle. Using input data from the previous section, the results are presented **Figure 40** for the case of CO_2 and in **Figure 41** for the case of air. In the case of air, the efficiency is also calculated if the inlet of the compressor is in atmospheric pressure, and illustrated with dots.

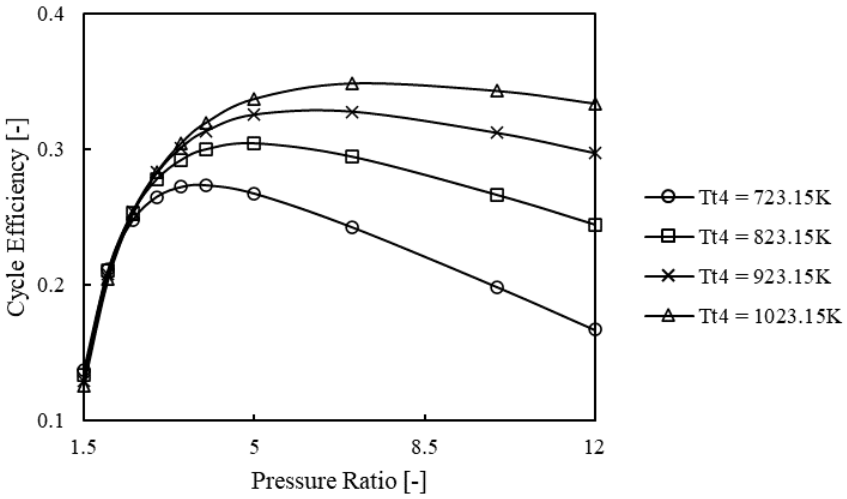

Figure 40. Cycle efficiency for different pressure ratios and turbine inlet temperature, working with CO_2.

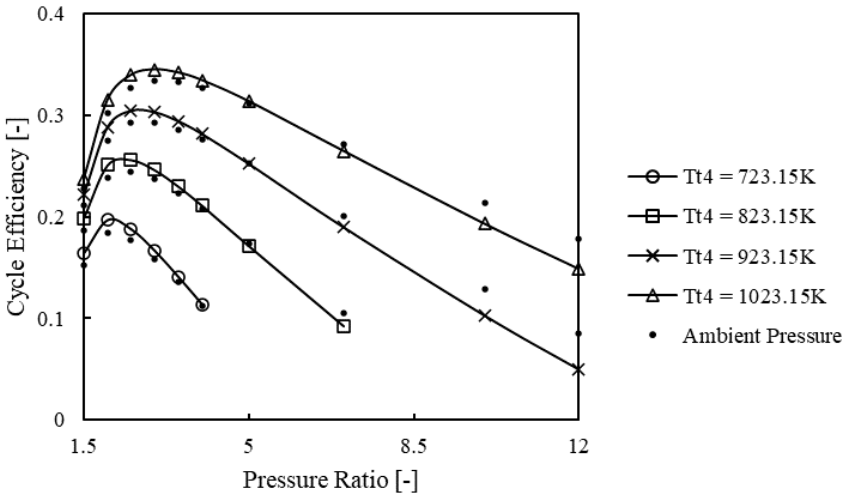

Figure 41. Cycle efficiency for different pressure ratios and turbine inlet temperature, working with air.

Similarly to the open cycle, working with air provides with a highest cycle efficiency for a relative low pressure ratio. CO_2 offers the ability to work on higher pressure ratios and achieve acceptable efficiencies.

In addition to the investigation of the compression process around the critical point, which was conducted in **3.3.2**, to depict the influence of the compressor's efficiency on the total efficiency of the cycle, a parametric study was carried out in which cycle efficiency was calculated as a function of the compressor's efficiency and inlet temperature. The results are presented in **Figure 42**.

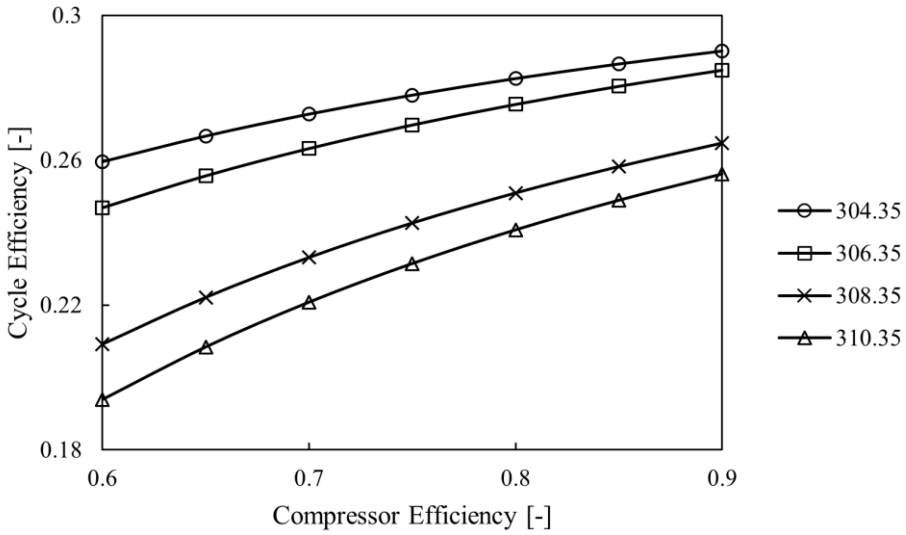

Figure 42. Cycle efficiency for different compressor efficiencies and inlet temperatures.

5.3.3 Concentrated Solar Power (CSP) Application

Several studies have been carried out concerning integration of CSP with sCO_2 [[24], [17], [25]], since it could contribute to greater efficiencies. The common thread among those studies is that they examine certain cycle configurations and investigate the operation of the components that are involved. For a tryout of the aforementioned equations for the recuperated cycle, the work of van der Westhuizen and Dobson [17] is selected as a reference, to perform a cycle calculation in a temperature range that is defined by CSP.

Van der Westhuizen and Dobson set as main objectives to contribute to the design, optimization, and control of CSP-sCO_2 systems. Their simulation is based on a simple recuperated Brayton cycle, presented in **Figure 43**, where the heater is a solar receiver. A centrifugal compressor is used, along with a radial inflow turbine, which are not mechanical connected. The heat sink is modelled as a natural cooled finned tube and the recuperator is a counter flow printed-circuit type.

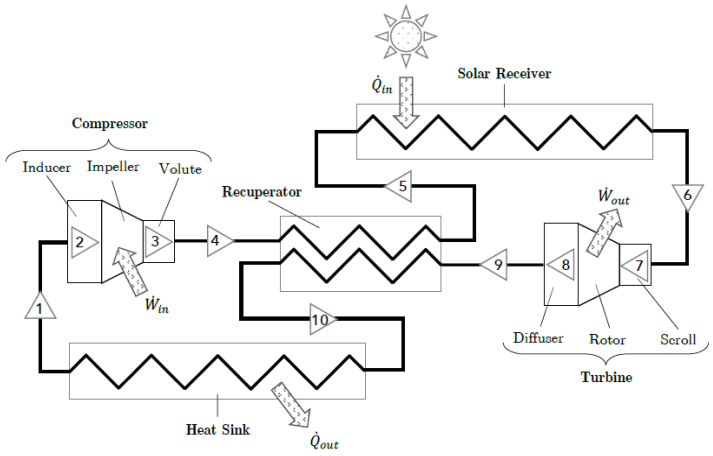

Figure 43. Overview of the simulated CSP-sCO₂ system [17].

They present their results in the form of diagrams, which are shown in **Figure 44**.

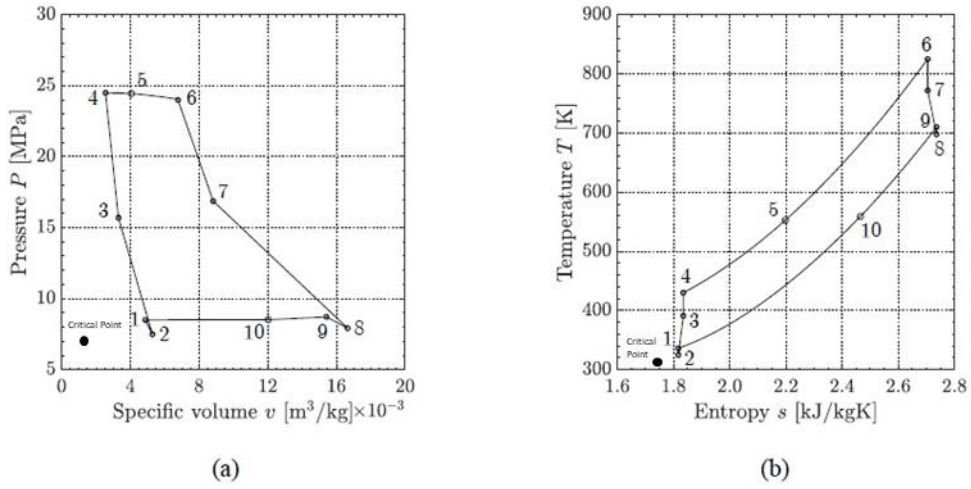

Figure 44. Van der Westhuizen and Dobson results in form of: P-v diagram (a); T-s diagram (b) [17].

The goal is to get similar results with the diagrams of **Figure 44**, and for this reason, they were turned into values, using *plot digitizer* [31], and presented in **Table 8**.

Table 8. Van der Westhuizen and Dobson results in form of table.

	1	2	3	4	5	6	7	8	9	10
T [K]	335.41	324.88	390.91	430.14	552.63	825.36	771.77	698.09	709.57	559.33
P [MPa]	8.54	7.53	15.69	24.57	24.49	24.01	16.90	7.93	8.74	8.54

As it was mentioned, van der Westhuizen and Dobson utilize a centrifugal compressor and a radial turbine, and they consider intermediate points in those components. The first attempt to reproduce their results, neglects those points and assumes that Point 1 and Point 4 are the inlet and outlet of the compressor, and Point 6 and 9 are the inlet and outlet of the turbine. The configuration of **Figure 45** was used.

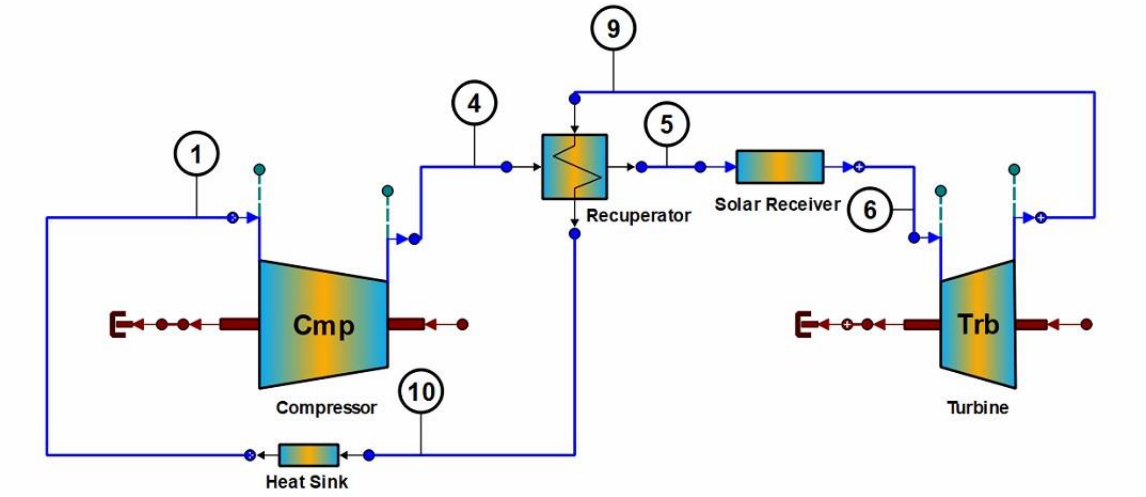

Figure 45. First configuration to reproduce the results.

By executing the simulation, the values of **Table 9** are achieved.

Table 9. Results produced using the configuration of Figure 45.

	1	4	5	6	9	10
T_{calc} [K]	335.41	430.10	553.02	825.36	710.74	557.49
P_{calc} [MPa]	8.54	24.57	24.49	24.01	8.74	8.54
T_{error} [%]	0.00	0.01	0.07	0.00	-0.16	0.33

To be more precise, Inducer, Volute, Scroll and Diffuser, were modelled as ducts which increase and decrease the temperature and the pressure, depending on the case. The configuration is now being presented in **Figure 47** and the results are summarized in **Figure 46**, depicting the goal temperature of each point of the configuration with the relative error that occurs to the calculation of temperature, using Berthelot and Span and Wanger equation of state.

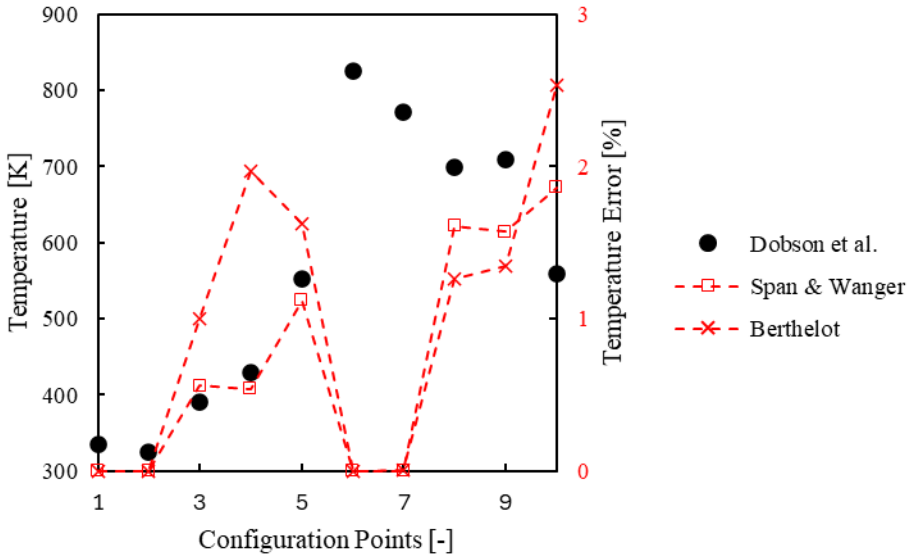

Figure 46. Goal temperature and relative error for the configuration of Figure 47.

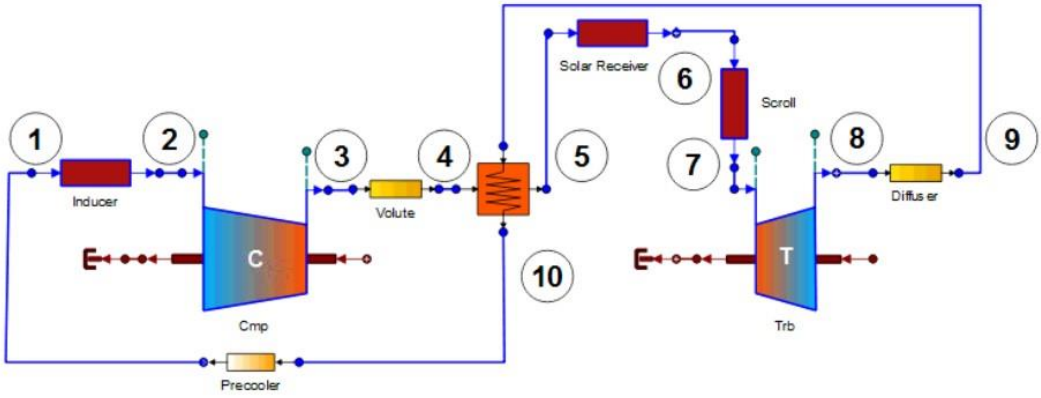

Figure 47. Final configuration with intermediate points 2,3 and 7,8.

For both **Table 9** and **Figure 46**, the relative error is calculated only for temperature since the pressure values are identical. The formula for the calculation is:

$$T_{error} = 100\frac{T - T_{calc}}{T} \tag{5.45}$$

5.4 Reheated Power Cycle Analysis

The first step towards the improvement of the efficiency of simple recuperated Brayton cycle, is to add a reheater and a second turbine. Those additions, improve the cycle efficiency by increasing the equivalent Carnot temperature for the cycle. Equivalent Carnot cycle is a cycle which achieves the same efficiency as the original thermodynamic cycle would achieve [6].

Based on Carnot's cycle theory, to increase the efficiency of the original cycle, either the average temperature of heat addition needs to be increased, or the average temperature of head rejection need to be reduced. By adding a reheat stage, the inlet temperature of the heater increases and consequently, the average temperature of heat additions is increased. The reheated Brayton cycle configuration is depicted in **Figure 48** and a typical temperature-entropy diagram can be found in **Figure 49**.

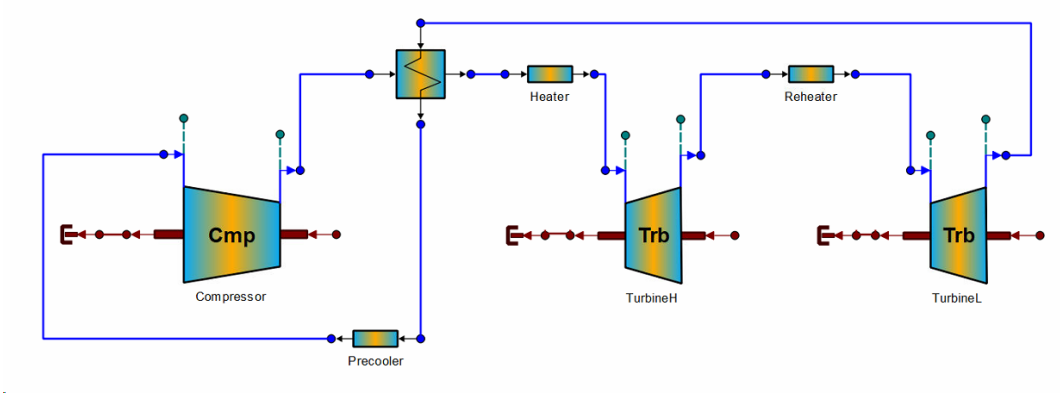

Figure 48. Reheated Brayton cycle configuration.

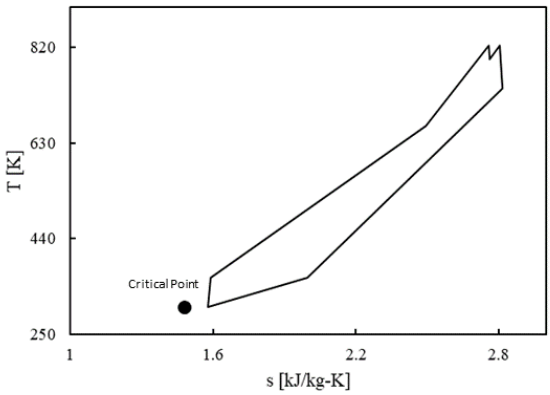

Figure 49. Typical T-s diagram of reheated Brayton cycle.

The cycle is similar to the simple Brayton cycle with recuperation, which was already studied in **5.3**. CO_2 undergoes a compression process to reach the maximum pressure of the cycle, then it is preheated in the recuperator before it enters the main heater and the high-pressure turbine. The difference is that the expansion process is divided to two turbines, high and low pressure, and there is an intermediate reheater. After the total expansion of the fluid, the recuperator takes advantage of the remaining heat, and finally, precooler rejects the excessive heat to reach the inlet conditions of the compressor.

In terms of modelling such configurations, the equations are the same as simple Brayton cycle. However, in this case, we need to define characteristics of the second turbine, i.e. efficiency and inlet temperature, and also the outlet pressure of the first turbine, which we will see how it affects cycle's efficiency in the following parametric analysis. The data used for this analysis is presented in **Table 10**. In addition, no pressure losses are considered.

Table 10. Data used for parametric analysis of reheated Brayton cycle.

Conditions	Values
Turbines Efficiency [-]	0.9
Compressor Efficiency [-]	0.85
Recuperator Effectiveness [-]	0.8
Main Compressor Inlet Temperature [K]	305
Main Compressor Inlet Pressure [MPa]	7.4
Turbine Inlet Temperature [K]	823.15
Pressure Ratio [-]	1.5 – 3.5

Figure 50 depicts the results of the parametric analysis. For three different pressure ratios, the efficiency of the cycle was calculated for different reheater inlet pressures. It seems that for a certain pressure ratio, the efficiency is not highly affected. However, there are wide variations of efficiency when the pressure ratio changes. For this reason, a second parametric analysis is carried out, with the same conditions, but this time pressure ratio is the main parameter. The results can be found in **Figure 51** and indicate the influence of the pressure ratio in the efficiency of the cycle.

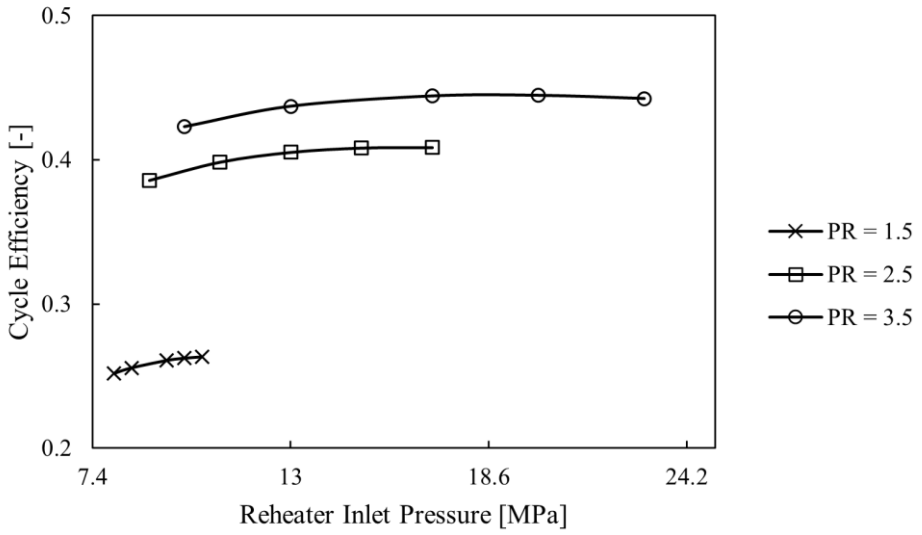

Figure 50. First parametric analysis results for reheated Brayton cycle.

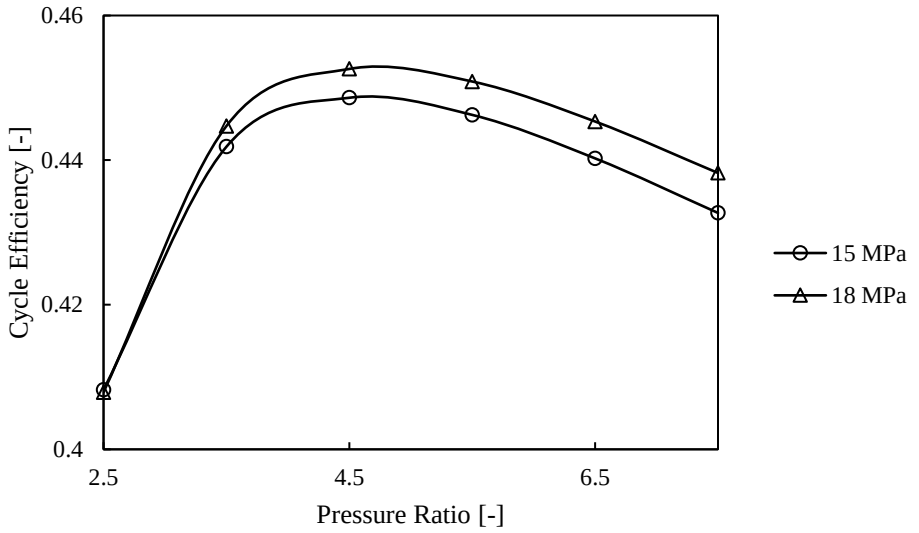

Figure 51. Second parametric analysis results for reheated Brayton cycle.

5.5 Recompression Power Cycle Analysis

In his PhD Thesis, Dostal [6] indicates that the recompression cycle has the biggest potential for efficiency improvement among the cycles he examines. The reason behind the improvement of the efficiency, is the reduction of heat rejection from the cycle by introducing another compressor before the precooler. In the layout of **Figure 52**, only a part of the total fluid flow is used for heat rejection in the precooler. Moreover, there are

now two recuperators instead of one, which was the case for cycles that were previously studied.

In this configuration, a fraction of fluid flow is compressed from Point 1 to Point 2, in the main compressor. In the low temperature recuperator, the fluid is preheated to the temperature of the recompression (Point 2 to Point 3). Then, the flow is merged in Point 4, and the total flow is now preheated in high temperature recuperator (Point 4 to Point 5). From Point 5 to Point 6, there is the heat addition of the cycle, and then, from Point 6 to Point 7, an expansion occurs. The exhaust fluid of the turbine is used for the preheat of the fluid in the recuperators (Point 7 to Point 8 and Point 8 to Point 9). Finally, the flow is splitted in Point 9 and a part of the flow is recompressed (Point 9 to Point 10), while the other is cooled in the precooler (Point 9 to Point 1).

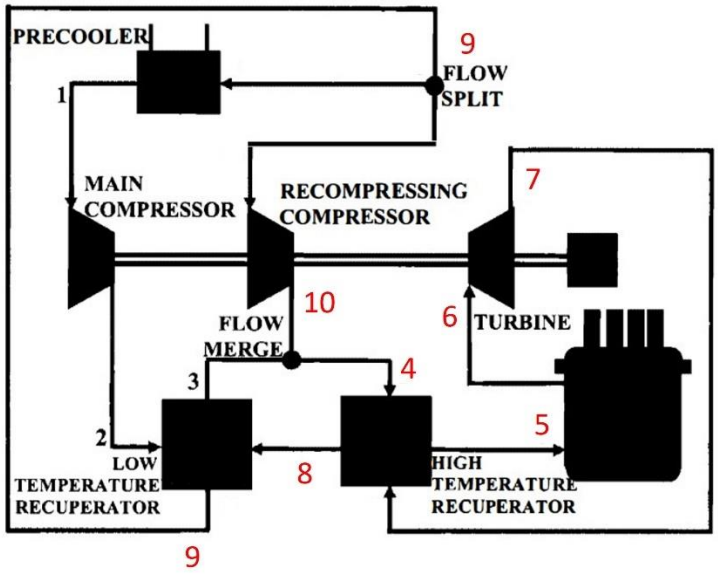

Figure 52. Recompression Brayton cycle layout [6].

To simulate such configurations, some variables need to be defined. Those include the inlet conditions of the main compressor (T_{t1}, p_{t1}), the efficiencies of the two compressors $(\eta_{C,main}, \eta_{C,rec})$ and the turbine (η_T), the effectiveness of the two recuperators (η_{LTR}, η_{HTR}), the pressure ratio of the two compressors (π_C), the split ratio (s_r), and the inlet temperature of the turbine (T_{t6}). For our study, we suppose that every point of the layout, is either in high or low pressure, i.e., there are no pressure drops in heat exchangers. Moreover, we consider the general case, where the outlet temperature of the recompression compressor is not the same as the outlet temperature of the cold stream of low temperature recuperator.

Starting off from Point 1, by knowing temperature and pressure, we can calculate all the other properties, since:

$$s_{t1} = f(T_{t1}, p_{t1}) = s_{t2,is} \tag{5.46}$$

$$h_{t1} = f(T_{t1}, p_{t1}) \tag{5.47}$$

Compressor

We can proceed to Point 2, in which we can directly calculate the pressure from:

$$p_{t2} = p_{t1}\pi_C \tag{5.48}$$

The known pressure p_{t2} and specific entropy $s_{t2,is}$, allow us to calculate the temperature and the specific enthalpy, if the compression was isentropic, since:

$$T_{t2,is} = f(s_{t2,is}, p_{t2}) \quad h_{t2,is} = f(T_{t2,is}, p_{t2}) \tag{5.49}$$

Now, h_{t2} can be calculated from isentropic efficiency definition for the main compressor:

$$h_{t2} = h_{t1} + \frac{h_{t2,is} - h_{t1}}{\eta_{C,main}} \tag{5.50}$$

and the total temperature from:

$$T_{t2} = f(h_{t2}, p_{t2}) \tag{5.51}$$

Since there are no pressure drops (ideal case), the pressures in every point are given by:

$$p_{t2} = p_{t3} = p_{t4} = p_{t6} = p_{t6} \tag{5.52}$$

$$p_{t3} = p_{t10} = p_{t9} = p_{t8} = p_{t7} \tag{5.53}$$

Turbine

For further calculations, we need to know turbine inlet temperature T_{t6}. Similarly with open cycle, T_{t6} and p_{t6} are already known, and so are the specific entropy and enthalpy since:

$$s_{t6} = f(T_{t6}, p_{t6}) = s_{t7,is} \tag{5.54}$$

$$h_{t6} = f(T_{t6}, p_{t6}) \tag{5.55}$$

The known pressure p_{t7} and specific entropy $s_{t7,is}$, allow us to calculate the temperature and the specific enthalpy, if the expansion was isentropic, since:

$$T_{t7,is} = f(s_{t7,is}, p_{t7}) \quad h_{t7,is} = f(T_{t7,is}, p_{t7}) \tag{5.56}$$

Now, h_{t7} can be calculated from isentropic efficiency definition for the turbines:

$$h_{t7} = h_{t6} - \eta_T(h_{t6} - h_{t7,is}) \tag{5.57}$$

And the total temperature from:

$$T_{t7} = f(h_{t7}, p_{t7}) \tag{5.58}$$

Recuperators

Up to this point, the equations are the same as in Section **5.3**. The remaining equations consist of the effectiveness and energy balance of recuperators, the efficiency of the recompression compressor and the energy balance in Point 4. The effectiveness of HTR and LTR are given as in [23].

For the High Temperature Recuperator:

$$T_{t8} = \varepsilon_{HTR}(T_{t4} - T_{t7}) + T_{t7} \quad h_{t5} = h_{t7} + h_{t4} - h_{t8} \tag{5.59}$$

For the Low Temperature Recuperator:

$$T_{t9} = \varepsilon_{LTR}(T_{t2} - T_{t8}) + T_{t8} \quad h_{t3} = h_{t2} + \frac{h_{t8} - h_{t9}}{s_r} \tag{5.60}$$

For the recompression compressor:

$$h_{t10} = h_{t9} + \frac{h_{t10,is} - h_{t9}}{\eta_{C,sec}} \tag{5.61}$$

For the energy balance in Point 4:

$$h_{t4} = s_r h_{t3} + (1 - s_r) h_{t10} \tag{5.62}$$

The previous six equations include seven unknown variables, and the iteration process of **Figure 53** is required.

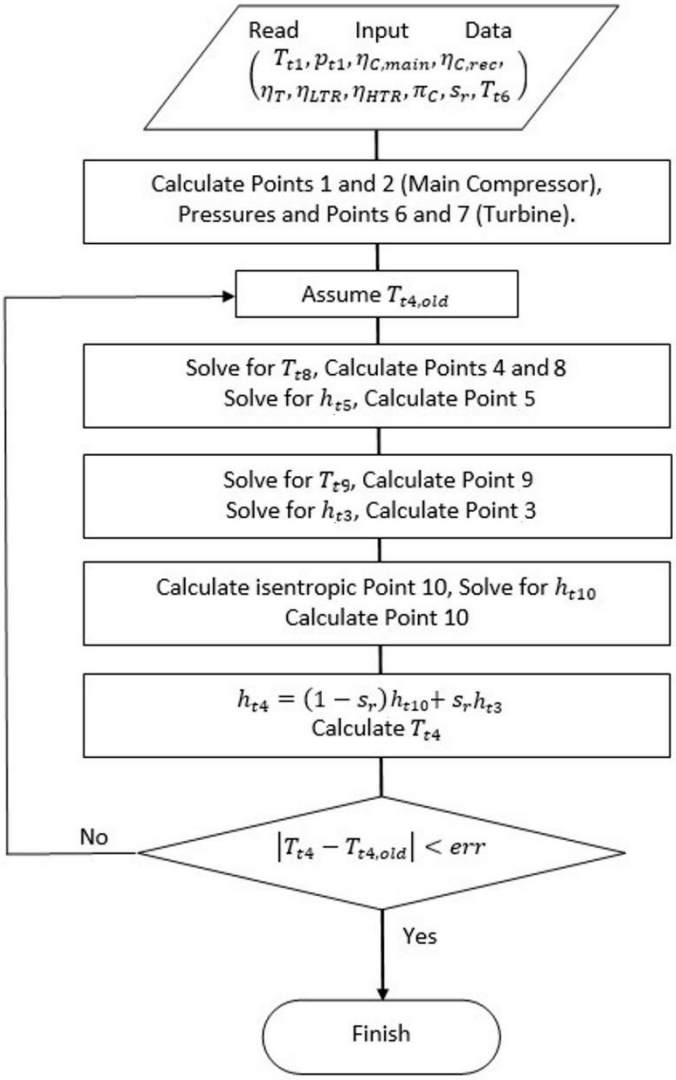

Figure 53. Flow chart for recompression cycle layout.

By converging the upper iteration process, every point of the layout is solved, and this allows us to calculate characteristics of the cycle, including works and efficiencies, with respect to mass flow rate.

$$\dot{q}_{pc} = h_{t9} - h_{t1} \tag{5.63}$$

$$\dot{q}_{heater} = h_{t6} - h_{t5} \tag{5.64}$$

$$\dot{w}_{cycle} = \dot{w}_{iT} - s_r \dot{w}_{iC,main} - (1 - s_r)\dot{w}_{iC,sec} \tag{5.65}$$

$$\eta_{Cycle} = \frac{\dot{w}_{cycle}}{\dot{q}_{heater}} = \frac{(h_{t6} - h_{t7}) - s_r(h_{t2} - h_{t1}) - (1 - s_r)(h_{t10} - h_{t9})}{h_{t6} - h_{t5}} \quad (5.66)$$

The previous equations complete the modeling of the recompression supercritical CO_2 cycle, and the cycle performance can be simulated. The first case which is examined, is an ideal case, where there are no pressure drops and the efficiencies and effectiveness are equal to 1. This case validates the equations since the results are compared with the results of Mohammadi et al. [23]. The data used for this case, can be found in **Table 11**.

Table 11. Cycle assumptions for the ideal case.

Conditions	Values
Turbine Efficiency [-]	1
Compressors Efficiency [-]	1
Recuperators Effectiveness [-]	1
Main Compressor Inlet Temperature [K]	308.15
Main Compressor Inlet Pressure [MPa]	7.4
Turbine Inlet Temperature [K]	823.15
Pressure Ratio [-]	3
Split Ratio [-]	0.703

The results of the ideal case in terms of temperature, the reference value of temperature as calculated in [23] and the relative error are presented in **Table 12**.

Table 12. Temperature for each point in recompression sCO_2 ideal cycle, compared to bibliography.

	1	2	3=4=10	5	6	7	8	9
T [K]	308.15	385.12	491.67	658.77	823.15	679.68	491.71	385.12
$\mathbf{T_{ref}}$ [K]	308.15	385.16	491.86	658.8	823.15	679.68	491.86	385.16
$\mathbf{T_{err}}$ [%]	0.00	-0.01	-0.04	0.00	0.00	0.00	-0.01	-0.01

After validating the calculations, we can proceed to further investigation of the recompression cycle. To study the effect of pressure and split ratios on the cycle performance some simulation conditions were assumed, as Kim et al. [32] suggest in their work. They can be found in **Table 13**.

Table 13. Simulation conditions for recompression cycle.

Conditions	Values
Turbine Efficiency [-]	0.90
Compressors Efficiency [-]	0.85
Recuperators Effectiveness [-]	0.95
Main Compressor Inlet Temperature [K]	305.15
Main Compressor Inlet Pressure [MPa]	7.4
Turbine Inlet Temperature [K]	823.15
Pressure Ratio [-]	1.5-4.5
Split Ratio [-]	0-1

Figure 54 depicts that pressure and split ratios have a serious impact on cycle efficiency, as previous researchers have stated [6]. Moreover, **Figure 54** signifies the potential that recompression may have, if values of pressure and split ratio are optimized.

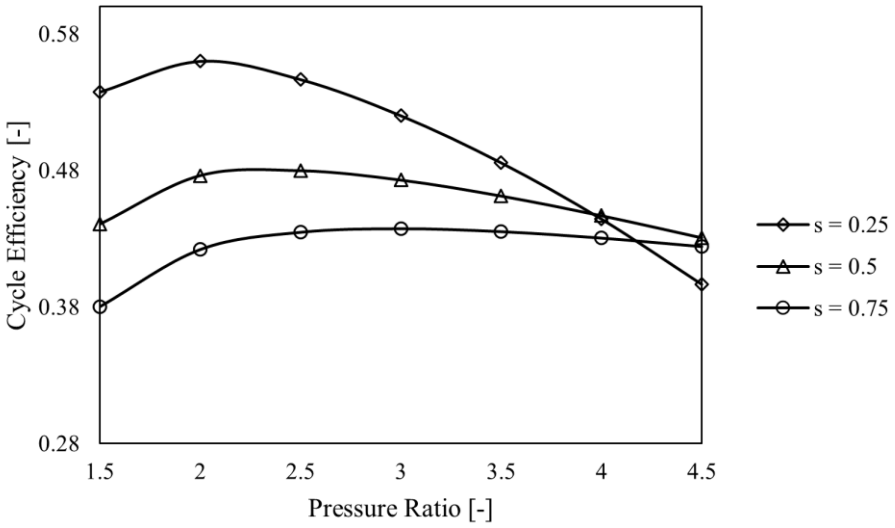

Figure 54. Recompression cycle efficiency for various pressure and split ratios.

5.6 Comparison of Power Cycles

Previously in this chapter, three of the main sCO_2 power cycles were examined. In practice, each cycle may be suitable for a different application, which corresponds to different heat sources and operating conditions.

In 1969, Angelino [16] proposed several cycle layouts, and later, many researchers including Dostal [6], examined the different variation of the sCO_2 cycles, in a similar way as the author did. For a better understanding of the need to study more complex cycles, four configurations are compared in terms of their efficiency. The three of those, are examined previously, and the fourth is a simple closed cycle, consisting of a compressor, a turbine, a heater and a cooler.

Every layout is shown in **Figure 55**. The inputs for each model, are summarized in

Table 14 and they are based on typical values of the litterature. In this analysis, pressure drops across heat exchangers are not considered. Of course, the results will be affected by the selected opperating conditions. To find out the potential of each cycle in a wider range, inlet temperature of the turbine is ranges from 823.15K to 1223.15K. Moreover, when it comes to more complex cycles, other parameters introduced, like split ratio, are not optimized.

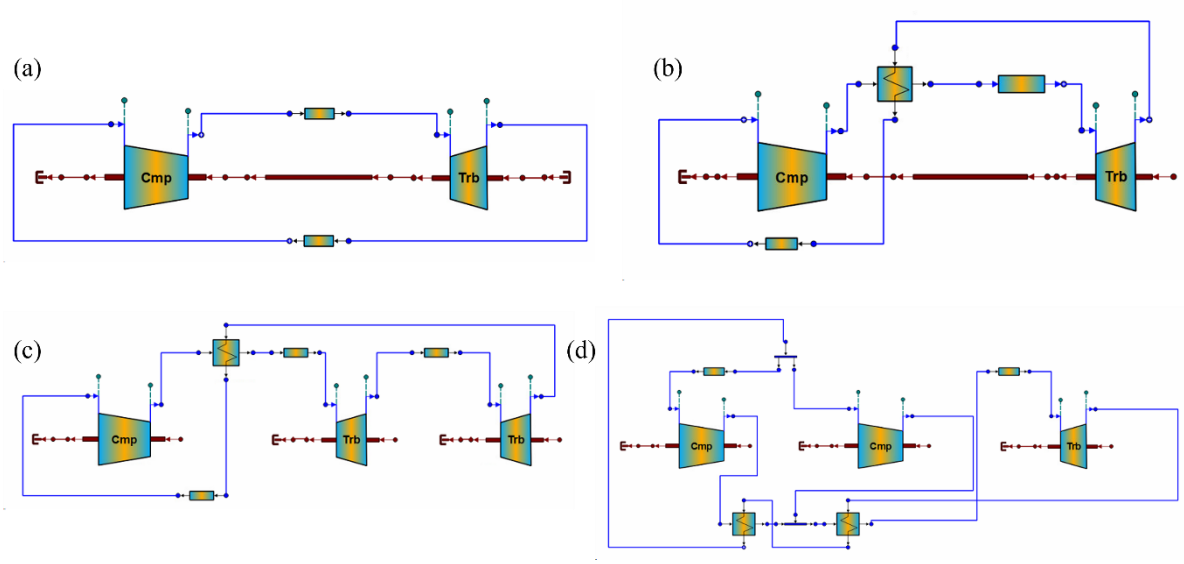

Figure 55. Examined cycles layouts; (a) Simple closed cycle, (b) Recuperated closed cycle, (c) Reheated-Recuperated closed cycle and (d) Closed cycle with recompression.

Table 14. Cycle inputs for the comparison.

Conditions	Values
Turbine Efficiency [-]	0.90
Compressor Efficiency [-]	0.85
Recuperators Effectiveness [-]	0.80
Main Compressor Inlet Temperature [K]	305.15
Main Compressor Inlet Pressure [MPa]	7.4
Pressure Ratio [-]	4
Split Ratio (Recompression) [-]	0.3

The results of the comparison, are depicted in **Figure 56**. As expected, the simplest version of the cycle, has the lowest efficiency with a value from 19.31% to 20.18% and is slightly influenced by the inlet temperature of the turbine. By adding a recuperator, the improvement of the efficiency is significant, since it reaches values from 43.91% to 49.39%. The reheated-recuperated version, is slightly better in lower turbine inlet temperatures than the simple recuperated and its efficiency varies from 44.90% to 49.24% . Finally, closed cycle with recompression achieves the highest efficiency (53.44%) for the conditions that were studied. However, it should be noted that for lower turbine inlet temperatures, the efficiency of the cycle is relative low.

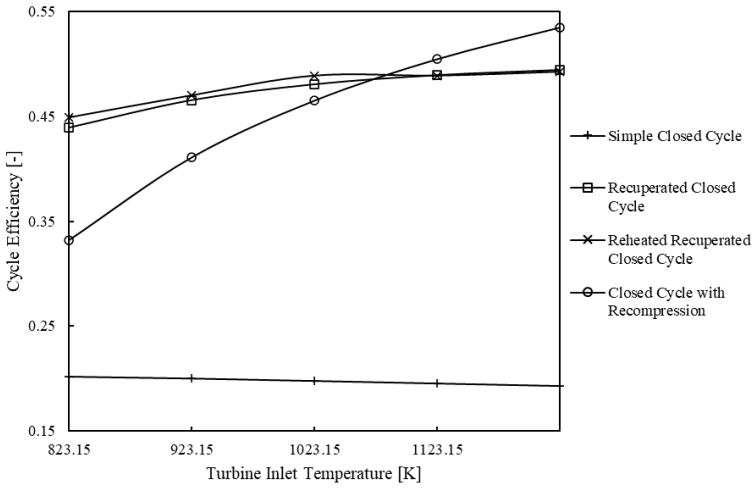

Figure 56. Cycle comparison results.

In an effort to examine how the pressure ratio affects the efficiency of the cycles, it is setted as the main parameter of the study. The turbine inlet temperature is the lowest and the highest of the previous study, and the results are depicted in **Figure 57** and **Figure 58** for the lowest and highest turbine inlet temperature, respectively.

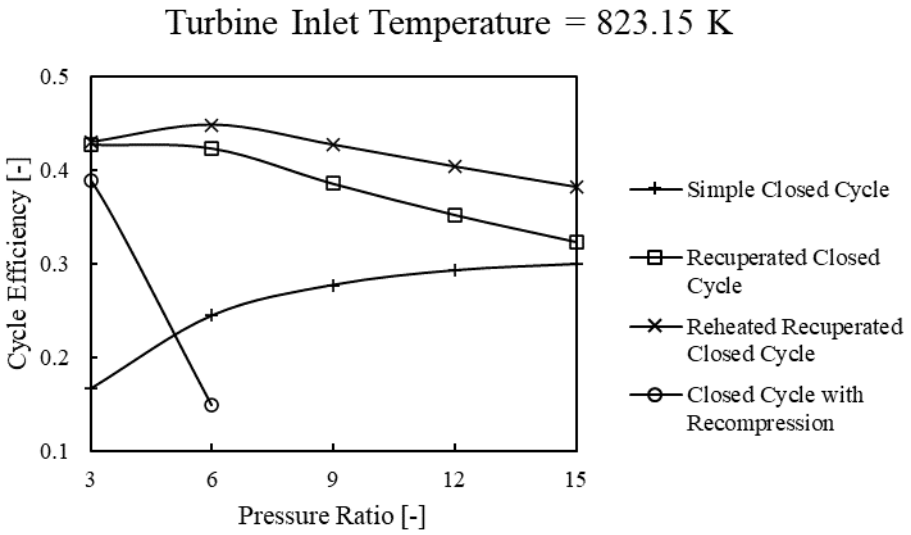

Figure 57. Cycle comparison results with varying pressure ratio, for turbine inlet temperature = 823.15 K.

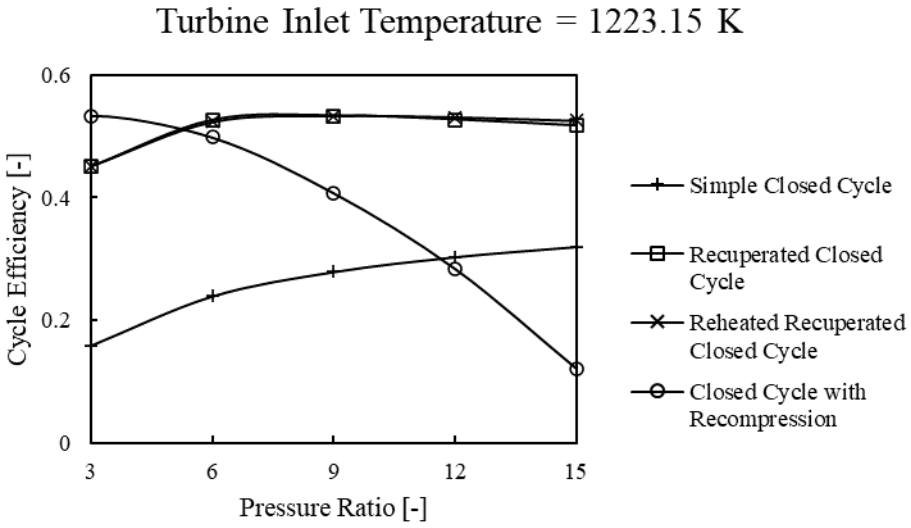

Figure 58. Cycle comparison results with varying pressure ratio, for turbine inlet temperature = 1223.15 K.

In the previous figures, especially in **Figure 57**, bigger fluctuations are observed, as the pressure ratio increases, compared to **Figure 56**, which indicates that the pressure ratio could affect the cycle significantly. For the certain split ratio, the use of closed cycle with recompression in high pressure ratio is unacceptable since the efficiency decreases. The simple recuperated cycle and the reheated-recuperated appear to operate well in every pressure ratio for both temperatures, while the simple closed cycle seems to be more affected by the pressure ratio that it is by the inlet temperature of the turbine.

5.7 Summary

The configurations that were examined in this chapter consist of the majority of the layouts that are used with sCO_2 as a working fluid. Apart from the different calculations that were carried out for a certain configuration, the importance of the proper EoS was mentioned by comparing the errors that were introduced. Moreover, a CSP application was presented, which is a typical heat source to be integrated with sCO_2 cycles. In addition, the potential of each layout was exhibited, and it was shown that more complex layouts could potentially lead to higher efficiencies, as demonstrated in **Figure 56**. However, adding extra parameters to a cycle, such as the split ratio, requires further analysis and optimization, since it can lead to worse efficiencies, as shown in **Figure 57**. The credibility of the computational tools that were developed, was certified through different applications found in global literature by providing similar results. Consequently, they set the basis for proceeding to the next step, which is the study of some of those cycles under off-design conditions.

6. OFF-DESIGN ANALYSIS

Once an engine has been designed and materialized, it is forced to operate within a range of conditions, since there are alternations in power production requirements, ambient condition and various other reasons. Off-design analysis is performed, to predict the performance of the cycle over the complete operating envelop. Off design analysis is useful already during the detailed design phase, it is essential when the control system has to be designed, while it is useful for monitoring and optimizing the operation of an installation. The constitution of off design performance models is discussed in this chapter. A major problem when producing such models is the constitution of turbo machinery component performance maps. We start by describing the procedure for obtaining such maps using scaling methods. The derivation of the performance models follows.

6.1 Map Scaling Process

The off-design performance of a component is typically predicted by a turbomachinery map, which provides the efficiency and the pressure ratio as a function of flow rate and rotational speed. Even though there are a lot of studies which evaluate and develop prediction models for air conditions, it is considered a relative unexplored topic when the working medium is sCO_2. Jeong et al. ([29], [30]) have already conducted relative research, by evaluating five existing similitude models, to compare their precision accuracy. At first sight, they distinguish Pham's model and propose a modification to overcome the drawback that sCO_2 arises.

The process that will be followed in this thesis, is based on [33] and its initial point is to introduce to the compressor and the turbine some suitable, but not necessarily the actual performance maps, and then use scale factors to scale them. Those factors either multiply the main parameter, when they contain the letter s, or they are being added when they contain the letter a, as underneath:

For the case of the compressor:

$$NcRdes = NcRdesMap * s_{NcRdes_{in}} + a_{NcRdes_{in}} \quad (6.1)$$

$$PR = (PRmap - 1) * s_{mapPR_{in}} + 1 \quad (6.2)$$

$$PRsurge = (PRsurgeMap - 1) * s_{mapPR_{in}} + 1 \tag{6.3}$$

$$eff = effMap * s_{mapEff_{in}} + a_{mapEff_{in}} \tag{6.4}$$

$$Wc = WcMap * s_{mapWc_{in}} + a_{mapWc_{in}} \tag{6.5}$$

Terms that include Map in their name, are data without any correction, as taken from the existing map. $NcRdes$ is the corrected rotational speed relative to design after all corrections. It is defined as:

$$NcRdes = \frac{Nmech}{\sqrt{\theta} NcDes} \tag{6.6}$$

where $Nmech$ is the rotational speed, $\theta = \gamma RT/\gamma_{ref} R_{ref} T_{ref}$ is practically the non-dimensional square of speed of sound and $NcDes$ the corrected rotational speed. PR and $PRsurge$ is the pressure ratio and the surge pressure ratio after the corrections, respectively. Wc is the corrected mass flow rate, defined as:

$$Wc = W\frac{\sqrt{\theta}}{\delta} = W\frac{\sqrt{\gamma RT/\gamma_{ref} R_{ref} T_{ref}}}{p/p_{ref}} \tag{6.7}$$

where $\delta = p/p_{ref}$ is the non-dimensional pressure.

For the turbine $s_{NcRdes_{in}}$ is named as $s_{mapNc_{in}}$ and a ZETA parameter is introduced, which refers to auxiliary coordinates to accommodate map interpolation. ZETA ranges from 0 to 1 and is defined as:

$$ZETA = \frac{PRmap - PRmap_{min}}{PRmap_{max} - PRmap_{min}} \tag{6.8}$$

If $PRmap_{min}$ and $PRmap_{max}$ are taken from the existing map,

$$PRmap = (1 - ZETA) * PRmap_{min} + ZETA * PRmap_{max} \tag{6.9}$$

The rest equations are the same as in case of the compressor. Moreover, for the compressor, BETA lines are introduced, which are curves that have unique intersections with the speed lines and their value range from 0 to 1. Typical unscaled maps are depicted in **Figure 59** and **Figure 60.**

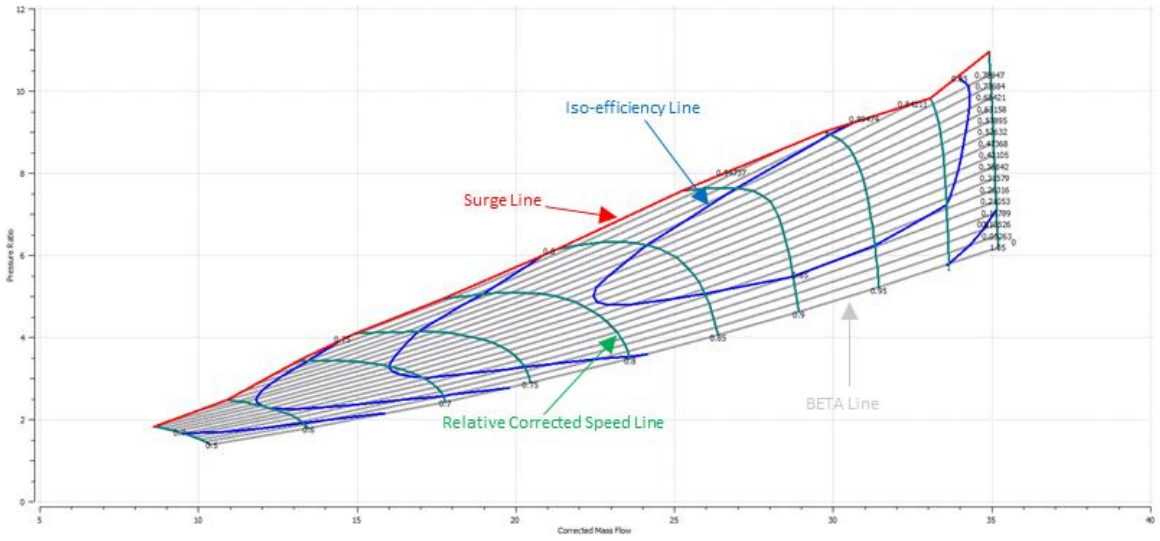

Figure 59. Unscaled map for the compressor.

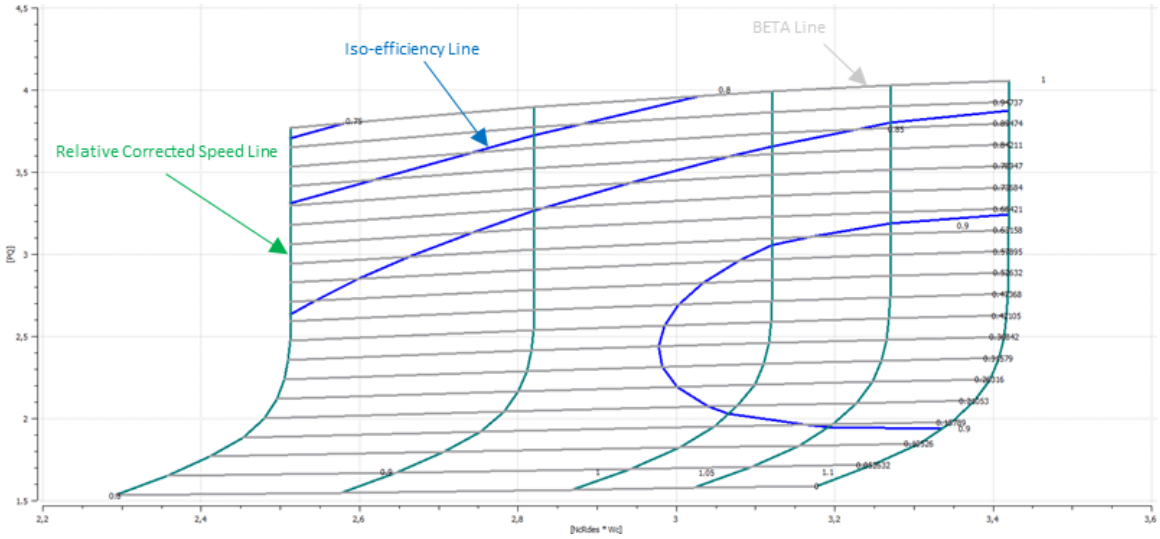

Figure 60. Unscaled map for the turbine.

6.1.1 Map Scaling Experiment

In order to examine how the previous equations operate, a new custom partition is created in PROOSIS, for a compressor and a turbine separately, shown in **Figure 61**. The option to transform data into unknown variables is selected. This allows us to calculate the map scaling factors and the corrected speed at design point which are presented in **Figure 62**. Only *s* type factors are included, neglecting the factors that are being added to the main parameters.

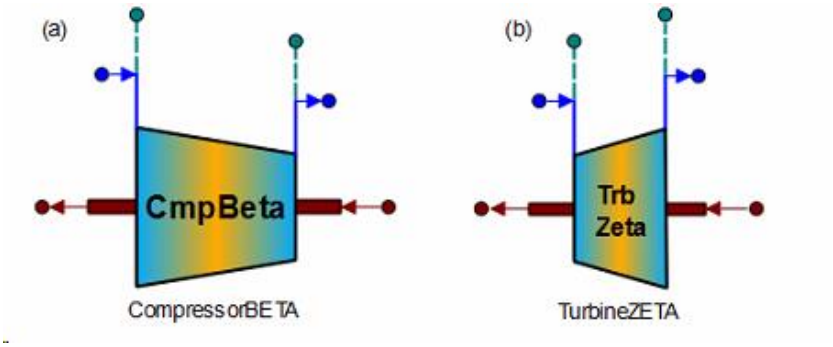

Figure 61. PROOSIS components with performance maps; (a) Compressor, (b) Turbine.

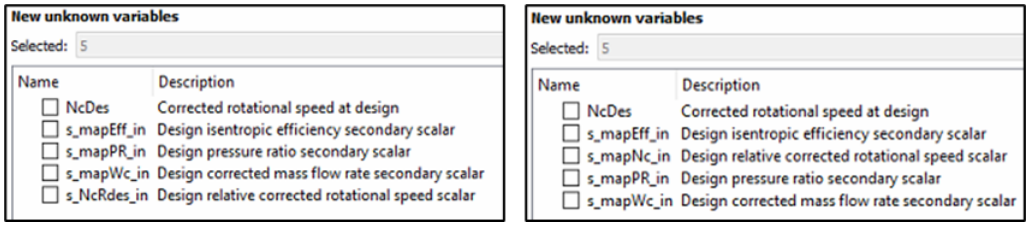

Figure 62. Design variables for compressor and turbine.

The goal of the experiment is to solve for the scaling factors. This is achieved through the following equations (*a* type factors are considered as 0):

$$NcDes = \frac{Nmech}{\sqrt{\theta} NcRDes} \tag{6.10}$$

$$s_{mapWc_{in}} = \frac{Wc - a_{mapWc_{in}}}{WcMap} \tag{6.11}$$

$$s_{mapPR_{in}} = \frac{PR - 1}{PRmap - 1} \tag{6.12}$$

$$s_{mapEff_{in}} = \frac{eff - a_{mapEff_{in}}}{effMap} \tag{6.13}$$

$$s_{mapNc_{in}} = s_{NcRdes_{in}} = \frac{NcRdes - a_{NcRdes_{in}}}{NcRdesMap} \tag{6.14}$$

For the compressor, the boundary variables which are selected, are presented in **Figure 63** with their corresponding value. The same in **Figure 64**, this time for the turbine. $BETA$,

$ZETA$, PR, eff and $NcRdesMap$ are used to determine the map scaling factors and $NcRdes$ is used to calculate $NcDes$.

	Name	Value	Units	
1	BETA	0.5	-	BETA parameter
2	F_in.Pt	101325	Pa	Total tressure
3	F_in.Tt	288.15	K	Total temperature
4	F_in.W	30	kg/s	Total mass flow
5	Me_in.Nmech	5000	rpm	Rotational speed
6	Me_in.inertia	0	kg·m^2	Inertia
7	Me_in.inertia_tot	0	kg·m^2	Overall inertia
8	Me_in.trq	0	N·m	Torque
9	NcRdes	1	-	Corrected rotational speed relative to design after all corrections
10	NcRdesMap	1	-	Corrected rotational speed relative to design before any corrections
11	PR	12	-	Pressure ratio
12	eff	0.9	-	Isentropic efficiency

Figure 63. Values of boundary variables for the component of compressor.

	Name	Value	Units	
1	F_in.Pt	1230000	Pa	Total tressure
2	F_in.Tt	1370	K	Total temperature
3	F_in.W	70	kg/s	Total mass flow
4	Me_in.Nmech	12000	rpm	Rotational speed
5	Me_in.inertia	0	kg·m^2	Inertia
6	Me_in.inertia_tot	0	kg·m^2	Overall inertia
7	Me_in.trq	0	N·m	Torque
8	NcRdes	1	-	Relative corrected speed
9	NcRdesMap	1	-	Relative corrected speed map value
10	PQ	3.8	-	Expansion ratio
11	ZETA	0.5	-	Map auxiliary coordinate
12	eff	0.9	-	Isentropic efficiency

Figure 64. Values of boundary variables for the component of turbine.

If the experiments are simulated in monitor, the results of **Table 15** are obtained. Moreover, the scaled maps for compressor and turbine, are presented in **Figure 65** and **Figure 66** respectively.

Table 15. Values of design variables for the experiments.

Map Scaling Factor	Compressor	Turbine
NcDes	5078.55	5841.88703
s_mapWc_in	0.882068031	3.79545279
s_mapPR_in	1.50443397	1.57459486
s_NcRdes_in / s_mapNc_in	1	1
s_mapEff_in	1.04630631	0.989560785

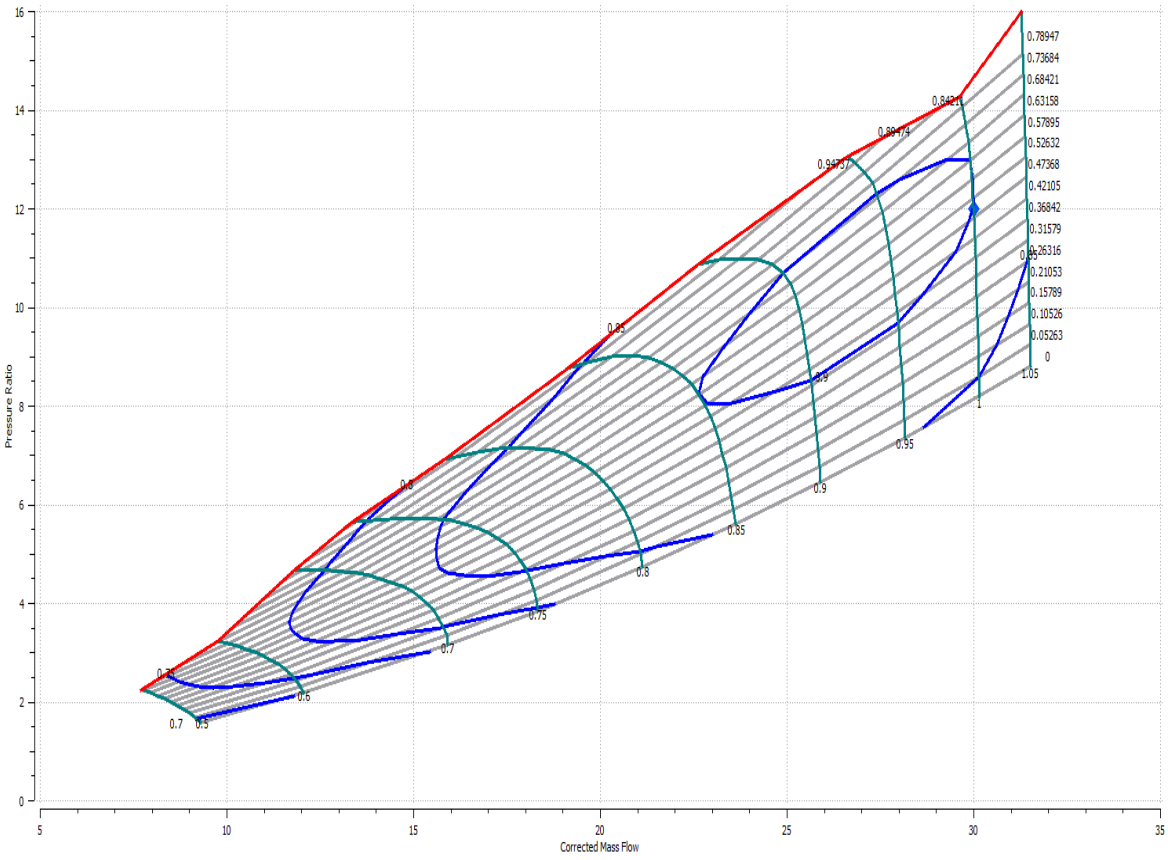

Figure 65. Scaled map for the compressor.

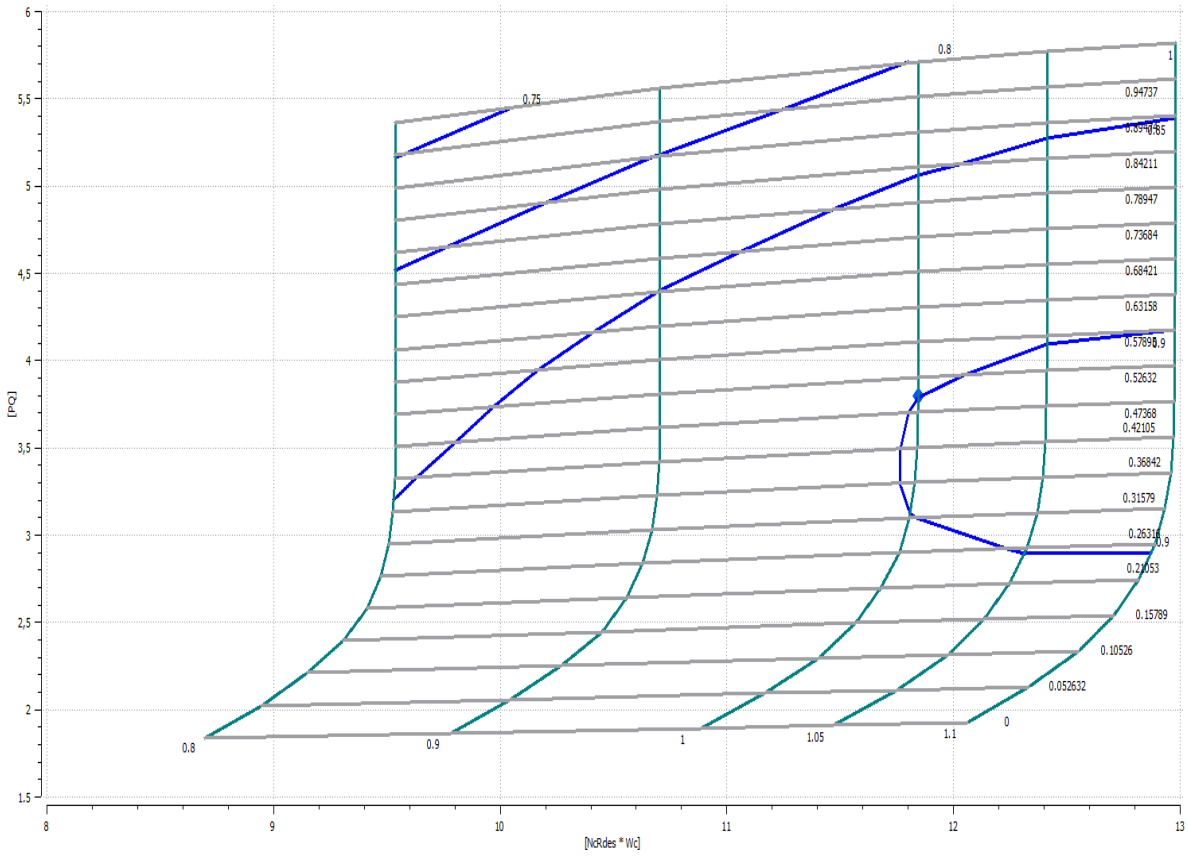

Figure 66. Scaled map for the turbine.

6.2 Off-Design Cycles Analysis

6.2.1 Simple Closed Cycle

The previous scaling process is now performed in closed thermodynamic cycles, starting with the simplest version, which incorporates a compressor, a heater, a turbine and a precooler.

The first goal is to scale the maps for compressor and turbine simultaneously, and to do so, the following procedure is employed. After creating the schematic of a simple closed cycle, shown in **Figure 67**, in which the numeration is not based on SAE Standards since no relative point is considered away from the inlet, a new partition is created in which the option *to transform data into unknown variables* is selected. The new unknown variables are presented in **Figure 68**, which are the combination of scaling factors for the compressor and the turbine in total, plus the design inlet flow capacity for the heater and the precooler.

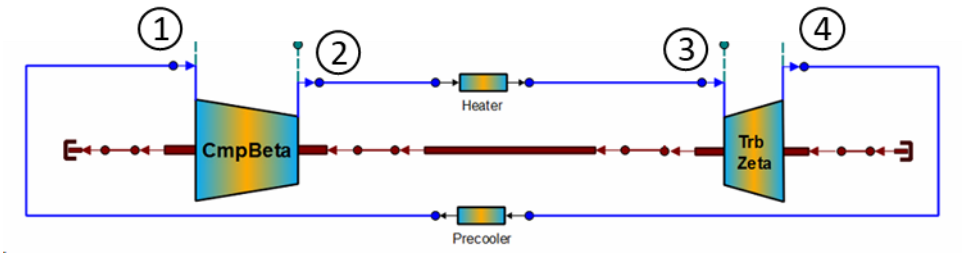

Figure 67. Simple closed cycle for off-design calculations.

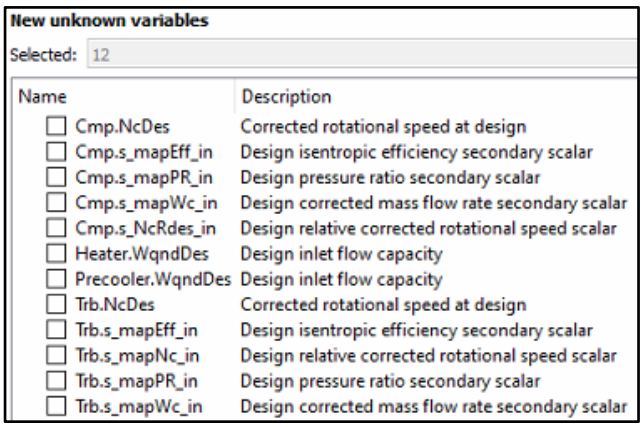

Figure 68. Design variables for the simple closed cycle.

The sixteen required boundary conditions with their respective values can be found in **Figure 69**.

	Name	Value	Units	
1	Cmp.BETA	0.5	-	BETA parameter
2	Cmp.F_in.W	40	kg/s	Total mass flow
3	Cmp.Me_in.Nmech	50000	rpm	Rotational speed
4	Cmp.NcRdes	1	-	Corrected rotational speed relative to design after all corrections
5	Cmp.NcRdesMap	1	-	Corrected rotational speed relative to design before any corrections
6	Cmp.PR	3	-	Pressure ratio
7	Cmp.eff	0.8	-	Isentropic efficiency
8	Cmp.fInfo_in.Pt	7.8*1e6	Pa	Total pressure
9	Cmp.fInfo_in.Tt	306.15	K	Total temperature
10	Heater.dPqP	0.01	-	Fractional pressure loss
11	Precooler.dPqP	0.01	-	Fractional pressure loss
12	Trb.NcRdes	1	-	Relative corrected speed
13	Trb.NcRdesMap	1	-	Relative corrected speed map value
14	Trb.ZETA	0.5	-	Map auxiliary coordinate
15	Trb.eff	0.9	-	Isentropic efficiency
16	Trb.fInfo_in.Tt	823.15	K	Total temperature

Figure 69. Values of boundary variables for the simple closed cycle.

The scaling factors and the design inlet flows of **Figure 70** are the results of the experiment.

Variable	Value	Units
Cmp.NcDes	70557.9834	rpm
Cmp.s_mapEff_in	0.930050056	-
Cmp.s_mapPR_in	0.273533449	-
Cmp.s_mapWc_in	0.0109965513	-
Cmp.s_NcRdes_in	1	-
Heater.WqndDes	0.26743379	
Precooler.WqndDes	0.772969142	
Trb.NcDes	29066.6633	rpm
Trb.s_mapEff_in	0.989560785	-
Trb.s_mapNc_in	1	-
Trb.s_mapPR_in	1.091138	-
Trb.s_mapWc_in	0.0964331464	-

Figure 70. Values of design variables for the closed cycle experiment.

After calculating the scaling factors and the design inlet flow capacities for the ducts, they can be used for further analysis of the cycle. This can be done by entering the values in the relevant components of the schematic manually, or by using a Restore State Calculation, which reads the report file of the Scale Factor calculation and adds them on the cases that follow, which makes the process more automatic.

Now that the maps for the compressor and the turbine are known, the next step is to declare the inlet conditions $\boldsymbol{T_{t1}}$, $\boldsymbol{p_{t1}}$, a constant rotating speed $\boldsymbol{Nmech}$ and the inlet temperature of the turbine $\boldsymbol{T_{t3}}$.

The equations for the off-design calculations are presented below and they are based on **Figure 67**:

The known inlet conditions allow the calculation of the other thermodynamic properties of Point 1:

$$s_{t1} = f(T_{t1}, p_{t1}) = s_{t2,is} \tag{6.15}$$

$$h_{t1} = f(T_{t1}, p_{t1}) \tag{6.16}$$

The corrected rotational speed relative to design of the compressor can be calculated through:

$$Cmp.NcRdes = \frac{Nmech}{\sqrt{\theta} Cmp.NcDes} = \frac{Nmech}{\sqrt{f(T_{t1}, p_{t1}) \Big/ \gamma_{ref} R_{ref} T_{ref}}\, Cmp.NcDes} \tag{6.17}$$

and then the corrected rotational speed before all the corrections:

$$Cmp.NcRdesMap = \frac{Nmech}{\frac{\sqrt{f(T_{t1}, p_{t1})}}{\gamma_{ref} R_{ref} T_{ref}}\, Cmp.NcDes}{Cmp.s_{NcRdes_{in}}} \tag{6.18}$$

For the compressor, the parameters of the original performance map, before the scaling process, are a function of $Cmp.NcRdesMap$ and $BETA$.

$$Cmp.WcMap = f(Cmp.NcRdesMap, BETA) \tag{6.19}$$

$$Cmp.effMap = f(Cmp.NcRdesMap, BETA) \tag{6.20}$$

$$Cmp.PRmap = f(Cmp.NcRdesMap, BETA) \tag{6.21}$$

By selecting the $\boldsymbol{BETA}$ parameter, mass flow rate, efficiency and pressure ratio of the compressor can be calculated.

$$Cmp.Wc = Cmp.WcMap * Cmp.s_{mapWc_{in}} \tag{6.22}$$

$$W = \frac{Cmp.Wc * \delta}{\sqrt{\theta}} = \frac{Cmp.Wc * {p_{t1}}/{p_{ref}}}{\sqrt{\frac{f(T_{t1}, p_{t1})}{\gamma_{ref} R_{ref} T_{ref}}}} \tag{6.23}$$

$$Cmp.eff = Cmp.effMap * Cmp.s_{mapEff_{in}} \tag{6.24}$$

$$Cmp.PR = (Cmp.PRmap - 1) * Cmp.s_{mapPR_{in}} + 1 \tag{6.25}$$

The know pressure ratio, allows the calculation of the pressure at the exit of the compressor:

$$p_{t2} = PR * p_{t1} \tag{6.26}$$

The known pressure p_{t2} and specific entropy $s_{t2,is}$, allow us to calculate the temperature and the specific enthalpy, if the compression was isentropic, since:

$$T_{t2,is} = f(s_{t2,is}, p_{t2}) \quad h_{t2,is} = f(T_{t2,is}, p_{t2}) \tag{6.27}$$

Now, h_{t2} can be calculated from isentropic efficiency definition for compressors:

$$h_{t2} = h_{t1} + \frac{h_{t2,is} - h_{t1}}{Cmp.eff} \tag{6.28}$$

and the total temperature from:

$$T_{t2} = f(h_{t2}, p_{t2}) \tag{6.29}$$

The inlet flow capacity of the heater and the relevant pressure loss can be calculated, through the following pressure loss model, by defining an input fractional pressure loss $dPqP_{in}$:

$$Heater.Wqnd = W \frac{\sqrt{f(T_{t2}, p_{t2}) / \gamma_{ref} R_{ref} T_{ref}}}{p_{t2} / p_{ref}} \tag{6.30}$$

$$Heater.dPqP = dPqP_{in} \left(\frac{Heater.Wqnd}{Heater.WqndDes} \right)^2 \tag{6.31}$$

The pressure at the exit of the heater, which is the same as at the inlet of the turbine can now be evaluated:

$$p_{t3} = (1 - Heater.dPqP) p_{t2} \tag{6.32}$$

In addition, for the inlet of the turbine:

$$s_{t3} = f(T_{t3}, p_{t3}) = s_{t4,is} \tag{6.33}$$

$$h_{t3} = f(T_{t3}, p_{t3}) \tag{6.34}$$

Which allows the calculation of δ for the turbine:

$$Trb.\delta = \frac{p_{t3}}{p_{ref}} \tag{6.35}$$

Moreover, the corrected rotational speed relative to design can also be calculated for the turbine:

$$Trb.NcRdes = \frac{Nmech}{\sqrt{\theta} Trb.NcDes} = \frac{Nmech}{\sqrt{f(T_{t3}, p_{t3}) / \gamma_{ref} R_{ref} T_{ref}}\, Trb.NcDes} \tag{6.36}$$

and then the corrected rotational speed before all the corrections:

$$Trb.NcRdesMap = \frac{Trb.NcRdes}{Trb.s_{NcRdes_{in}}} \tag{6.37}$$

Moreover the variables $Trb.PRmap_{min}$ and $Trb.PRmap_{max}$ which are needed for the calculation of $ZETA$, can be found since they are a function of the $Trb.NcRdesMap$.

$$Trb.PRmap_{min} = f(NcRdesMap) \tag{6.38}$$

$$Trb.PRmap_{max} = f(NcRdesMap) \tag{6.39}$$

By selecting the $\boldsymbol{ZETA}$ parameter, the mass flow rate before any corrections can be calculated:

$$Trb.WcMap = f(Trb.NcRdesMap, ZETA) \tag{6.40}$$

then the mass flow rate of the turbine:

$$Trb.Wc = Trb.WcMap * s_{mapWc_{in}} \tag{4.41}$$

However, $Trb.\delta$ can also be calculated from the following function:

$$Trb.\delta = W\frac{\sqrt{f(T_{t3}, p_{t3})/\gamma_{ref}R_{ref}T_{ref}}}{Trb.Wc} \tag{6.42}$$

The two different ways of $Trb.\delta$ lead to the first residual equation, for the $BETA$ parameter

$$error_B = \left| W\frac{\sqrt{f(T_{t3}, p_{t3})/\gamma_{ref}R_{ref}T_{ref}}}{Trb.Wc} - \frac{p_{t3}}{p_{ref}} \right| < \varepsilon \tag{6.43}$$

The known $ZETA$ parameter, allows us to proceed to the following calculations for the pressures and the efficiency.

$$Trb.effMap = f(Trb.NcRdesMap, ZETA) \tag{6.44}$$

$$Trb.eff = Trb.effMap * Trb.s_{mapEff_{in}} \tag{6.45}$$

$$Trb.PRmap = ZETA(Trb.PRmap_{max} - Trb.PRmap_{min}) + Trb.PRmap_{min} \tag{6.46}$$

$$Trb.PQ = Trb.s_{mapPR_{in}} * (Trb.PRmap - 1) + 1 \tag{6.47}$$

$$p_{t4} = \frac{p_{t3}}{Trb.PQ} \tag{6.48}$$

$$Precooler.dPqP = 1 - \frac{p_{t1}}{p_{t4}} \tag{6.49}$$

The known pressure p_{t4} and specific entropy $s_{t4,is}$, allow us to calculate the temperature and the specific enthalpy, if the expansion was isentropic, since:

$$T_{t4,is} = f(s_{t4,is}, p_{t4}) \quad h_{t4,is} = f(T_{t4,is}, p_{t4}) \tag{6.50}$$

Now h_{t4} can be calculated from isentropic efficiency definition for turbines:

$$h_{t4} = h_{t3} - Trb.eff(h_{t3} - h_{t4,is}) \tag{6.51}$$

And the total temperature is:

$$T_{t4} = f(h_{t4}, p_{t4}) h_{t4,is} = f(T_{t4,is}, p_{t4}) \tag{6.52}$$

Finally, the inlet flow capacity of the precooler and the pressure loss fraction can be calculated from the two following equations:

$$Precooler.Wqnd = W \frac{\sqrt{f(T_{t4}, p_{t4}) / \gamma_{ref} R_{ref} T_{ref}}}{p_{t4} / p_{ref}} \tag{6.53}$$

$$Precooler.dPqP = dPqP_{in} \left(\frac{Precooler.Wqnd}{Precooler.WqndDes} \right)^2 \tag{6.54}$$

which create the residual equation for the $ZETA$:

$$error_Z = \left| 1 - \frac{p_{t1}}{p_{t4}} - dPqP_{in} \left(\frac{Precooler.Wqnd}{Precooler.WqndDes} \right)^2 \right| < \varepsilon \tag{6.55}$$

If Equations 6.43 and 6.55 are satisfied simultaneously, the previous iteration process is converged, and every other parameter of the cycle can be calculated. Otherwise, different values for $BETA$ or $ZETA$ must be selected.

For example, a parametric study can be carried out, for given inlet conditions and rotational speed, while the inlet temperature of the turbine varies. The design point of this study is when $T_{t3} = 823.15K$. The selected conditions are presented in **Table 16**.

Table 16. Conditions for off-design calculations of the simple closed cycle.

T_{t1} [K]	306.15
p_{t1} [MPa]	7.8
$Nmech$ [RPM]	50000
T_{t3} [K]	723.15 : 50 : 1023.15

The following diagrams are obtained, starting with the operation lines on the performance map for the compressor and the turbine in **Figure 71** and **Figure 72** respectively.

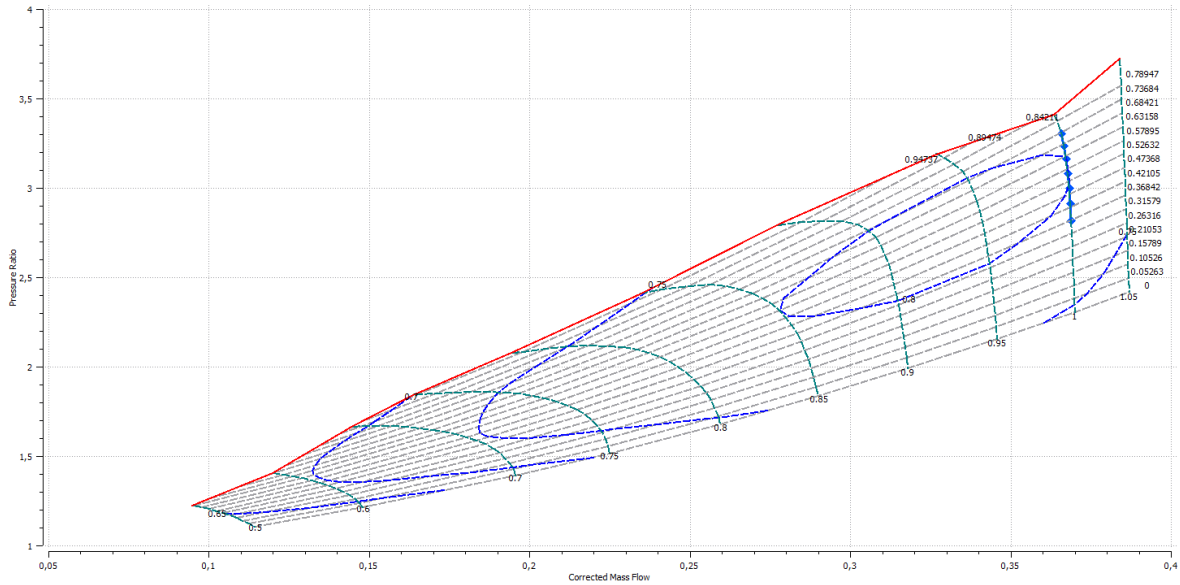

Figure 71. Scaled performance map for the compressor in a simple closed cycle.

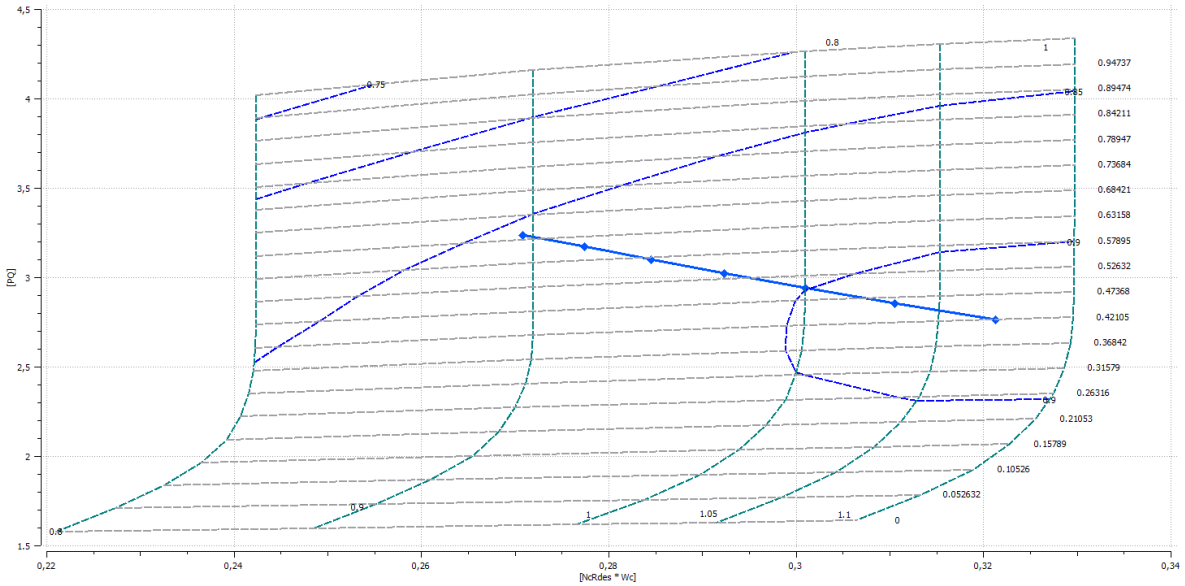

Figure 72. Scaled performance map for the turbine in a simple closed cycle.

In addition, diagrams concerning the efficiency and the power of the turbomachinery (**Figure 73** and **Figure 74**), the total efficiency of the cycle (**Figure 75**), the mass flow rate and the pressure ratio of the compressor (**Figure 76**), and the fractional pressure loss of the ducts (**Figure 77**), are presented below as a function of turbine inlet temperature.

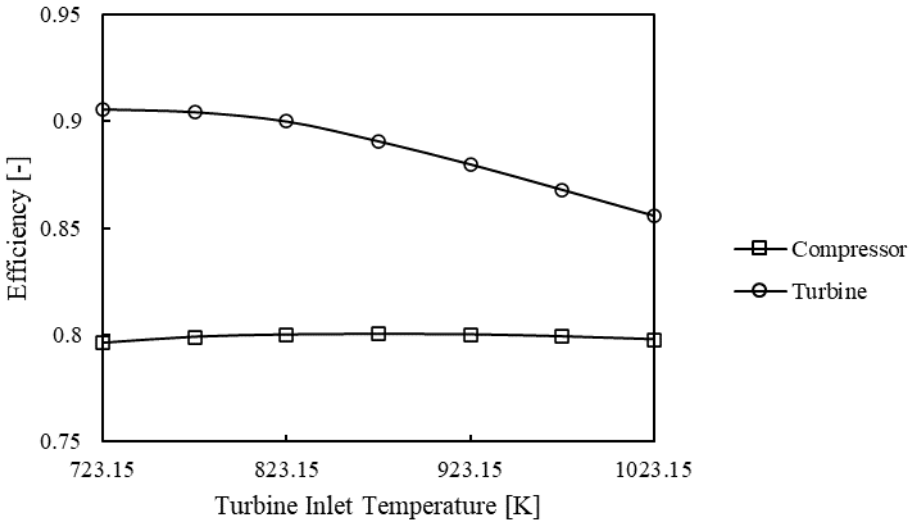

Figure 73. Efficiency of the turbomachinery in an off-design simple closed cycle.

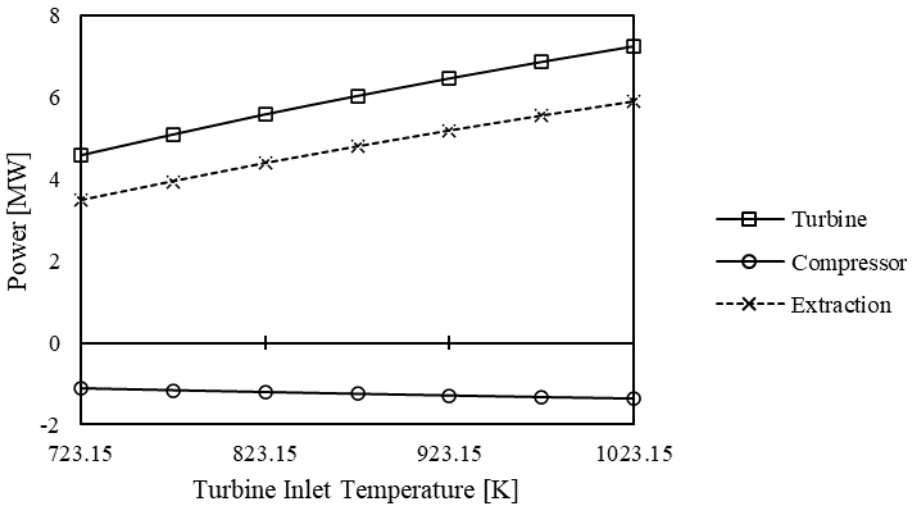

Figure 74. Power of the turbomachinery and power extraction in an off-design simple closed cycle.

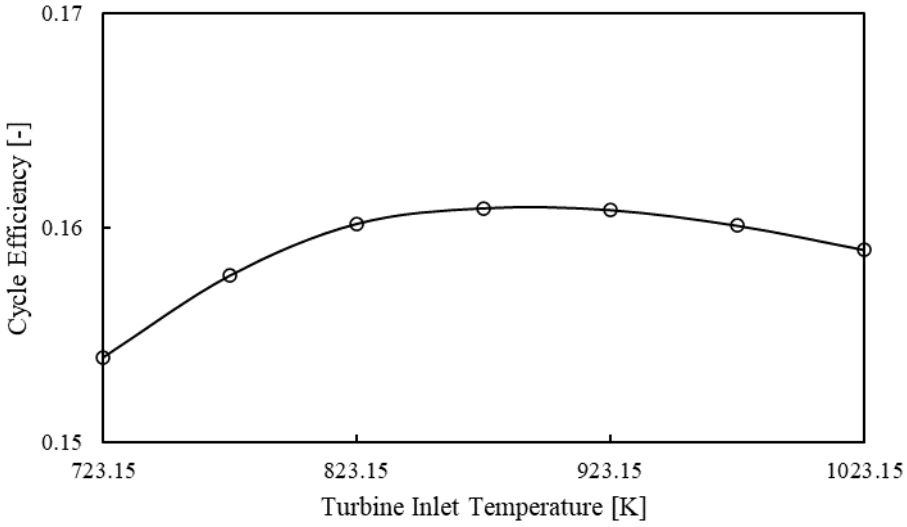

Figure 75. Total efficiency of a simple closed cycle in off-design calculations.

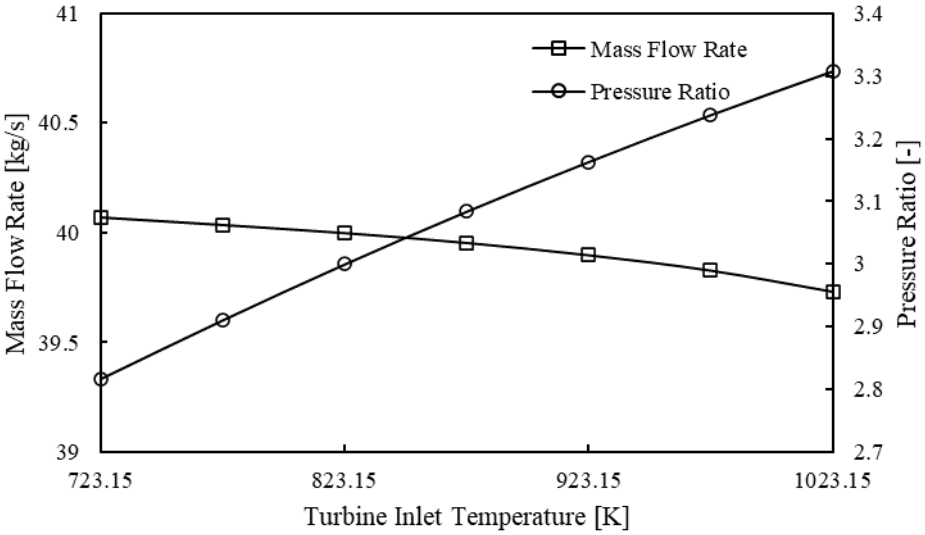

Figure 76. Mass flow rate and pressure ratio of the compressor in an off-design simple closed cycle.

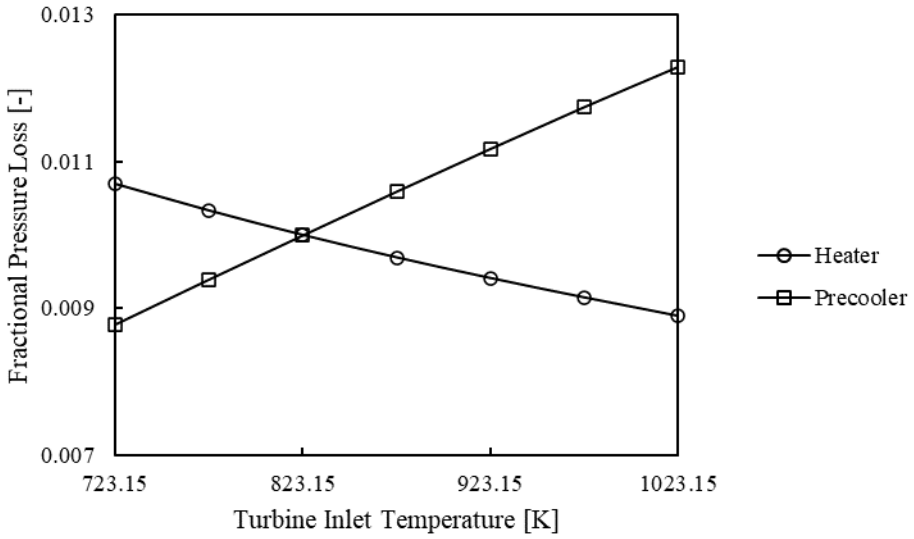

Figure 77. Fractional pressure loss of the heat exchangers in an off-design simple closed cycle.

6.2.2 Recuperated Closed Cycle

The same process is also performed for the recuperated closed cycle of **Figure 78**. The first step is to scale the maps for compressor and turbine simultaneously. A new partition is created in which the option *to transform data into unknown variables* is selected. The new unknown variables are presented in **Figure 79**, which are the combination of scaling factors

for the compressor and the turbine in total, plus the design inlet flow capacity for the heater, the precooler and the two streams of the recuperator.

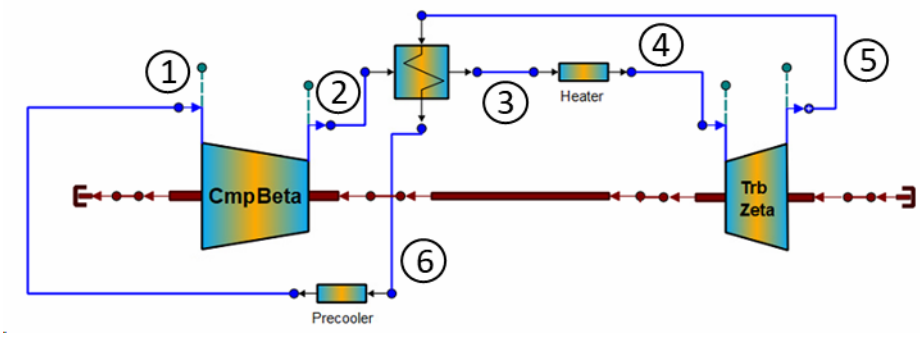

Figure 78. Recuperated closed cycle for off-design calculations.

New unknown variables

Selected: 14

Name	Description
Cmp.NcDes	Corrected rotational speed at design
Cmp.s_mapEff_in	Design isentropic efficiency secondary scalar
Cmp.s_mapPR_in	Design pressure ratio secondary scalar
Cmp.s_mapWc_in	Design corrected mass flow rate secondary scalar
Cmp.s_NcRdes_in	Design relative corrected rotational speed scalar
Heater.WqndDes	Design inlet flow capacity
Precooler.WqndDes	Design inlet flow capacity
Rec.WqndDesG	Design inlet flow capacity fo the secondary stream
Rec.WqndDesR	Design inlet flow capacity for the main stream
Trb.NcDes	Corrected rotational speed at design
Trb.s_mapEff_in	Design isentropic efficiency secondary scalar
Trb.s_mapNc_in	Design relative corrected rotational speed scalar
Trb.s_mapPR_in	Design pressure ratio secondary scalar
Trb.s_mapWc_in	Design corrected mass flow rate secondary scalar

Figure 79. Design variables for the recuperated closed cycle.

The eighteen required boundary conditions with their respective values can be found in **Figure 80.**

	Name	Value	Units	
1	Cmp.BETA	0.5	-	BETA parameter
2	Cmp.Me_in.Nmech	50000	rpm	Rotational speed
3	Cmp.NcRdes	1	-	Corrected rotational speed relative to design after all corrections
4	Cmp.NcRdesMap	1	-	Corrected rotational speed relative to design before any corrections
5	Cmp.PR	3	-	Pressure ratio
6	Cmp.eff	0.8	-	Isentropic efficiency
7	Cmp.flnfo_in.Pt	7.8 * 1e6	Pa	Total pressure
8	Cmp.flnfo_in.Tt	306.15	K	Total temperature
9	Heater.F_in.W	40	kg/s	Total mass flow
10	Heater.dPqP	0.01	-	Fractional pressure loss
11	Precooler.dPqP	0.01	-	Fractional pressure loss
12	Rec.dPqPrr	0.01	-	Fractional pressure loss
13	Rec.dPqPrrG	0.01	-	Fractional pressure loss of the exhaust gas stream
14	Trb.NcRdes	1	-	Relative corrected speed
15	Trb.NcRdesMap	1	-	Relative corrected speed map value
16	Trb.ZETA	0.5	-	Map auxiliary coordinate
17	Trb.eff	0.9	-	Isentropic efficiency
18	Trb.flnfo_in.Tt	823.15	K	Total temperature

Figure 80. Values of boundary variables for the recuperated closed cycle.

The scaling factors and the design inlet flows of **Figure 81** are the results of the experiment.

Variable	Value	Units
Cmp.NcDes	70557.9834	rpm
Cmp.s_mapEff_in	0.930050056	-
Cmp.s_mapPR_in	0.273533449	-
Cmp.s_mapWc_in	0.0109965513	-
Cmp.s_NcRdes_in	1	-
Heater.WqndDes	0.263118632	
Precooler.WqndDes	0.449694493	
Rec.WqndDesG	0.766656394	
Rec.WqndDesR	0.26743379	
Trb.NcDes	29091.7676	rpm
Trb.s_mapEff_in	0.989560785	-
Trb.s_mapNc_in	1	-
Trb.s_mapPR_in	1.05823349	-
Trb.s_mapWc_in	0.0973231625	-

Figure 81. Values of design variables for the recuperated cycle experiment.

After calculating the scaling factors and the design inlet flow capacities for the ducts and the recuperator, they can be used for further analysis of the cycle. This can be done by entering the values in the relevant components of the schematic manually, or by using a Restore State Calculation, which reads the report file of the Scale Factor calculation and adds them on the cases that follow, which makes the process more automatic.

Now that the maps for the compressor and the turbine are known, the next step is to declare the inlet conditions $\boldsymbol{T_{t1}}$, $\boldsymbol{p_{t1}}$, a constant rotating speed $\boldsymbol{Nmech}$ and the inlet temperature of the turbine $\boldsymbol{T_{t4}}$.

A similar set of equation, as in case of the simple closed cycle, describes the recuperated configuration. For the sake of simplicity, only the iteration loop will be presented, since the first equations are the same as before.

By selecting the $\boldsymbol{BETA}$ parameter, mass flow rate, efficiency and pressure ratio of the compressor can be calculated.

$$Cmp.Wc = Cmp.WcMap * Cmp.s_{mapWc_{in}} \tag{6.56}$$

$$W = \frac{Cmp.Wc * \delta}{\sqrt{\theta}} = \frac{Cmp.Wc * {p_{t1}}/{p_{ref}}}{\sqrt{{f(T_{t1}, p_{t1})}/{\gamma_{ref} R_{ref} T_{ref}}}} \tag{6.57}$$

$$Cmp.eff = Cmp.effMap * Cmp.s_{mapEff_{in}} \tag{6.58}$$

$$Cmp.PR = (Cmp.PRmap - 1) * Cmp.s_{mapPR_{in}} + 1 \tag{6.59}$$

The know pressure ratio, allows the calculation of the pressure at the exit of the compressor:

$$p_{t2} = PR * p_{t1} \tag{6.60}$$

The known pressure p_{t2} and specific entropy $s_{t2,is}$, allow us to calculate the temperature and the specific enthalpy, if the compression was isentropic, since:

$$T_{t2,is} = f(s_{t2,is}, p_{t2}) \quad h_{t2,is} = f(T_{t2,is}, p_{t2}) \tag{6.61}$$

Now, h_{t2} can be calculated from isentropic efficiency definition for compressors:

$$h_{t2} = h_{t1} + \frac{h_{t2,is} - h_{t1}}{Cmp.eff} \tag{6.62}$$

and the total temperature from:

$$T_{t2} = f(h_{t2}, p_{t2}) \tag{6.63}$$

The inlet flow capacity of the cold stream of the recuperator and the relevant pressure loss can be calculated, by defining an input fractional pressure loss $dPqP_{in}$:

$$Rec.WqndR = W \frac{\sqrt{f(T_{t2}, p_{t2}) / \gamma_{ref} R_{ref} T_{ref}}}{p_{t2} / p_{ref}} \tag{6.64}$$

$$Rec.dPqPrr = dPqPrr_{in} \left(\frac{Rec.WqndR}{Rec.WqndDesR} \right)^2 \tag{6.65}$$

The pressure at the exit of the cold stream of the recuperator, which is the same as at the inlet of the heater can now be evaluated:

$$p_{t3} = (1 - Rec.dPqPrr) p_{t2} \tag{6.66}$$

By selecting the $\boldsymbol{p_{t4}}$ parameter, the following variables can be calculated:

$$Heater.dPqP = 1 - \frac{p_{t4}}{p_{t3}} \tag{6.67}$$

For the inlet of the turbine:

$$s_{t4} = f(T_{t4}, p_{t4}) = s_{t5,is} \tag{6.68}$$

$$h_{t4} = f(T_{t4}, p_{t4}) \tag{6.69}$$

The corrected rotational speed relative to design can also be calculated for the turbine:

$$Trb.NcRdes = \frac{Nmech}{\sqrt{\theta} Trb.NcDes} = \frac{Nmech}{\sqrt{f(T_{t4}, p_{t4}) / \gamma_{ref} R_{ref} T_{ref}}\, Trb.NcDes} \tag{6.70}$$

and then the corrected rotational speed before all the corrections is:

$$Trb.NcRdesMap = \frac{Trb.NcRdes}{Trb.s_{NcRdes_{in}}} \tag{6.71}$$

Moreover the variables $Trb.PRmap_{min}$ and $Trb.PRmap_{max}$ which are needed for the calculation of $ZETA$, can be found since they are a function of the $Trb.NcRdesMap$.

$$Trb.PRmap_{min} = f(NcRdesMap) \tag{6.72}$$

$$Trb.PRmap_{max} = f(NcRdesMap) \tag{6.73}$$

By selecting the $\boldsymbol{ZETA}$ parameter, the following variables can be calculated:

$$Trb.WcMap = f(Trb.NcRdesMap, ZETA) \tag{6.74}$$

$$Trb.Wc = Trb.WcMap * Trb.s_{mapWc_{in}} \tag{6.75}$$

$$Trb.\delta = W\frac{\sqrt{f(T_{t4}, p_{t4})/\gamma_{ref}R_{ref}T_{ref}}}{Trb.Wc} \tag{6.76}$$

$$Trb.\delta = \frac{p_{t4}}{p_{ref}} \tag{6.77}$$

This leads to two equations for the calculation of $Trb.\delta$, which lead to the first residual equation for the $BETA$ variable:

$$error_B = \left| W\frac{\sqrt{f(T_{t4}, p_{t4})/\gamma_{ref}R_{ref}T_{ref}}}{Trb.Wc} - \frac{p_{t4}}{p_{ref}} \right| < \varepsilon \tag{6.78}$$

The known $ZETA$ parameter, allows us to proceed to the following calculations for the pressures and the efficiency.

$$Trb.effMap = f(Trb.NcRdesMap, ZETA) \tag{6.79}$$

$$Trb.eff = Trb.effMap * Trb.s_{mapEff_{in}} \tag{6.80}$$

$$Trb.PRmap = ZETA(Trb.PRmap_{max} - Trb.PRmap_{min}) + Trb.PRmap_{min} \tag{6.81}$$

$$Trb.PQ = Trb.s_{mapPR_{in}} * (Trb.PRmap - 1) + 1 \tag{6.82}$$

$$p_{t5} = \frac{p_{t4}}{Trb.PQ} \tag{6.83}$$

The known pressure p_{t5} and specific entropy $s_{t5,is}$, allow us to calculate the temperature and the specific enthalpy, if the expansion was isentropic, since:

$$T_{t5,is} = f(s_{t5,is}, p_{t5}) \quad h_{t5,is} = f(T_{t5,is}, p_{t5}) \tag{6.84}$$

Now h_{t5} can be calculated from isentropic efficiency definition for turbines:

$$h_{t5} = h_{t4} - Trb.eff\left(h_{t4} - h_{t5,is}\right) \tag{6.85}$$

And the total temperature is:

$$T_{t5} = f(h_{t5}, p_{t5}) \tag{6.86}$$

The inlet temperature of the heater can be calculated from the given effectiveness of the recuperator:

$$T_{t3} = Rec.eff(T_{t5} - T_{t2}) + T_{t2} \tag{6.87}$$

and as a result, the inlet flow capacity of the heater:

$$Heater.Wqnd = W\frac{\sqrt{f(T_{t3}, p_{t3})/\gamma_{ref}R_{ref}T_{ref}}}{p_{t3}/p_{ref}} \tag{6.88}$$

Apart from Eq. 6.67, the fractional pressure loss of the heater can be calculated from:

$$Heater.dPqP = dPqP_{in}\left(\frac{Heater.Wqnd}{Heater.WqndDes}\right)^2 \tag{6.89}$$

which lead to a residual equation for the $ZETA$ variable:

$$error_Z = \left|1 - \frac{p_{t4}}{p_{t3}} - dPqP_{in}\left(\frac{Heater.Wqnd}{Heater.WqndDes}\right)^2\right| < \varepsilon \tag{6.90}$$

Afterwards, the energy balance of the recuperator is utilized:

$$h_{t3} = f(T_{t3}, p_{t3}) \quad h_{t5} = f(T_{t5}, p_{t5}) \tag{6.91}$$

$$h_{t6} = h_{t2} + h_{t5} - h_{t3} \tag{6.92}$$

And the inlet flow capacity and fractional pressure loss for the hot stream are calculated:

$$Rec.WqndG = W\frac{\sqrt{f(T_{t5},p_5)/\gamma_{ref}R_{ref}T_{ref}}}{p_{t5}/p_{ref}} \quad (6.93)$$

$$Rec.dPqPrrG = dPqPrrG_{in}\left(\frac{Rec.WqndG}{Rec.WqndDesG}\right)^2 \quad (6.94)$$

The third residual equation for the $\boldsymbol{p_{t4}}$ parameter is defined from the precooler:

$$p_{t6} = p_{t5}(1 - Rec.dPqPrrG) \quad (6.95)$$

$$Precooler.dPqP = 1 - \frac{p_{t1}}{p_{t6}} \quad (6.96)$$

$$T_{t6} = f(h_{t6}, p_{t6}) \quad (6.97)$$

$$Precooler.Wqnd = W\frac{\sqrt{f(T_{t6},p_6)/\gamma_{ref}R_{ref}T_{ref}}}{p_{t6}/p_{ref}} \quad (6.98)$$

$$Precooler.dPqP = dPqP_{in}\left(\frac{Precooler.Wqnd}{Precooler.WqndDes}\right)^2 \quad (6.99)$$

The two previous equations for the calculation of $Precooler.dPqP$ lead to:

$$error_{p_{t4}} = \left|1 - \frac{p_{t1}}{p_{t6}} - dPqP_{in}\left(\frac{Precooler.Wqnd}{Precooler.WqndDes}\right)^2\right| < \varepsilon \quad (6.100)$$

If Equations 6.78, 6.90, 6.100 are satisfied simultaneously, the previous iteration process is converged, and every other parameter of the cycle can be calculated. Otherwise, different values for $BETA$, $ZETA$ or p_{t4} must be selected.

For example, a parametric study can be carried out, for given inlet conditions and rotational speed, while the inlet temperature of the turbine varies. The design point of this study is when $T_{t4} = 823.15K$. The selected conditions are presented in **Table 17**.

Table 17. Conditions for off-design calculations of the recuperated cycle.

T_{t1} [K]	306.15
p_{t1} [MPa]	7.8
$Nmech$ [RPM]	50000
T_{t4} [K]	723.15 : 50 : 1023.15

The following diagrams are obtained, starting with the operation lines on the performance map for the compressor and the turbine in **Figure 82** and **Figure 83** respectively.

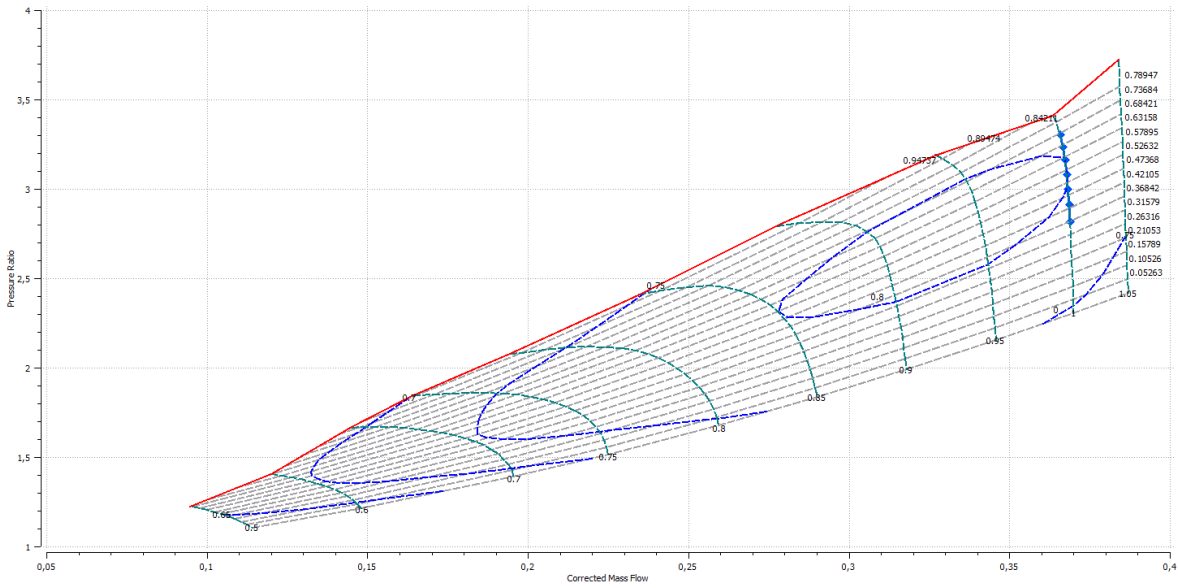

Figure 82. Scaled performance map for the compressor in a recuperated closed cycle.

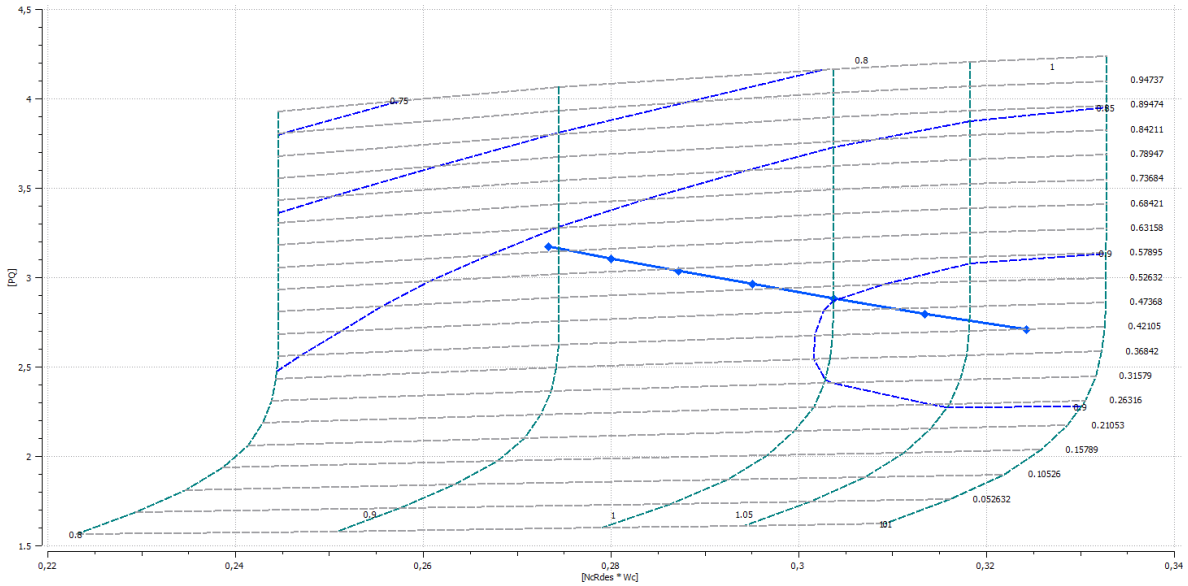

Figure 83. Scaled performance map for the turbine in a recuperated closed cycle.

In addition, diagrams concerning the efficiency and the power of the turbomachinery (**Figure 84** and **Figure 85**), the total efficiency of the cycle (**Figure 86**), the mass flow rate and the pressure ratio of the compressor (**Figure 87**), and the fractional pressure loss of the ducts and the recuperator (**Figure 88**), are presented below as a function of turbine inlet temperature.

Between the following diagrams, the impact of the recuperator is illustrated in the efficiency of the cycle (**Figure 86**) if it is compared to the efficiency of the cycle without the recuperator (**Figure 73**). The efficiency of the turbomachinery, the mass flow rate and the pressure ratio are almost the same. Moreover, by examining **Figure 74** and **Figure 85**, we note that the power extraction among the two cycles is comparable. This leads to the conclusion that the installation of a recuperator reduces the heat that needs to be added to the cycle. Taking into account the definition of the cycle's efficiency and the values of **Figure 73** and **Figure 86**, the recuperator reduces the added heat by almost three times, demonstrating its significance.

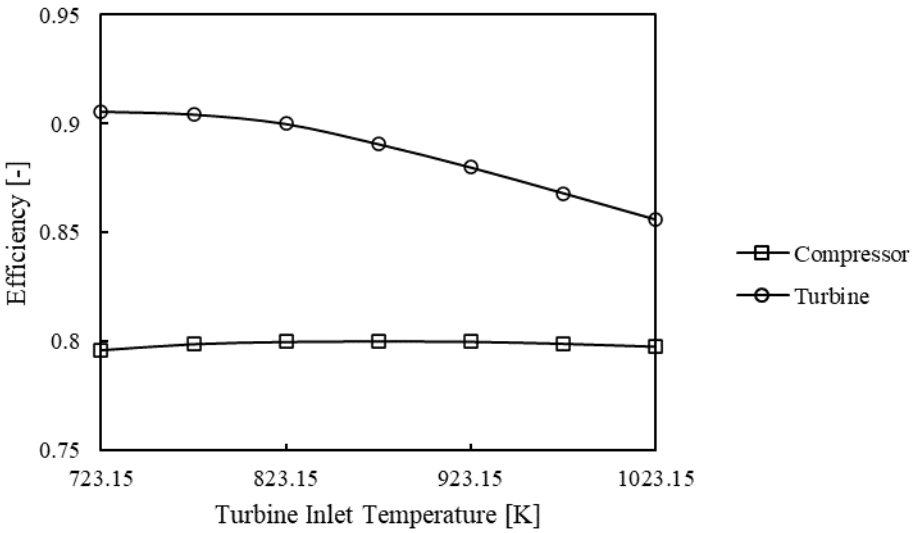

Figure 84. Efficiency of the turbomachinery in an off-design recuperated closed cycle.

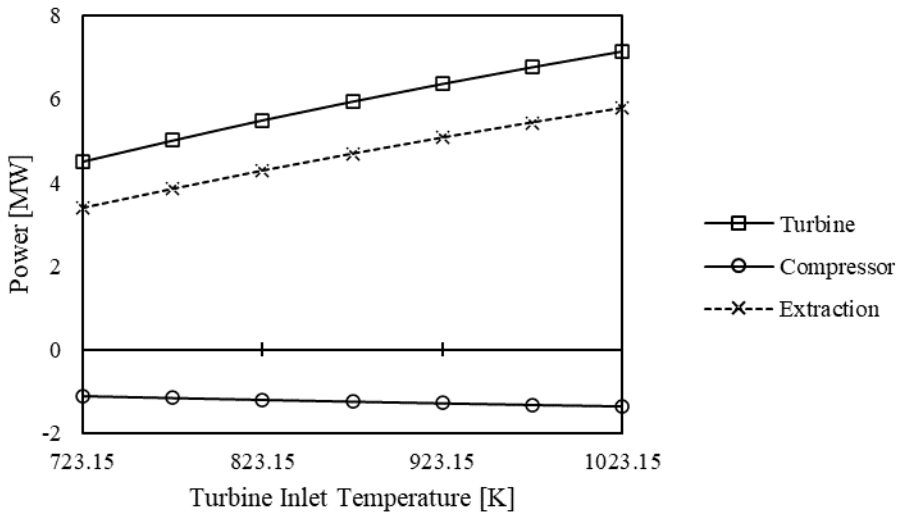

Figure 85. Power of the turbomachinery and power extraction in an off-design recuperated closed cycle.

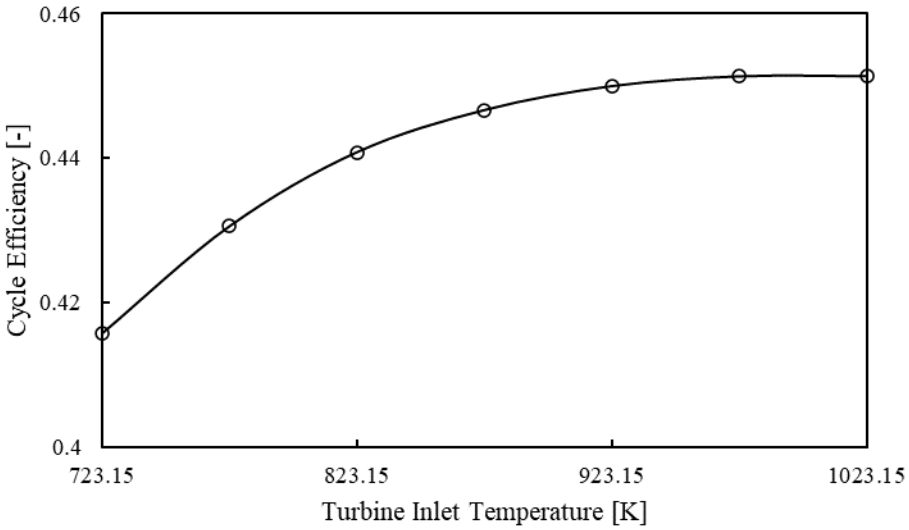

Figure 86. Total efficiency of a recuperated closed cycle in off-design calculations.

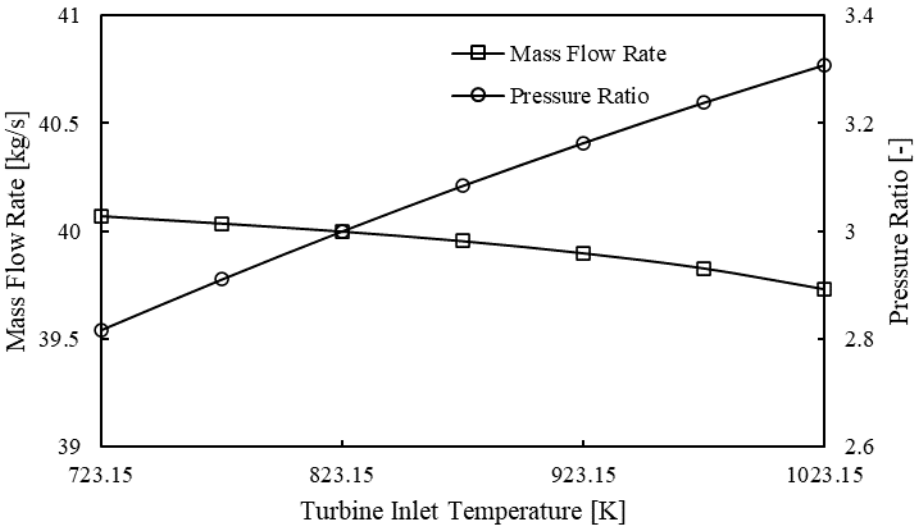

Figure 87. Mass flow rate and pressure ratio of the compressor in an off-design recuperated closed cycle.

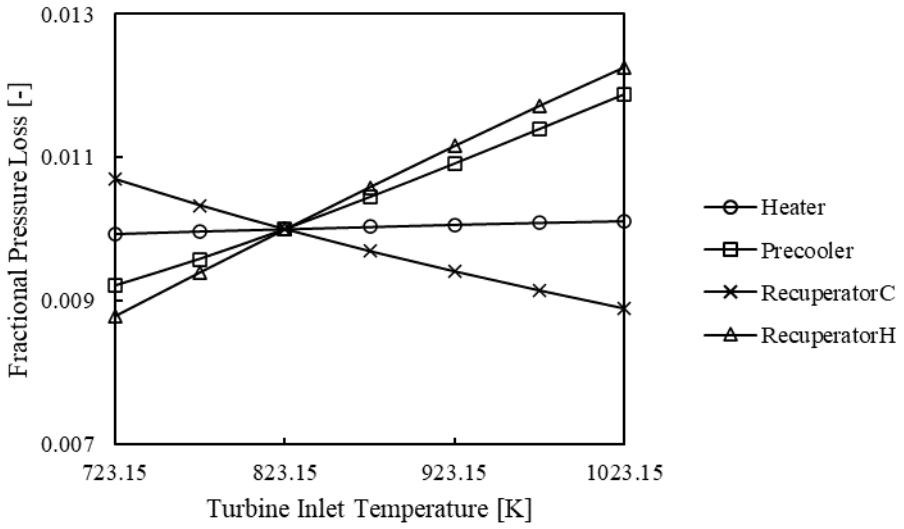

Figure 88. Fractional pressure loss of the heat exchangers in an off-design recuperated closed cycle.

The simple similitude model, which was presented in this chapter, appears to be able to capture the operation of a recuperated cycle, when the turbine inlet temperature alternates. This can be helpful in applications when the power source is not stable, such as solar power. It is also important to examine whether the prediction model is able to represent the operation of the cycle when the inlet conditions change. The design point of the study is presented in **Table 18**, while the inlet pressure of the compressor and the inlet temperature of turbine vary.

Table 18. Design point for off-design calculations of the recuperated cycle.

T_{t1} [K]	306.15
p_{t1} [MPa]	7.8
$Nmech$ [RPM]	50000
T_{t4} [K]	823.15

The turbomachinery maps and the operating lines that occur, are presented in **Figure 89** for the compressor and in **Figure 90** for the turbine. The inlet pressure of the compressor varies in a range from 6 to 8.5 MPa, with the design point at 7.8 MPa.

By observing the performance maps, an operating line appears to be out of the boundaries that the scaling process imposed, already for a small deviation from the design point. This signifies that a better similitude model needs to be utilized, to predict the performance of the cycle in different inlet conditions. Such results, indicate a future work that could be conducted by the Laboratory of Thermal Turbomachines.

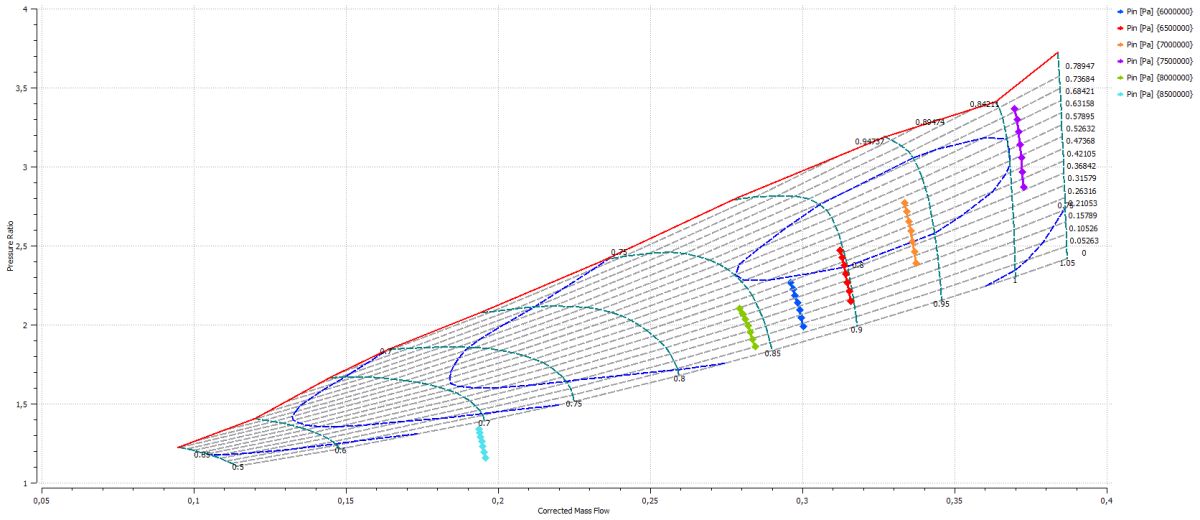

Figure 89. Operating lines of the compressor, for different compressor inlet pressures.

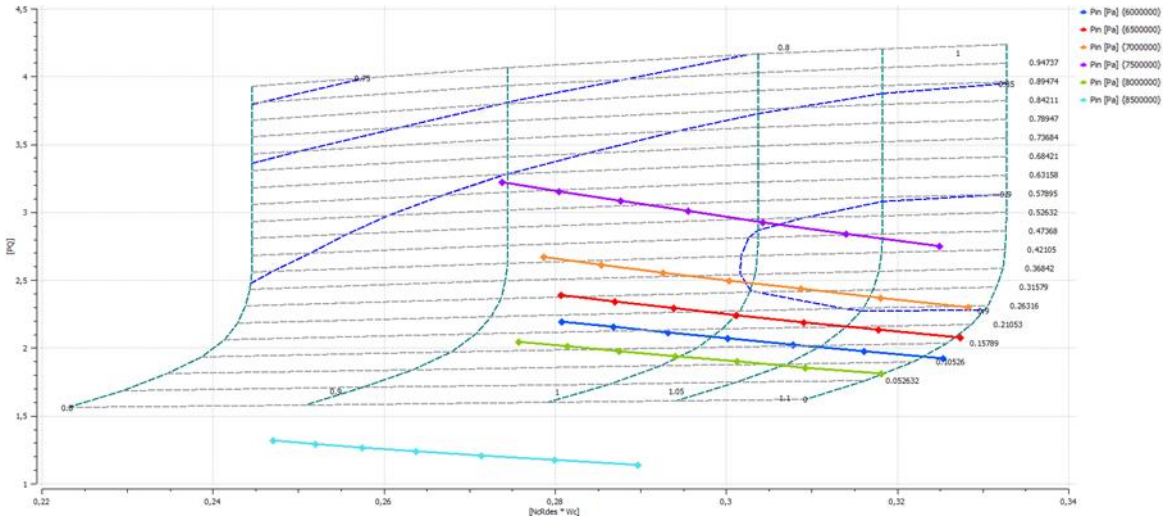

Figure 90. Operating lines of the turbine, for different compressor inlet pressures.

6.3 Summary

The last chapter of the thesis aims to a more comprehensive look on how off-design power cycles operate, with CO_2 as the working medium. A map scaling process is presented for the turbomachinery of the cycles, by using the appropriate factors and applying the suitable equations, since CO_2 should be handled as a real gas fluid. A simple closed loop and a recuperated loop are being studied, and several key parameters are being calculated and compared. While the deviation in the inlet temperature of the turbine can be handled by the current scaling process, there is inadequacy when the inlet pressure alternates. This indicates the future work that should be conducted to be able to predict the performance of a recuperated sCO_2 cycle, in total.

7. SUMMARY AND CONCLUSIONS

This thesis unfolds with an extensive literature review that serves as a guiding framework. The central focus encompasses two key domains: the properties of supercritical carbon dioxide (sCO_2) and power cycles. Drawing from global literature, this exploration becomes particularly pertinent in the attempt to introduce sCO_2 as a working fluid within the Laboratory of Thermal Turbomachines at NTUA. The initial phase involves a detailed modeling of sCO_2 properties.

The investigation reveals that the thermodynamic properties of CO_2 in the supercritical region introduce complexities, yet offer a distinct advantage in compressing the fluid near the critical point with reduced work requirements. The selection of an appropriate Equation of State (EoS), such as the specialized Span and Wagner EoS, proves crucial for accurate calculations, contrasting with the inadequacy of obsolete and simpler EoS like vdW and RK. The specialized EoS of Span and Wanger is integrated into PROOSIS and sets the stage for future thermodynamic property calculations. Cycle analysis has been performed for typical gas turbine cycles and their features have been commented.

Moving forward, the thermodynamic analysis of sCO_2 systems components necessitates a variation from ideal gas assumptions, given the significant deviation of sCO_2 from ideal gas behavior. Every thermodynamic property becomes a function of two state variables, forming the basis for subsequent thermodynamic cycle constructions. Components capable to handle such substances have been developed, in order to allow modelling of installations using them as working media and the corresponding thermodynamic cycles.

Various cycle configurations associated with sCO_2 as a working fluid have been modeled and studied. Calculations for specific configurations underscore the importance of the chosen EoS, concerning the accuracy of the calculations, while the potential of more intricate layouts, hints at higher efficiencies. However, caution is warranted when introducing additional parameters such as the split ratio, as they may impact efficiency adversely. The reliability of developed computational tools is demonstrated through comparisons with results from the open literature, providing a solid foundation for advancing to the study of selected cycles under off-design conditions. The advantage of the recuperated cycle over the simple one is once again confirmed. Example studies of operation at varying conditions are performed.

The studies performed in this work have demonstrated that in order to perform calculations with CO_2 as a working medium, it is essential to use the computation framework developed, while behavior that is customary with gas turbines operating with air as working medium is quite different. Apart from the dependence of properties on two independent variables, other steps such as the scaling of turbomachinery performance maps, has to be carefully performed, in order to have a realistic representation of components behavior. This fact points out to the need for further work, that will allow more accurate component maps for off-design studies, by following "zooming" approaches

that produce much more accurate performance characteristics for any set of conditions that can be encountered during operation, be they close or not to the critical CO_2 thermodynamic conditions.

8. BIBLIOGRAPHY

[1] E. P. Agency, "epa.gov," US EPA, 2023. [Online]. Available: https://www.epa.gov/ghgemissions/overview-greenhouse-gases.

[2] I. Tiseo, "Statista," 2023. [Online]. Available: https://www.statista.com/statistics/276629/global-co2-emissions/.

[3] P. &. M. S. &. K. V. &. S. s. p. Maurya, "Roadmap to sustainable carbon-neutral energy and environment: can we cross the barrier of biomass productivity?," *Environmental Science and Pollution Research,* 2021.

[4] N. D. Baltadjiev, "An Investigation of Real Gas Effects in Supercritical CO2 Compressors," Massachusetts Institute of Technology, 2012.

[5] J. M. M. M. a. M. L. R. Kurz, "Compressor Applications in the Decarbonization Discussion," *IEEE Transactions on Industry Applications,* pp. 1-12, 2023.

[6] H. Li, "Thermodynamic Properties of CO2 Mixtures and Their Applications in Advanced Power Cycles with CO2 Capture Processes," Stockholm, 2008.

[7] V. Dostal, A Supercritical Carbon Dioxide Cycle for Next Generation Nuclear Reactors, Massachusetts Institute of Technology, 2004.

[8] M. Marchionni, "Supercritical Carbon Dioxide Power Cycles for Waste Heat Recovery Applications," Brunel University London, London, 2021.

[9] P. F. R. D. Klaus Brun, Fundamentals and Applications of Supercritical Carbon Dioxide (sCO2) Based Power Cycles, Elsevier Ltd, 2017.

[10] R. B. A. A. I. A. Nikolai Polikhronidi, "Supercritical CO2: Properties and Technological Applications - A Review," *Journal of Thermal Science,* 2019.

[11] A. &. M. M. &. R. S. Witkowski, "Analysis of pipeline transportation systems for carbon dioxide sequestration.," *Archives of Thermodynamics.,* pp. 117-140, 2014 .

[12] J. T. O. K. R. L. C.-H. P. NORBERT BÖTTCHER, "Comparison of equations of state for carbon dioxide for numerical simulations," *IAHS,* 2012.

[13] R. a. W. W. Span, "A New Equation of State for Carbon Dioxide Covering the Fluid Region from the Triple Point Temperature to 1100 K at Pressures up to 800 MPa.," *Journal of Physical and Chemical Reference Data,* pp. 1509-1596, 1996.

[14] G. B. L. C. S. A. T. A. I. S. Martin T. White, "Review of supercritical CO2 technologies and systems for power generation," *Applied Thermal Engineering,* 2021.

[15] J. J. M. J. C. W. K. B. Timothy C. Allison, "Turbomachinery Overview for Supercritical CO2 Power Cycles," in *46th TURBOMACHINERY & 33rd PUMP SYMPOSIA*, Houston, Texas, 2017.

[16] E. Feher, "The supercritical thermodynamic power cycle," *Energy Conversion,* pp. 85-90, 1968.

[17] G. Angelino, "Real Gas Effects in Carbon Dioxide Cycles," *ASME,* 1969.

[18] R. T. D. Ruan van der Westhuizen, "Modelling and simulation of a supercritical carbon dioxide (sCO2) concentrated solar power (CSP) system," in *AIP Conference Proceedings*, 2019.

[19] W. L. Q. Z. W. Z. J. X. Zhiyuan Liu, "Preliminary Design and Model Assessment of a Supercritical CO2 Compressor," *Applied Sciences,* 2018.

[20] LTT-NTUA, "WP1: State Equations and Fluid Properties Summary for the RGTM PROOSIS Library," Athens, 2022.

[21] NIST. [Online]. Available: https://trc.nist.gov/refprop/MINIREF/MINIREF.HTM.

[22] I. H. a. W. J. a. Q. S. a. L. V. Bell, "Pure and Pseudo-pure Fluid Thermophysical Property Evaluation and the Open-Source Thermophysical Property Library CoolProp," *Industrial & Engineering Chemistry Research,* pp. 2498-2508, 2014.

[23] S. N. Laboratories, "Operation and Analysis of a Supercritical CO2 Brayton Cycle," Albuquerque and Livermore, 2010.

[24] J. L. S. G. K. J. I. L. J. E. C. S.-W. L. Yoonhan Ahn, "Design consideration of supercritical CO2 power cycle integral experiment loop," *Energy,* pp. 115-127, 2015.

[25] M. F. S. S. M. Z. Mohammadi, "Advanced exergy analysis of recompression supercritical CO2 cycle," *Energy,* pp. 631-643, 2019.

[26] Y. C. M. S. K. M. K. Sunjin Kim, "Characteristics and optimization of supercritical CO2 recompression power cycle and the influence of pinch point temperature difference of recuperators," *Energy,* pp. 1216-1226, 2018.

[27] C. T. T. Neises, "A Comparison of Supercritical Carbon Dioxide Power Cycle Configurations with an Emphasis on CSP Applications," *Energy Procedia,* pp. 1187-1196, 2014.

[28] M. A. S. C. G. M. P. S. Marco Binotti, "Preliminary assessment of sCO2 cycles for power generation in CSP solar tower plants.," *Applied Energy,* pp. 1007-1017, 2017.

[29] S. S. S. K. C. J. I. L. Yongju Jeong, "An improved off-design prediction model based on similarity analysis for turbomachinery under S-CO2 Conditions," in *The 7th International Supercritical CO2 Power Cycles Symposium*, San Antonio, Texas, 2022.

[30] S. K. C. I. W. S. J. I. L. Yongju Jeong, "Evaluation of off-design scaling methods of supercritical CO2 compressor with experimental data," *Energy,* 2023.

[31] A. M. R. J. M. S. V. S. M. B. P. C. Florian Jacob, "Performance of a Supercritical CO2 Bottoming Cycle for Aero Applications," *Applied Sciences,* 2017.

[32] J. L. Modisette, "Equation of State Tutorial.," in *PSIG Annual Meeting*, Savannah, Georgia, 2000.

[33] J. D. V. D. Waals, On the Continuity of the Gaseous and Liquid States, 1873.

[34] NIST. [Online]. Available: https://shorturl.at/fhNQW.

[35] [Online]. Available: https://plotdigitizer.com/app.

[36] A. Alexiou, "Introduction To Gas Turbine Modelling With PROOSIS," Empresarios Agrupados International (EAI) S.A., 2015.

9. APPENDIX

9.1 Equations of State

9.1.1 Berthelot Equation of State Analysis

For the sake of completeness, the mathematical formulas needed for the Berthelot model to calculate real gas properties, are presented, based on LLT's Report [19].

First, partial derivatives of pressure w.r.t. temperature (f_T, f_{TT}, f_{Tv}) and specific volume (f_v, f_{vv}, f_{vT}) are obtained, by differentiating Eq. 3.5:

$$f_T = \left(\frac{\partial p}{\partial T}\right)_v = \frac{R_g}{u-b} + \frac{a}{u^2 T^2}$$

$$f_{TT} = \left(\frac{\partial^2 p}{\partial T^2}\right)_v = -\frac{2a}{u^2 T^3}$$

$$f_v = \left(\frac{\partial p}{\partial v}\right)_T = \frac{2a}{v^3 T} - \frac{R_g T}{(u-b)^2}$$

$$f_{vv} = \left(\frac{\partial^2 p}{\partial v^2}\right)_T = \frac{2R_g T}{(u-b)^3} - \frac{6a}{v^4 T}$$

$$f_{vT} = f_{Tv} = \frac{\partial^2 p}{\partial v \partial T} = \frac{\partial^2 p}{\partial T \partial v} = -\frac{R_g}{(u-b)^2} - \frac{2a}{u^3 T^2}$$

For a given condition (T, v), to calculate the specific entropy, enthalpy and internal energy, the equation for the Helmholtz free energy residual is needed. Its general formula derives from Gibbs relation and is given by [19]:

$$a_H^r = a_H - a_H^0 = \int_v^\infty \left(p - \frac{R_g T}{v}\right) dv$$

and specifically for Berthelot EoS:

$$a_H^r = -\left(R_g T \ln\left|\frac{v-b}{v}\right| + \frac{a}{vT}\right)$$

We can now calculate the residual specific entropy (s^r), the specific internal energy since it is related to the Helmholtz free energy residual:

$$s^r = s - s^0 = -\left(\frac{\partial a_H^r}{\partial T}\right)_v = R_g \ln\left|\frac{v-b}{v}\right| - \frac{a}{vT^2}$$

The term s^0 is the ideal-gas specific entropy, which is equal to:

$$s^0 = s^0(T,v) = s_{ref} + \varphi^0(T) - \varphi^0(T_{ref}) - R_{g,j} \ln\frac{p_j^0}{p_{ref}}$$

Finally, the real-gas entropy function is obtained by:

$$s(T,v) = s^r(T,v) + s^0(T,v)$$

When it comes to specific internal energy, in an equivalent way as specific entropy, the residual specific internal energy (u^r) can be calculated by:

$$u^r = u - u^0 = a_H^r + Ts^r$$

Where the ideal-gas specific internal energy (u^0) is given by:

$$u^0 = u^0(T) = h^0(T) - R_gT$$

So, the real-gas internal energy function for Berthelot model is obtained by:

$$u(T,v) = u^r(T,v) + u^0(T,v) \Longrightarrow$$

$$\Longrightarrow u(T,v) = -\left(R_gT \ln\left|\frac{v-b}{v}\right| + \frac{a}{vT}\right) + T\left(R_g \ln\left|\frac{v-b}{v}\right| - \frac{a}{vT^2}\right) + h^0(T) - R_gT$$

Then, specific enthalpy is defined as:

$$h = u + pv$$

and its residual by:

$$h^r = h - h^0 = u^r + pv - p^0v = u^r + pv - R_gT$$

For Berthelot model:

$$h(T,v) = h^r(T,v) + h^0(T) \Longrightarrow$$

$$\Longrightarrow h(T,v) = -\left(R_g T \ln\left|\frac{v-b}{v}\right| + \frac{a}{vT}\right) + T\left(R_g \ln\left|\frac{v-b}{v}\right| - \frac{a}{vT^2}\right) + pv + R_g T$$

Now, we continue with the equations for heat capacity at constant volume. Its definition is:

$$C_v = \left(\frac{\partial u}{\partial T}\right)_v$$

The residual is given by:

$$C_v^r = C_v - C_v^0 = \left(\frac{\partial u^r}{\partial T}\right)_v$$

Where the C_v^0 is the specific heat capacity at constant volume for the ideal-gas at the same temperature. It can be calculated as:

$$C_v^0 = C_p^0(T) - R_g$$

We know that:

$$\left(\frac{\partial u^r}{\partial T}\right)_v = \left(\frac{\partial a_H^r}{\partial T}\right)_v + s^r + T\left(\frac{\partial s^r}{\partial T}\right)_v$$

And $s^r = -\left(\frac{\partial a_H^r}{\partial T}\right)_v$. So,

$$C_v^r = T\left(\frac{\partial s^r}{\partial T}\right)_v$$

For Berthelot model,

$$C_v(T,v) = C_v^r(T,v) + C_v^0(T) \Longrightarrow$$

$$\Longrightarrow C_v(T,v) = \frac{2a}{vT^2} + C_p^0(T) - R_g$$

The coefficient of thermal expansion is defined as:

$$\beta = \frac{1}{v}\left(\frac{\partial v}{\partial T}\right)_p$$

Its final formula for Berthelot model, is given through the partial derivatives that were previously calculated:

$$\beta = -\frac{1}{v}\frac{f_T}{f_v} = -\frac{1}{v}\left(\frac{\frac{R_g}{u-b}+\frac{a}{u^2T^2}}{\frac{2a}{v^3T}-\frac{R_gT}{(u-b)^2}}\right)$$

The isothermal compressibility factor is defined as:

$$k = -\frac{1}{v}\left(\frac{\partial v}{\partial p}\right)_T$$

Its final formula for Berthelot model, is given through the partial derivatives that were previously calculated:

$$k = -\frac{1}{vf_v} = -\frac{1}{v\left(\frac{2a}{v^3T}-\frac{R_gT}{(u-b)^2}\right)}$$

Heat capacity at constant pressure (C_p) is given through Mayer's relation by:

$$C_p = C_v + \frac{\beta^2}{k}vT$$

In terms of residual quantities, it can be written as:

$$C_p^r = C_p - C_p^0 = C_v^r + \frac{\beta^2}{k}vT - R_g$$

For Berthelot model:

$$C_p(T,v) = C_p^r(T,v) + C_p^0(T) \Longrightarrow$$

$$\Longrightarrow C_p(T,v) = \frac{2a}{vT^2} + \frac{\beta^2}{k}vT - R_g + C_p^0(T)$$

The Joule-Thompson coefficient is defined as:

$$\mu_{JT} = \left(\frac{\partial T}{\partial p}\right)_h$$

Its final formula for Berthelot model, is given through C_p and β that were previously calculated:

$$\mu_{JT} = \frac{v}{C_p}(\beta T - 1) = -\frac{v}{\frac{2a}{vT^2} + \frac{\beta^2}{k}vT - R_g + C_p^0(T)}\left(\frac{T}{v}\left(\frac{\frac{R_g}{u-b} + \frac{a}{u^2T^2}}{\frac{2a}{v^3T} - \frac{R_gT}{(u-b)^2}}\right) + 1\right)$$

The speed of sound is defined as:

$$w^2 = \left(\frac{\partial p}{\partial \rho}\right)_s$$

Its final formula for Berthelot model, is given through C_p, k and β that were previously calculated:

$$w = \sqrt{\frac{vC_p}{kC_p - \beta^2 vT}} \Longrightarrow$$

$$\Longrightarrow w = \sqrt{\frac{v\left(\frac{2a}{vT^2} + \frac{\beta^2}{k}vT - R_g + C_p^0(T)\right)}{\left(-\frac{\frac{2a}{vT^2} + \frac{\beta^2}{k}vT - R_g + C_p^0(T)}{v\left(\frac{2a}{v^3T} - \frac{R_gT}{(u-b)^2}\right)}\right) - \left(-\frac{1}{v}\left(\frac{\frac{R_g}{u-b} + \frac{a}{u^2T^2}}{\frac{2a}{v^3T} - \frac{R_gT}{(u-b)^2}}\right)\right)^2 vT}}$$

The isentropic expansion coefficient is defined as:

$$\gamma = -\frac{v}{p}\left(\frac{\partial p}{\partial v}\right)_s$$

Its final formula for Berthelot model, is given through C_p, k and β that were previously calculated:

$$\gamma = \frac{\frac{2a}{vT^2} + \frac{\beta^2}{k}vT - R_g + C_p^0(T)}{p\left(-\frac{\left(\frac{2a}{vT^2} + \frac{\beta^2}{k}vT - R_g + C_p^0(T)\right)}{v\left(\frac{2a}{v^3T} - \frac{R_gT}{(u-b)^2}\right)} - \left(-\frac{1}{v}\left(\frac{\frac{R_g}{u-b} + \frac{a}{u^2T^2}}{\frac{2a}{v^3T} - \frac{R_gT}{(u-b)^2}}\right)\right)^2 vT\right)}$$

9.2 Typical Experiment from Schematics

After writing the scripts for the components and creating their symbol, as shown in **PROOSIS Components**, schematics can be created, and several experiments can be conducted. A typical example is the following Parametric Study, which examines how the inlet temperature of the turbine affects a recuperated cycle.

The first step is to create a New Default Partition. The following variables will be used as Boundary Variables.

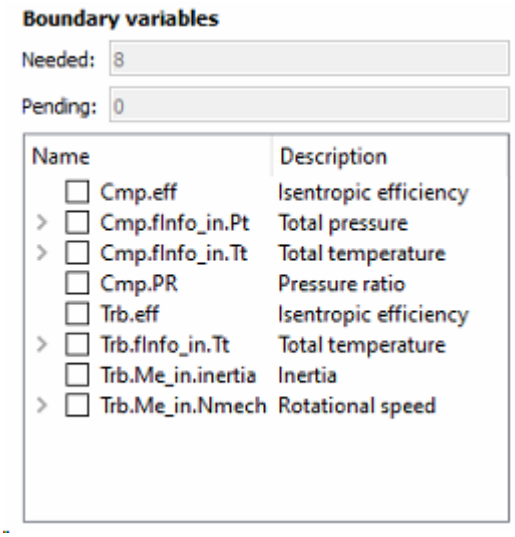

Then, we create a Wizard Experiment, and we add a Standard Case. Under this case, we add a Steady and a Parametric calculation. Steady Calculation, will calculate the cycle for the Boundary Values that we enter in Initialize tab.

	Name	Value	Units	
1	Cmp.PR	20/7.78	-	Pressure ratio
2	Cmp.eff	0.65	-	Isentropic efficiency
3	Cmp.flnfo_in.Pt	7.78 * 1E6	Pa	Total pressure
4	Cmp.flnfo_in.Tt	306.35	K	Total temperature
5	Trb.Me_in.Nmech	111000	rpm	Rotational speed
6	Trb.Me_in.inertia	1	kg·m^2	Inertia
7	Trb.eff	0.85	-	Isentropic efficiency
8	Trb.flnfo_in.Tt	773.15	K	Total temperature

In Parametric Calculation, we add the inlet temperature of the compressor as a Parameter, by pressing the white-green cross.

Parameters

Name	Type	Mode	Submode	Value	Units	Category	Description
Cmp.fInfo_in.Tt	REAL	INTERVAL	By Final Value	initial=295;final=315;step=20;	K	BOUNDARY	Total temperature

And we select the following range of inlet temperatures.

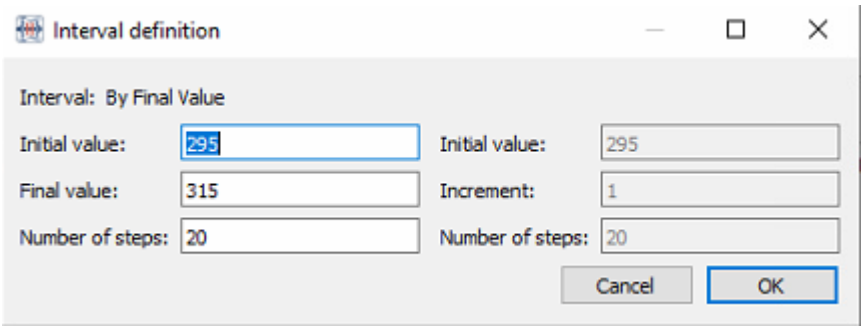

In Initialize tab we enter the previous values, and then we can run our simulation. An example of results is the following.

1	2	3	4	5	6	7	8	9	10	11	12	13	14	15	16
Name	Alias	Station	1	2	3	4	5	6	7	8	9	10	11	12	13
#Calculation id	--	--	steady2(#1)-ste...	parametric1(#2...	parametric1(#2...	parametric1(#2...	parametric1(#2...	parametric1(#2...	parametric1(#2...	parametric1(#2...	parametric1(#2...	parametric1(#2...	parametric1(#2...	parametric1(#2...	parametric1(#2...
#Status	--	--	STEADY_OK	STEADY_OK	STEADY_OK	STEADY_OK	STEADY_OK	STEADY_OK	STEADY_OK	STEADY_OK	STEADY_OK	STEADY_OK	STEADY_OK	STEADY_OK	STEADY_OK
#ESI	--	--	0	0	0	0	0	0	0	0	0	0	0	0	0
#Case	--	--	case2(#1)	case2(#1)	case2(#1)	case2(#1)	case2(#1)	case2(#1)	case2(#1)	case2(#1)	case2(#1)	case2(#1)	case2(#1)	case2(#1)	case2(#1)
#Point	--	--													
Cmp.F_in.Tt (K)	--	--	306.35	295	296	297	298	299	300	301	302	303	304	305	306
Cmp.F_out.Tt (K)	--	--	347.409239	396.046288	397.257652	398.468797	399.679726	400.89044	402.100943	403.311236	404.521322	405.731202	406.94088	408.150356	409.359633
Heater.F_in.Tt (K)	--	--	542.113707	566.023329	566.513932	567.004445	567.494872	567.985211	568.475465	568.965633	569.455718	569.94572	570.435639	570.925477	571.415234
Heater.F_out.Tt ...	--	--	773.15	773.15	773.15	773.15	773.15	773.15	773.15	773.15	773.15	773.15	773.15	773.15	773.15
Precooler.F_in.T...	--	--	389.508025	523.83866	524.436905	525.035872	525.63556	526.235965	526.837085	527.438915	528.041454	528.644698	529.248644	529.853289	530.458631
Precooler.F_out...	--	--	306.35	295	296	297	298	299	300	301	302	303	304	305	306
Recuperator.F_i...	--	--	347.409239	396.046288	397.257652	398.468797	399.679726	400.89044	402.100943	403.311236	404.521322	405.731202	406.94088	408.150356	409.359633
Recuperator.F_i...	--	--	674.64364	681.721988	681.721988	681.721988	681.721988	681.721988	681.721988	681.721988	681.721988	681.721988	681.721988	681.721988	681.721988
Recuperator.F_...	--	--	542.113707	566.023329	566.513932	567.004445	567.494872	567.985211	568.475465	568.965633	569.455718	569.94572	570.435639	570.925477	571.415234
Recuperator.F_...	--	--	389.508025	523.83866	524.436905	525.035872	525.63556	526.235965	526.837085	527.438915	528.041454	528.644698	529.248644	529.853289	530.458631
Trb.fInfo_in.Tt (K)	--	--	773.15	773.15	773.15	773.15	773.15	773.15	773.15	773.15	773.15	773.15	773.15	773.15	773.15
Trb.fInfo_out.Tt ...	--	--	674.64364	681.721988	681.721988	681.721988	681.721988	681.721988	681.721988	681.721988	681.721988	681.721988	681.721988	681.721988	681.721988

10. FIGURES

11. TABLES